AN AERODYNAMIC ANALYSIS OF AEROFOILS USING A SPLINE VELOCITY SINGULARITY METHOD

by

Rob Dunn

Department of Mechanical Engineering

McGill University

Montreal Quebec, Canada.

This Thesis, submitted to the Faculty of Graduate Studies and Research, completes the requirements towards a Masters degree in Engineering.

June, 1993

©Rob Dunn, 1993.

Abstract

This thesis presents a new approach based on a spline formulation for the analysis of thin aerofoils using the velocity singularity method. The method of velocity singularities was originally developed by Mateescu and Newman in conjunction with a polynomial representation of the normal perturbation velocities. The present method uses a cubic spline representation of the aerofoil contour, which led to improvements in the accuracy and stability of the solution, especially in the case of the jet-flapped aerofoils.

This method has been first validated for the cases of rigid and flexible aerofoils. The pressure distributions obtained with the spline formulation have proven to be in good agreement with the previous solutions based on conformal transformation, or obtained by Thwaites, Nielsen, and by Mateescu and Newman.

The spline-velocity singularity method has been used for the jet flapped aerofoils and then extended to analyze the aerofoils with multiple sections, such as aerofoils with a flap. The solutions for these problems have been found to be in good agreement with the results obtained theoretically or experimentally by Spence, and Dimmock, and by Seebohm and Newman, based on a surface vortex method.

The spline-velocity singularity method displayed a better accuracy and an enhanced stability of the solution, in comparison with the polynomial formulation, especially in the cases when the aerofoil contour is not known a priori, such as for the flexible or jet-flapped aerofoils.

Sommaire

Cette thèse présente une nouvelle approche à l'analyse de aerofoil par la methode de singularité de vitesse en utilisant des splmes cubiques. La méthode des singularites de vitesse fut initiallement developpée par Mateescu et Newman en utilisant une représentation polynomiale pour les vitesses verticales de perturbation. Par contre, la méthode devel oppée dans cette thèse utilise une représentation du contour du profil aèrodynamique basée sur des splines cubiques; ça à conduit a l'amélioration de la précision et la stabilité de la solution, specialement dans le cas des profils aérodynamiques avec des ailetons à jet.

Cette mèthode a été validée pour les cas des profils aérodynamiques rigides ou flex ibles. Les distributions des pressions obtenues avec cette mèthode ont été trouvées en bon accord avec les solutions existantes basées sur des transformations conformes, or obtenues par Thwaites, Nielsen, et par Mateescu et Newman.

La mèthode spline-singularités de vitesse a été utilisée pour l'étude des profiles aéro dynamique avec des ailerons à jet, et puis une extension a été developée pour l'analyse des profils avec plusieurs elements, comme les profils munis des ailerons. Les solutions obtenues pour ces problèmes ont été trouvées en bon accord avec les résultats théoriques ou experimentaux obtenus par Spence, Dimmock, ou par Scebohm et Newman, basés sur une méthode tourbillonaire de surface.

La méthode spline-singularités de vitesse a demontrée une meilleure précision et une stabilité ameliorée de la solution, en comparaison avec la représentation polynomiale, specialement dans les cas où la géometrie du profil n'est pas connuc d'avance, comme dans les cas des profils aérodynamiques flexibles ou munis des ailerons à jet.

Acknowledgements

I would like to thank my thesis supervisor, Professor Dan F. Mateescu, for his help, knowledge, and patience throughout the course of this work. His own research was a basis for this work.

I am grateful to Joyce, and to my family for their social and financial encouragement.

I would like to thank all my friends in Goderich.

Contents

		Abstract	
		Sommaire	i
		Acknowledgements	ii
		Table of Contents	i۱
		List of Figures	vi
		List of Tables	>
		Nomenclature	x
1	Inti	roduction	1
	1.1	General Considerations	ı
	1.2	Scope of Thesis	4
2	Rev	view of Selected Aerofoil Theories	6
	2.1	Basic Equations	ϵ
	2.2	Conformal Transformation Method	8
	2.3	Method of Velocity Singularities	9
		2.3.1 Basic Equations and General Considerations for the Velocity Sin-	
		gularity Method	9

		2.3.2	Thin Aerofoil Solutions	10
		2.3.3	Aerofoils of Symmetrical Thickness	14
		2.3.4	Local Linearization Solution	16
3	A S	pline l	Formulation for the Method of Velocity Singularities	18
	3.1	Gener	al Considerations for Spline Formulation	18
		3.1.1	Spline Formulation for Thin Aerofoils	21
		3.1.2	Spline Formulation for Aerofoils of Symmetrical Thickness	22
		3.1.3	Spline Formulation for Aerofoils Using Local Linearization	23
	3.2	Applic	cations of the Spline Formulation for Aerofoils of Fixed Geometry .	24
		3.2.1	Cambered Thin Aerofoils	24
		3.2.2	Aerofoils With Pointed Leading Edges	29
		3.2.3	Aerofoils with Rounded Leading Edges	38
4	Ana	alysis d	of Flexible Aerofoils	47
	4.1	Gener	al Theory of a Flexible Aerofoil	48
	4.2	Spline	Formulation For Flexible Aerofoils	49
	4.3	Soluti	ons for Flexible Aerofoils and Discussion of Results	52
5	Ana	alysis d	of Jet Flapped Aerofoils	61
	5.1	Gener	al Theory of a Jet Flapped Aerofoil	62
	5.2	Spline	Formulation for Jet Flapped Aerofoils	64
	5.3	Soluti	ons for Jet Flapped Aerofoils and Discussion of Results	68

6	Ana	alysis of Multi-Element Aerofoils	73		
	6.1	Flow Field Solution outside the Aerofoil Contour by the Method of Velocity			
		Singularities	73		
		6.1.1 Thin Aerofoil Solutions	71		
		6.1.2 Aerofoils of Symmetrical Thickness	77		
	6.2	Analysis of Two-Element Aerofoils	78		
		6.2.1 Antisymmetrical Part of the Solution	80		
		6.2.2 Symmetrical Part of the Solution	82		
	6.3	Results and Comparisons for Two-Element Aerofoils	81		
7	Conclusions				
	Bibliography				
	Ap	pendices			
A	Con	nformal Transformation	97		
	A.1	Karman-Trefftz Transformation	97		
	A.2	Flow Around A Circle With Circulation	99		
В	Per	turbation Velocity Formulation	101		
	B.1	The Antisymmetrical Velocity field	101		
		B.1.1 Complex Conjugate Disturbance Velocity Function	101		
		B.1.2 Spline Formulation	103		
		B.1.3 Derivation of Integral $K_k^i(x)$	104		
	B.2	The Symmetrical Velocity Field	100		

		B.2.1	Complex Conjugate Disturbance Velocity Function	106
		B.2.2	Spline Formulation	107
		B.2.3	Derivation of Integral $J_k^i(x)$	108
	B.3	Modifi	ed Expansion Field - Local Linearization	109
		B.3 .1	Derivation of Integral $J_{M_k}^i(x)$	109
\mathbf{C}	Cul	oic Spli	ne Formulation	110
	C.1	Introd	uction	110
		C.1.1	Cubic Spline Using Tri-Diagonal Matrix	110
		C.1.2	Cubic Spline Using Second Derivatives	113
D	Ima	ginary	Perturbation Regime	114
	D.1	Imagin	ary Part of the Ridge Function	114
	D .2	lmagin	ary Part of the Antisymmetrical Velocity Function outside the Aero-	
		foil Co	ntour	115
		D.2.1	Derivation of Integral $Q_k^i(x)$	116
E	Con	nputer	Subroutines	118
	E.1	Subrou	tine for Antisymmetrical Velocities	119
	E.2	Subrou	tine for Symmetrical Velocities	120
	E.3	Subrou	tine using Local Linearization	121
	E.4	Subrou	tine for Integral $K_k^i(x)$	122
	E.5		tine for Integral $J_k^i(x)$	123
	E.6		tine for Integral $J_{M_k}^i(x)$	124
	E.7		tine for Spline Formulation	195

E.8	Subroutine for Flexible Membranes	•	-126
E.9	Subroutine for Jet Flapped Aerofods		129
E.10	Subroutine for Multi-Element Aerofoils		1 (+)

List of Figures

2.1	Simple flapped plate	11
2.2	Double wedge aerofoil	15
2.3	Normal and tangential perturbation components on a rounded	
	leading edged aerofoil	17
3.1	Camberline coefficients for crescent shaped aerofoils	19
3.2	Pressure coefficients for circular arc aerofoil $f/c=0.025$ at various	
	angles of attack.	26
3.3	Pressure coefficients for circular arc aerofoil $f/c=0.05$ at various	
	angles of attack.	27
3.4	Lift coefficients for circular arcs with $f/c = 0.02$, and $f/c = 0.05$.	28
3.5	Pressure coefficients for symmetrical lenticular aerofoil $e/c=0.05$	
	at various angles of attack	31
3.6	Pressure coefficients for symmetrical lenticular aerofoil $e/c=0.1$	
	at various angles of attack	32
3.7	Lift coefficients for symmetrical lenticular aexofoils with $e/c=$	
	0.05, and $e/c = 0.1$	33

3.8	Pressure coefficients for crescent shaped aerofoil $e/c = 0.05$ and	
	f/c = 0.025 at various angles of attack	34
3.9	Pressure coefficients for crescent shaped aerofoil $e/c=0.1$ and	
	f/c = 0.05 at various angles of attack	35
3.10	Pressure coefficients for cambered lenticular aerofoil $e/c=0.05$	
	and $f/c = 0.01$ at various angles of attack	36
3.11	Lift coefficients for two crescent shaped and a cambered lentic-	
	ular aerofoil	37
3.12	Pressure coefficients for symmetrical Joukowski aerofoil at $lpha=0^{\circ}$	
	using regular expansion.	40
3.13	Pressure coefficients for symmetrical Joukowski aerofoil at $lpha=0^{ m o}$	
	using modified expansion.	41
3.14	Pressure coefficients for symmetrical Joukowski aerofoil with	
	e/c=0.05 at various angles of attack	43
3.15	Pressure coefficients for symmetrical Joukowski aerofoil with	
	e/c = 0.1 at various angles of attack	44
3.16	Pressure coefficients for a cambered Joukowski aerofoil with $e/c=$	
	0.05 and $f/c = 0.025$ at various angles of attack	45
3.17	Lift coefficients for three Joukowski aerofoils.	46
4.1	Typical side picture of two-dimensional flexible aerofoil	48
4.2	Flexible-aerofoil geometry for various tension coefficients C_T com-	
	pared with Mateescu and Newman.	57

4.3	Pressure coefficients vs chordwise position for various tension	
	coefficients ('T	58
4.4	Lift coefficients vs various tension coefficients C_T	59
4.5	Centers of pressure for various tension coefficients C_T	60
5.1	Geometry of a jet flapped aerofoil	62
5.2	Jet flap panel arrangement	64
5.3	Nondimensional pressure difference ΔC_P across a jet flapped	
	symmetrical aerofoil at zero incidence compared to Dimmock's,	
	experimental results ($\alpha=0^{\circ},\ \beta=31^{\circ},\ C_J=0.3$)	70
5.4	Lift slope, $\frac{\partial C_L}{\partial \beta}$, compared to Spence's solution and Spence's ex-	
	perimental values.	71
5.5	Plot of the jet-flap length L against jet coefficients C_J	72
6.1	Flapped aerofoil at incidence α and flap incidence β	78
6.2	Decomposition of (a) antisymmetrical and (b) symmetrical parts	
	of a two-element aerofoil.	79
6.3	Two thin cambered aerofoils to determine the antisymmetrical	
	velocity flow field.	80
6.4	Two symmetrical aerofoils to determine the symmetrical velocity	
	flow field.	82
6.5	Pressure coefficients for an aerofoil with a rounded leading edge	
	$(c/c = 0.05, f/c = 0.02)$ and a 35% flap $(\alpha = 0^{\circ}, \beta = 15^{\circ})$	86
6.6	Pressure coefficients for an aerofoil with a rounded leading edge	
	$(\epsilon/c = 0.05, f/c = 0.02)$ and a 35% flap $(\alpha = 10^{\circ}, \beta = 15^{\circ})$.	87

6.7	Pressure coefficients for a symmetrical Joukowski aerofoil ($\epsilon/c=$	
	0.05) with 35% flap ($\alpha = 0^{\circ}$, $\beta = 20^{\circ}$)	88
6.8	Pressure coefficients for a symmetrical Joukowski aerofoil ($\epsilon/c=$	
	0.05) with 35% flap ($\alpha = 10^{\circ}$, $\beta = 20^{\circ}$)	89
B .1	Geometric notations of camberline panels used for the cubic	
	spline representation of the aerofoil camberline	103
C.1	Geometric notations of camberline panels used for the cubic	
	spline representation of the aerofoil camberline	111

List of Tables

3.1	Accuracy of the present spline-velocity singularity method and	
	polynomial method in comparison with the conformal transfor-	
	mation method for a symmetrical Joukowski aerofoil (e/c = 0.05 ,	
	$\alpha = 0^{\circ}$)	39
4.1	Comparison of lift coefficients and excess membrane length for	
	various tension coefficients C_T	55
4.2	Comparison of $h(x)/\alpha$ for various tension coefficients C_T . The	
	position of maximum camber is outlined	56
5.1	Coefficients of lift for a jet-flapped aerofoil with $\beta=31.4^{\circ},$ com-	
	pared to Spence's solution.	68
6.1	Real and imaginary parts of the ridge function found in the com-	
	plex conjugate perturbation function.	74
6.2	Definitions for c and c_o for aerofoil 1 and aerofoil 2	78
6.3	Definitions of two types of aerofoils.	84
A.1	Summary of aerofoil parameters used in Karman-Trefftz trans-	
	formation.	99

Nomenclature

a, b, nconformal transformation parameters $A_{\mathfrak{t}}, B_{\mathfrak{t}}, C_{\mathfrak{t}}, D_{\mathfrak{t}}$ spline coefficients C_J jet momentum coefficient C_L lift coefficient C_{M} moment coefficient C_{P} pressure coefficient C_T tension coefficient chord c e/ccamber ratio f/cthickness ratio g(x), h(x)thickness and camber coordinates \boldsymbol{J} jet momentum j(x)ordinate of the jet sheet $J_k^{\imath}(x)$ integral defined by equation B.13 $J^{\imath}_{M_k}(x)$ integral defined by equation B.17 $K_k^i(x)$ integral defined by equation 3.15 leading edge LE M Mach number normal unit vector $\cdot n$ R aerofoil ridge TE trailing edge

membrane tension

T

u, v perturbation velocity components

 $ec{V}$ total velocity vector

 U_{∞} undisturbed flow velocity

W(z) complex conjugate perturbation velocity function

z = x + iy, complex variable

Greek Symbols

 α angle of incidence

 β, ϵ Karman-Trefftz conformal transformation parameters

 β jet flap angle

 δ leading edge angle

 ϵ excess membrane length

 Γ total circulation

 $\gamma(x)$ local circulation

 λ integral defined by equation 3.16

Λ integral defined by equation 3.17

 μ viscosity coefficient

 ϕ veloctiy potential

 ψ streamline function

 ρ fluid density

 σ nondimensional parameter defined by equation 2.32

au trailing edge angle, aerfoil surface slope

□ integration constant defined in section 4.2

 $\zeta = \xi + i\eta$

$\underline{Subscripts}$

 ${\cal A}$ antisymmetrical

S symmetrical

 ∞ unperturbed

u, l upper, lower

 L_E Leading Edge

 C_P Center of Pressure

Chapter 1

Introduction

1.1 General Considerations

The analysis of thin aerofoil theory has been a subject under research for many years. Classical theories for rigid aerofoils of arbitrary shape began with Glauert [5] and Birnbaum where the aerofoil was replaced by a vortex sheet on the camberline, and circulation was formulated by the use of Fourier series. Stewart [30] modified this method by transforming the aerofoil into a circle plane where the complex velocity perturbation function consisted of a series of singularities. This resulted in a Fourier series expression for pressure differences which was similar to that of Glauert's. The advent of the modern computer introduced methods where large matrices could be convieniently solved. This produced boundary element methods based on source, doublet and or vortex distributions [10,13,20]. This type of method could handle thicker aerofoils at the expense of computing time. Another method based on the use of a computer was developed by Halsey [8], in which the complex potential was iterated by conformal transformations.

Exact flow solutions around certain aerofoils can be found through conformal transformation, the problem being that their shapes are limited.

Methods of this type were derived for ideal fluid flow situations. An airplane in regular cruising conditions would have aerfoils operating under low angles of attack (ideal fluid flow situation). For an airplane cruising under conditions where compressibility becomes a factor (i.e. at Mach numbers greater than 0.3) the influence of compressibility has to be taken into account, whereby Prantl's concepts need to be introduced. For aerofoils subjected to large angles of attack (which usually occurs under slow flight conditions) the effects of viscosity and flow separation need to be accounted for.

Topics related to thin aerofoil theory have included the analysis of flexible aerofoils and aerofoils with jet flapped arrangements. The flexible aerofoil which is better known as a sail, has been under analytical research since the early sixties. Nielsen [23] and Thwaites [33] were the first to publish research based on a long Fourier series approach, solved by an eigenvalue approach. Also Newman [21,22], and more recently Mateescu and Newman [16,17] took an interest in the subject.

A jet flapped aerofoil increases lift on the aerofoil (without the use of a mechanical flap) by expelling a jet of fluid at the trailing edge of the aerofoil. Published research by Spence [27,28,29] analyzed an infinitely thin jet expelled out of the trailing edge at a specific angle with a high velocity. He first used a Fourier series approach and then found simple equations to predict lift and pressure variations. These equations compared quite well with experimental results. O'Mahoney and Smith [24] used a circle transformation method, which sometimes required several iterations becoming quite cumbersome.

Another interesting related topic is that of aerofoils with multiple sections (for example an aerofoil with a flap). Research by Hess and Smith [9] analyzed this topic using a

source panel method. Another panel method using vortices on the surface of the aerofoils was developed by Seebohm and Newman [26]. This method could also account for
viscosity which becomes important on the flap of the aerofoil which can be under large
deflections.

The present analysis represents an extension of the method of velocity singularities developed by Mateescu and Newman [16,17], in which special singularities at the aerofoil leading edge and ridges along the aerofoil are used to determine the complex conjugate velocity around the aerofoil. The mathematical expressions of these singularities are determined to implicitly satisfy the boundary conditions outside the aerofoil and the Kutta condition at the trailing edge. The velocity field around the aerofoil is thus determined by a simple integration of these singularities based on the variation of the slope of the aerofoil contour. This method is characterized by a simple and direct approach, leading to closed-form solutions in all cases when the aerofoil contour is specified. In addition, the method of velocity singularities has proven to be particularly suitable for solving the special problems in which the aerofoil contour is not known a priori, such as the problems of flexible aerofoils and jet-flapped aerofoils, in which the shape of the flexible membrane or of the jet sheet depends on the pressure difference across them [17].

The method of velocity singularities has been developed by Mateescu and Newman as a linear theory, using a polynomial representation of the aerofoil contour [15,17]. Later, Mateescu and one of his students, Nadeau, extended this method to the nonlinear analysis of the aerofoils [18,20].

1.2 Scope of Thesis

The polynomial representation of the aerofoil contour has proven to be very convenient and adequate for a large class of aerofoils of specified geometries, such as the five digit series of the NACA aerofoils, which are characterized by a polynomial representation of the camberline. However, in some special problems, for example, the case of the jet-flapped aerofoils, the polynomial representation of the aerofoil-contour can lead to high-order polynomials with large coefficients which can have adverse effects on the accuracy of the solution. In this respect, a smooth representation of the aerofoil contour, such as a cubic, will certainly contribute to improve the accuracy of the solution in these special problems.

In the present work, the method of velocity singularities is developed in conjunction with a cubic spline representation of the aerofoil contour. This spline representation will contribute to a higher accuracy and stability of the solution in special problems such as the jet-flapped aerofoils, and in general will have a beneficial effect on the application of the method of velocity singularities in all cases.

This thesis will focus on the method of velocity singularities using a linear approach incorporating cubic splines. In chapter 2 the method of velocity singularities will be described. This will form the basis for the work of chapter 3, where the spline formulation will be presented. The method of solution will be followed by solutions for various aerofoils comparing the use of cubic splines to the polynomials. The two methods will be checked by the exact solution of the Karman-Trefftz conformal transformation. Once the accuracy and validity of the method is shown, the method using cubic splines will be used for the analysis of special problems.

Chapter 4 will describe the analysis of flexible aerofoils. In this chapter the general theory will be described along with solutions for flexible aerofoils. The solutions will show how the method of velocity singularities is particularily suited for this type of problem. Solutions will be compared to experimental and analytical results obtained by Thwaites [33] and Nielsen [23].

The analysis of jet flapped aerofoils will be investigated in chapter 5. In this section it will be shown how the method of velocity singularities has a clear advantage when using cubic splines as opposed to large polynomials. Solutions for jet flaps will be compared to the solutions obtained by Spence [27,28,29] and experimental results by Dimmock [32].

In chapter 6, the flow field outside of the aerofoil will be investigated to analyze aerofoils with multiple sections. Solutions for various cases of aerofoils with flaps will be compared to that of the inviscid case of the surface vortex method developed by Seebohm and Newman [26].

Chapter 2

Review of Selected Aerofoil

Theories

This chapter focuses on thin aerofoil theory, characterized by an aerofoil consisting of moderate thickness and camber, subjected to small angles of attack.

2.1 Basic Equations

This work refers to two-dimensional, incompressible, and irrotational fluid flows. For incompressible flows, the continuity equation requires that:

$$\nabla \cdot \vec{V} = 0. \tag{2.1}$$

This allows the flow to be represented by a streamline function $\psi(x,y)$. For irrotational flows, $\nabla \times \vec{V} = 0$, the fluid velocity derives from a velocity potential $\phi(x,y)$:

$$\vec{V} = \nabla \phi. \tag{2.2}$$

These two flow functions (ϕ and ψ) are harmonic and satisfy Laplace's equation:

$$\nabla^2 \phi = 0, \tag{2.3}$$

$$\nabla^2 \psi = 0. \tag{2.4}$$

The solution of Laplace's equation allows for superposition of different simple flows and gives a complex potential for the fluid field:

$$F(z) = \phi + i\psi, \qquad (2.5)$$

where z = x + iy.

The velocity components can be obtained from the complex conjugate velocity defined as the derivative of the complex potential,

$$F'(z) = u - \imath v, \tag{2.6}$$

where u represents the velocity component in the x direction and v is the velocity component in the y direction (Cartesian coordinates). Pressures can be found using the momentum equation

$$(\vec{V} \cdot \nabla)\vec{V} = -\frac{1}{\rho}\nabla P. \tag{2.7}$$

Integrating this equation along a streamline results in Bernoulli's equation:

$$P_{\infty} + \frac{1}{2}\rho U_{\infty}^2 = P + \frac{1}{2}\rho \vec{V}^2. \tag{2.8}$$

Because inviscid, irrotational flows are being dealt with, Bernoulli's equation can be applied along and across the streamlines (the stagnation pressure, P_o , is the same everywhere). The pressure coefficient defined as:

$$C_P = \frac{P - P_{\infty}}{\frac{1}{2}\rho U_{\infty}^2},\tag{2.9}$$

can be expressed using Bernoulli's equation (2.8) in the form

$$C_P = 1 - \left(\frac{V}{U_\infty}\right)^2. \tag{2.10}$$

The boundary condition on the aerofoil can be expressed as

$$\vec{V} \cdot \vec{n} = 0, \tag{2.11}$$

where \vec{n} is the unit vector normal to the surface of the aerofoil. Perturbation velocities are assumed to be small, therefore far upstream and downstream of the aerofoil these perturbations become negligible with the oncoming fluid flow

$$\lim_{z \to \pm \infty} \vec{V} = U_{\infty}. \tag{2.12}$$

2.2 Conformal Transformation Method

By use of conformal transformation, an aerofoil can be transformed to the z plane from a circle in the ζ plane. This idea makes use of the already known solution for the flow with circulation around a circle in order to find velocity components on the aerofoil.

The Karman-Trefftz aerofoil has been chosen because it can be used for several types of aerofoils (i.e. Joukowski, circular arcs, lenticular, etc.). The transformation itself is defined as:

$$\frac{z-nb}{z+nb} = \left(\frac{\zeta-b}{\zeta+b}\right)^n,\tag{2.13}$$

where b is a constant, $\zeta = \xi + i\eta$ are the coordinates in the complex ζ plane, and n is a nondimensional constant, with a value between 1 and 2, that defines the trailing edge angle

$$\tau = (2-n)\pi. \tag{2.14}$$

Clearly if n=2 (known as the Joukowski transformation), the trailing edge angle becomes zero, forming a cusp. The circle of radius a in the z plane is defined by $a=b(1+\epsilon)/\cos\gamma$. Details of the Karman-Trefftz transformation are discussed in Appendix A.1. The complex conjugate velocity in the aerofoil plane, z can be obtained from the complex potential around the circle, $F(\zeta)$, from

$$\frac{dF}{dz} = \frac{dF}{d\zeta}\frac{d\zeta}{dz},\tag{2.15}$$

where

$$\frac{dz}{d\zeta} = \frac{(z - nb)(z + nb)}{(\zeta - b)(\zeta + b)}. (2.16)$$

A review of the potential flow around a circle with circulation is presented in Appendix A.2.

2.3 Method of Velocity Singularities

The potential flow analysis of thin aerofoils based on the velocity singularity method, was originally developed by Mateescu and Newman [15,17]. This method was then further extended by Mateescu and Nadeau [18,20] for the nonlinear analysis of aerofoils using polynomial expansions.

2.3.1 Basic Equations and General Considerations for the Velocity Singularity Method

Velocity perturbations imposed by the aerofoil are represented as u in the x direction and v in the y direction (using Cartesian coordinates). These perturbation velocities can be superimposed over the undisturbed velocity U_{∞} because u and v are harmonic functions

satisfying Laplace's equation

$$V_x = \vec{U}_{\infty} \cdot \vec{i} + u, \qquad (2.17)$$

$$V_y = \vec{U}_{\infty} \cdot \vec{j} + v. \tag{2.18}$$

The perturbation velocity components, u and v, in an incompressible irrotational flow must satisfy

$$\frac{\partial v}{\partial x} = \frac{\partial u}{\partial y},\tag{2.19}$$

$$\frac{\partial u}{\partial x} = -\frac{\partial v}{\partial y}. (2.20)$$

The boundary conditions on the aerofoil will be expressed using a complex function W(z) defined in the form

$$W(z) = u(x, y) - i[v(x, y) - v_o], \qquad (2.21)$$

where z = x + iy, x and y are coordinates of the physical plane where the aerofoil lies, and v_o is a conveniently chosen constant, which will be determined later.

2.3.2 Thin Aerofoil Solutions

This complex potential will be first analyzed by a simple flapped plate aerofoil at an incidence α (as seen in Figure 2.1). The analysis for this geometry was originally developed by Mateescu and Newman, by considering the singular behaviour of the perturbation velocities at the leading edge and at the ridge R at x = s. Using thin aerofoil theory, the boundary conditions on the aerofoil surface (transferred to the chordline) are expressed by using the complex conjugate perturbation function in the form

Imag[W(x)] =
$$(v_o - v) = \begin{cases} 0 & \text{for } 0 < x < s, \\ -\Delta v & \text{for } s < x < c, \end{cases}$$
 (2.22)

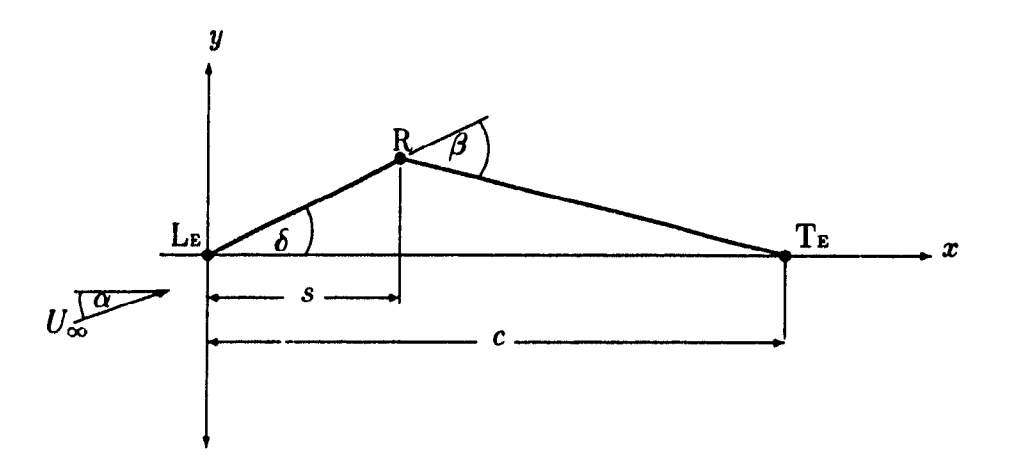


Figure 2.1: Simple flapped plate

where

$$\Delta v = U_{\infty} \cos \alpha [\tan (\delta - \beta) - \tan \delta] \approx -\beta U_{\infty}. \tag{2.23}$$

The perturbation velocities are assumed to be small, becoming negligible at large distances from the aerofoil when compared to the oncoming flow U_{∞} :

$$W(z)_{z\to\infty} = iv_o. (2.24)$$

In thin aerofoil theory perturbation velocities are assumed to have the same magnitude on the top, as well as on the bottom of the aerofoil. On a thin cambered aerofoil, the perturbation velocity u creates a discontinuity leading to an antisymmetrical flow with respect to the x axis:

$$u(x)_{top} = -u(x)_{bottom}, (2.25)$$

$$v(x)_{top} = v(x)_{bottom}. (2.26)$$

Ahead and behind of the aerofoil the perturbation velocity u on the aerofoil axis (y = 0) is zero. This also satisfies the Kutta condition and accounts for the antisymmetrical nature of the flow, and it can be expressed using the complex conjugate velocity function

in the form

$$Real[W(x)]_{y=0} = 0; \text{ for } x < 0, \ x > c.$$
 (2.27)

The assumed constant v_o can now be determined as

$$v_o = [-\sin\alpha + \cos\alpha \tan\delta]U_\infty \approx (-\alpha + \delta)U_\infty.$$
 (2.28)

The function W(z) is now mapped from the physical z plane to an auxillary ζ plane using a Schwartz-Christoffel type conformal transformation (noting that the velocity components do not change under this transformation):

$$\zeta^2 = \frac{z}{c-z}$$
, where $\zeta = \xi + i\eta$. (2.29)

Now the boundary conditions in the auxillary plane become:

Imag[
$$W(\zeta)$$
] _{$\eta=0$} =
$$\begin{cases} 0 & \text{for } -\sigma < \xi < \sigma \\ -\Delta v & \text{for } \xi < -\sigma, \ \xi > \sigma \end{cases}$$
 (2.30)

$$\operatorname{Real}[W(\zeta)]_{\xi=0} = 0, \tag{2.31}$$

where
$$\sigma = \sqrt{\frac{s}{c-s}}$$
. (2.32)

Discontinuities in the imaginary parts of $W(\zeta)$ at $\zeta = \sigma$ and $\zeta = -\sigma$ can be represented by the logarithmic singularities:

$$[W(\zeta)]_{\zeta \to \sigma} = \frac{\Delta v}{\pi} \ln(\zeta - \sigma), \qquad (2.33)$$

$$[W(\zeta)]_{\zeta \to -\sigma} = -\frac{\Delta v}{\pi} \ln(\zeta + \sigma). \tag{2.34}$$

The real part of $W(\zeta)$ presents a singularity at the leading edge which becomes a doublet corresponding to the sudden change of fluid flow:

$$[W(\zeta)]_{\zeta \to 0} = \frac{A}{\zeta},\tag{2.35}$$

where A is the doublet intensity. The singularity at the ridge can be represented by:

$$[W(\zeta)]_{\zeta \to \pm \sigma} = \pm \frac{\Delta v}{\pi} \left[\ln \left(\frac{\zeta - \sigma}{\zeta + \sigma} \right) - i \pi \right]. \tag{2.36}$$

By superposition (Laplace's equation is satisfied), the solution for $W(\zeta)$ is

$$W(\zeta) = \frac{A}{\zeta} + \frac{\Delta v}{\pi} \left[\ln \left(\frac{\zeta - \sigma}{\zeta + \sigma} \right) - i \pi \right], \tag{2.37}$$

where A is a constant. Transforming this equation back into the physical z plane, one obtains

$$W(z) = A\sqrt{\frac{c-z}{z}} - \frac{2}{\pi}\Delta v \cosh^{-1}\sqrt{\frac{(c-z)s}{c(s-z)}}.$$
 (2.38)

The constant A can now be determined by using equations 2.24, and 2.38:

$$A = -\left[v_o + \frac{2}{\pi}\Delta v \cos^{-1}\sqrt{\frac{s}{c}}\right]. \tag{2.39}$$

On the upper surface of the aerofoil (y = 0 and z = x), the chordwise perturbation velocity is

$$u_A(x) = \text{Real}[W(z)] = A\sqrt{\frac{c-x}{x}} - \frac{2}{\pi}\Delta v \cdot G(c, s, x), \qquad (2.40)$$

where the subscript A denotes the antisymmetrical nature and the singular ridge function G(c, s, x) is defined as

$$G(c, s, x) = \begin{cases} \cosh^{-1} \sqrt{\frac{s(c-x)}{c(s-x)}} & \text{for } 0 < x < s \\ \sinh^{-1} \sqrt{\frac{(c-x)s}{c(x-s)}} & \text{for } s < x < c \\ 0 & \text{for } x < 0, \ x > c. \end{cases}$$
 (2.41)

The first term of $u_A(x)$ represents the leading edge singularity and the second term represents the ridge singularity; the Kutta condition at the trailing edge is satisfied by both terms.

For a continuously cambered thin aerofoil (Figure 3.1), the solution can be obtained by considering a continuous distribution of elementary ridges. Using equation (3.14), the chordwise perturbation velocity is obtained in the form

$$u_{A}(x) = \left\{-v(0) - \frac{2}{\pi} \int_{0}^{c} \left(\frac{dv_{A}}{dx}\right)_{x=s} \cos^{-1} \sqrt{\frac{s}{c}} ds\right\} \sqrt{\frac{c-x}{x}}$$
$$-\frac{2}{\pi} \int_{0}^{c} \left(\frac{dv_{A}}{dx}\right)_{x=s} \cosh^{-1} \sqrt{\frac{s(c-x)}{c(s-x)}} ds, \tag{2.42}$$

where the normal-to-chord velocity component on the aerofoil is defined by

$$v_A(x) = [-\alpha + h'(x)] U_{\infty},$$
 (2.43)

in which h'(x) represents the slope fo the camberline (Figure 3.1). After integration by parts, equation (2.42) becomes

$$u_A(x) = -\frac{1}{\pi} \sqrt{\frac{c-x}{x}} \int_0^c v(s) \sqrt{\frac{s}{c-s}} \frac{ds}{s-x}.$$
 (2.44)

Details about this integration can be found in Appendix B.1.

2.3.3 Aerofoils of Symmetrical Thickness

A diamond shaped aerofoil is first considered at zero incidence. This gives a simple symmetrical aerofoil to analyze. The complex conjugate velocity for symmetrical cases is solved for in the same manner as the antisymmetrical cases, by investigating the singularities at the leading edge (x = 0), ridge R (x = s), and trailing edge (x = c). On a symmetrical aerofoil, the perturbation velocities can be defined on the top and bottom surfaces as:

$$u(x)_{top} = u(x)_{bottom}, (2.45)$$

$$v(x)_{top} = -v(x)_{bottom}. (2.46)$$

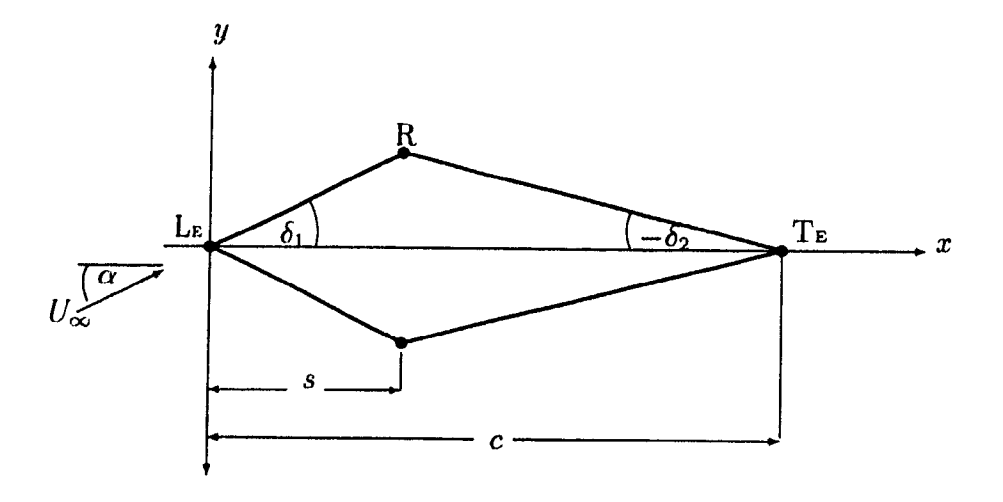


Figure 2.2: Double wedge aerofoil

This signifies the fact that there is no circulation around the aerofoil at zero incidence (i.e. $\Gamma = 0$). Using the regular assumptions of small aerofoil thickness, the boundary conditions can be expressed in the form

$$\operatorname{Imag}[W(z)_{z=x}] = \begin{cases} -v_1 & \text{for } 0 < x < s \\ -v_2 & \text{for } s < x < c \\ 0 & \text{for } x < 0, \ x > c, \end{cases}$$
 (2.47)

where the constant v_o is set to zero in equation (2.21), while $v_1 = U_\infty \tan \delta_1$ and $v_2 = -U_\infty \tan \delta_2$ are the normal-to-chord velocities on the first and second panels of the upper surface of the aerofoil. Using this, the complex conjugate velocity is expressed in the form

$$W(z) = \frac{1}{\pi} \left[v_1 \ln(z) + \Delta v \ln(z - s) - v_2 \ln(z - c) \right], \qquad (2.48)$$

where $\Delta v = v_2 - v_1$.

For an aerofoil with a continuously variable camber, g(x), the chordwise perturbation velocity can be obtained in the form (by considering a continuous distribution of elementary ridges):

$$u_S(x) = \frac{1}{\pi} \left\{ v_S(0) \ln z + \int_0^c \left(\frac{dv_S}{dx} \right)_{x=s} \ln (z - s) ds - v_S(c) \ln (z - c) \right\}, \tag{2.49}$$

where the normal-to-chord velocity on the aerofoil is defined by

$$v_S(x) = g'(x)U_{\infty},\tag{2.50}$$

in which g'(x) represents the slope of the aerofoil contour (Figure 3.1). Here the subscript S denotes the symmetrical nature of the velocity field. After integration (which can be found in Appendix B.2.1), one obtains

$$u_S(x) = \frac{1}{\pi} \int_0^c v_S(x) \frac{ds}{s - x}.$$
 (2.51)

This pure linear solution may be sufficiently accurate for the most part of the chord, except the aerofoil extremities where it predicts an infinite velocity at the leading edge, instead of a stagnation point which really exists. The correct flow behaviour at the leading and trailing edges is better predicted by the local linearization method (Mateescu [10,15]) or by using a non-linear approach (Mateescu and Nadeau [15]).

2.3.4 Local Linearization Solution

For symmetrical aerofoils with rounded leading edges at zero incidence, it was found that the purely linear solution defined in Section 2.3.3 was not giving very good results, especially near the leading edge. For these aerofoils, a local linearization approach [13,18,20] had to be used instead, in order to obtain a better accuracy of the solution. This method uses the tangential free stream velocity

$$U_{\infty_{\mathbf{t}}} = U_{\infty} \cos \tau, \tag{2.52}$$

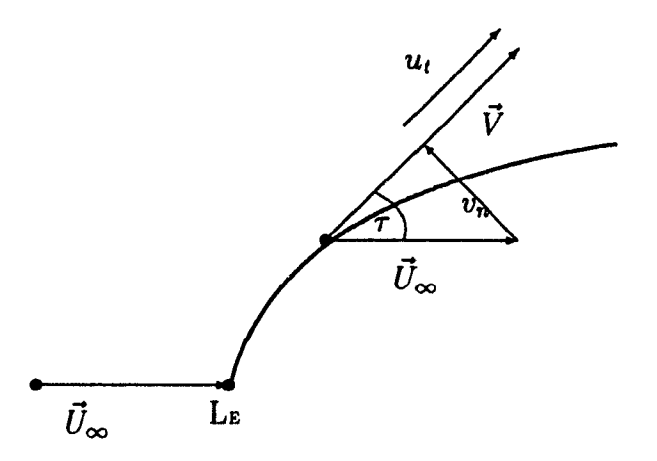


Figure 2.3: Normal and tangential perturbation components on a rounded leading edged aerofoil

where U_{∞_t} is used to normalize the tangential and normal components of the perturbation velocity u_t and v_n [18]. The associated normal perturbation component v_n is referred as g'(x) the camberline coefficient:

$$\frac{v_n}{U_{\infty_t}} = \frac{U_{\infty} \sin \tau}{U_{\infty_t}}. (2.53)$$

This equation acts as a boundary condition on the aerofoil where the large slopes of the rounded-leading-edge can be modelled by

$$\frac{v_n}{U_{\infty_t}} = g'(x)\sqrt{\frac{x}{c-x}}. (2.54)$$

This equation positions the stagnation point at the leading edge of the aerofoil and the Kutta condition is satisfied by the small slope at the trailing edge. Once the normal component is found the tangential component can be expressed as

$$\frac{u_t}{U_{\infty_t}} = \frac{V - U_{\infty_t}}{U_{\infty_t}}. (2.55)$$

This method of solution found very accurate results even for thicker aerofoils (which shows the stability of the solution).

Chapter 3

A Spline Formulation for the

Method of Velocity Singularities

The method of velocity singularities was first developed in conjunction with a polynomial representation of the aerofoil contour. This may lead in some cases to high-order polynomials with large coefficients which may affect the accuracy of the solution. The present method uses instead, a cubic spline formulation to represent the geometry of the aerofoil contour.

3.1 General Considerations for Spline Formulation

In this analysis, the method of velocity singularities is developed in conjunction with a cubic spline representation of the aerofoil contour.

To begin, the chordline c will be set to unity, and x will now be thought of as $\frac{x}{c}$, which

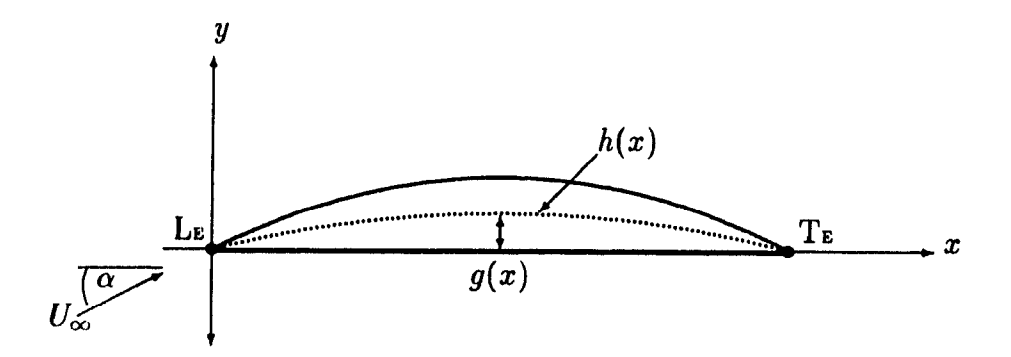


Figure 3.1: Camberline coefficients for crescent shaped aerofoils

is simply converted to x. Using these notations, the boundary conditions are applied as

$$v_A(x) = U_{\infty}[-\alpha + h'(x)], \qquad (3.1)$$

$$v_S(x) = U_{\infty}g'(x), \tag{3.2}$$

where h'(x) and g'(x) are derivatives of the camberline contour and the aerofoil thickness; h(x) and g(x) are defined as

$$h(x) = \frac{1}{2} [y_u + y_l], \qquad (3.3)$$

$$g(x) = \frac{1}{2} [y_u - y_l], \qquad (3.4)$$

where y_u represents the upper surface of the aerofoil, and y_l the lower surface. It becomes clear that by these equations g(x) = 0 for a circular arc (where only antisymmetrical velocities are found) and h(x) = 0 for a symmetrical aerofoil (where only symmetrical velocities are found). Approximating the camberline coefficients by a cubic spline, any function $f_i(x)$, such as $v_A(x)$, $v_S(x)$ or h(x), g'(x), can be expressed on the interval $x_{i-1} < x < x_i$ in the form:

$$f_i(x) = A_i + B_i(x - x_{i-1}) + C_i(x - x_{i-1})^2 + D_i(x - x_{i-1})^3, \tag{3.5}$$

or, in the more formal manner,

$$f_i(x) = \sum_{k=0}^{3} F_k^i(x - x_{i-1})^k.$$
 (3.6)

The cubic spline becomes a function of cubic order between two points x_{i-1} and x_i . Many boundary conditions can be used to formulate a cubic spline equation, two different types of splines are derived in Appendix C. The most important condition in the spline is the requirement of the slopes being equal at the interface between two consecutive intervals:

$$f_i'(x_i) = f_{i+1}'(x_i). (3.7)$$

Using this type of condition ensures that the series of splines will fit smoothly through the data points.

Once the velocities are found on the surface of the aerofoil, pressure coefficients can also be found. On aerofoils with just one type of velocity this can be easily done by finding the total velocity and using the well known pressure equation as defined by equation (2.10), which can be applied for both the top and bottom of the aerofoil surface. If the aerofoil has both antisymmetrical velocities and symmetrical velocities, pressure coefficients can be found by:

$$C_{P_u}(x) = 1 - \left[\cos\alpha + \frac{u_A(x)}{U_\infty} + \frac{u_S(x)}{U_\infty}\right]^2 - \left[\sin\alpha + \frac{v_A(x)}{U_\infty} + \frac{v_S(x)}{U_\infty}\right]^2$$
 (3.8)

$$C_{P_l}(x) = 1 - \left[\cos\alpha - \frac{u_A(x)}{U_\infty} + \frac{u_S(x)}{U_\infty}\right]^2 - \left[\sin\alpha + \frac{v_A(x)}{U_\infty} - \frac{v_S(x)}{U_\infty}\right]^2$$
 (3.9)

where the upper pressure coefficient is denoted by $C_{P_u}(x)$ and the lower by $C_{P_l}(x)$. To find the difference of pressures across the aerofoil:

$$\Delta C_P(x) = C_{P_u}(x) - C_{P_u}(x). \tag{3.10}$$

Knowing the pressure difference allows one to find many other aerodynamic characteristics such as lift and moments about the leading edge:

$$C_L = \int_0^c \Delta C_P(x) dx, \qquad (3.11)$$

$$C_{M_{L_E}} = \int_0^c \Delta C_P(x) x \, dx. \tag{3.12}$$

3.1.1 Spline Formulation for Thin Aerofoils

Antisymmetrical perturbation velocities are a resultant of thin cambered aerofoils. Using the cubic spline of equation (3.6) the aerofoil boundary conditions can be expressed as

$$v_A(x) = U_{\infty}[-\alpha + \sum_{k=0}^{3} H_k^i (x - x_{i-1})^k], \qquad (3.13)$$

where H_i represents the spline coefficients as described in Appendix C. After the antisymmetrical velocities are applied to the complex conjugate velocity W(x):

$$\frac{u_A(x)}{U_{\infty}} = \sqrt{\frac{(1-x)}{x}} \left(\alpha - \frac{1}{\pi} \sum_{i=1}^{N} \sum_{k=0}^{3} H_k^i K_k^i(x) \right), \tag{3.14}$$

$$K_k^i(x) = \sum_{q=0}^k C_k^q x_{i-1}^q \left\{ \sum_{l=0}^{k-q} x^l \Lambda_{k-q-l} + \lambda_{k-q} \right\}, \tag{3.15}$$

where:
$$\lambda_p = \frac{-2x^{p+1}}{\sqrt{x(1-x)}} \begin{cases} \cosh^{-1}\sqrt{\frac{s(1-x)}{s-x}} & \text{for } s > x \\ \sinh^{-1}\sqrt{\frac{s(1-x)}{x-s}} & \text{for } x > s, \end{cases}$$
 (3.16)

$$\Lambda_p = \int_{x_{i-1}}^{x_i} \frac{s^p ds}{\sqrt{s(1-s)}}. (3.17)$$

The integration for Λ_p results in:

•
$$p = 0$$

$$\Lambda_0 = \int_{x_{i-1}}^{x_i} \frac{ds}{\sqrt{s(1-s)}} = \left[\cos^{-1}(1-2s)\right]_{x_{i-1}}^{x_i}.$$

• p = 1

$$\Lambda_1 = \int_{x_{i-1}}^{x_i} \frac{sds}{\sqrt{s(1-s)}} = \left[\frac{1}{2}\cos^{-1}\left(1-2s\right) - \sqrt{s(1-s)}\right]_{x_{i-1}}^{x_i}.$$

• p = 2

$$\Lambda_2 = \int_{x_{i-1}}^{x_i} \frac{s^2 ds}{\sqrt{s(1-s)}} = \left[\frac{3}{8} \cos^{-1} \left(1 - 2s \right) - \left(\frac{s}{2} + \frac{3}{4} \right) \sqrt{s(1-s)} \right]_{x_{i-1}}^{x_i}.$$

• p = 3

$$\Lambda_3 = \int_{x_{i-1}}^{x_i} \frac{s^3 ds}{\sqrt{s(1-s)}} = \left[\frac{5}{16} \cos^{-1} (1-2s) - \left(\frac{s^2}{3} + \frac{5s}{12} + \frac{5}{8} \right) \sqrt{s(1-s)} \right]_{x_{i-1}}^{x_i}.$$

The constant C_k^q represents the coefficients of the binomial expansion $(x-x_{i-1})^k$ [i.e. $C_k^q = (-1)^q \frac{k!}{q!(k-q)}$]. The integration and algebra to find these velocities can be found in Appendix B.

3.1.2 Spline Formulation for Aerofoils of Symmetrical Thickness

For aerofoils of symmetrical thickness the perturbation velocities are treated differently than thin cambered aerofoils. Using the spline formulation of equation (3.6) with the linear theory described by equation (3.2)

$$v_S(x) = U_{\infty} \sum_{k=0}^{3} G_k^i (x - x_{i-1})^k.$$
 (3.18)

Again the spline coefficients G_k^i are described in Appendix C. Once the spline formulation is applied to the complex conjugate velocity W(x):

$$\frac{u_S(x)}{U_\infty} = -\frac{1}{\pi} \sum_{i=1}^N \sum_{k=0}^3 G_k^i J_k^i(x), \tag{3.19}$$

$$J_k^i(x) = \sum_{q=0}^k C_k^q x_{i-1}^q \left\{ \sum_{l=0}^{k-q-1} \frac{x^l}{k-l-q} (x_i^{k-l-q} - x_{i-1}^{k-l-q}) + x^{k-q} \ln \left| \frac{x_i - x}{x_{i-1} - x} \right| \right\}$$
(3.20)

The constant C_k^q is the same as previously expressed and the integration and algebra can be found in Appendix B.

3.1.3 Spline Formulation for Aerofoils Using Local Linearization

For rounded leading edged aerofoils of symmetrical thickness at zero incidence the normal method of calculating symmetrical velocities did not account for the stagnation point at the leading edge. This can be overcome by using local linearization techniques with the spline formulation:

$$\frac{v_n}{U_\infty} = g'(x)\sqrt{\frac{x}{1-x}} = \sum_{k=0}^3 G_k^i (x - x_{i-1})^k,$$
 (3.21)

where the factor $\sqrt{\frac{x}{1-x}}$ creates a stagnation point at the leading edge. The Kutta condition is also satisfied with the low values of g'(x) at the trailing edge, which also cancels out the infinite values predicted by the zero denominator in $\sqrt{\frac{x}{1-x}}$. Finding the tangential perturbation component was found through the integration:

$$\frac{u_t}{U_{\infty}} = -\frac{1}{\pi} \sum_{i=1}^{N} \sum_{k=0}^{3} G_k^i \int_{x_{i-1}}^{x_i} \sqrt{\frac{1-s}{s}} (s-x_i)^k \frac{ds}{s-x}, \tag{3.22}$$

where the integral is represented by $J_{M_k}^i(x)$

$$\frac{u_t}{U_{\infty}} = -\frac{1}{\pi} \sum_{i=1}^{N} \sum_{k=0}^{3} G_k^i J_{M_k}^i(x). \tag{3.23}$$

This integration is performed in Appendix B, where the end result is:

$$J_{M_k}^{i}(x) = \sum_{q=0}^{k} C_q^k x_{i-1}^q \left\{ (1-x) \left(\sum_{l=0}^{k-q-1} x^l \Lambda_{k-q-l-1} - \frac{\lambda_{k-q}}{x} \right) - \Lambda_{k-q} \right\}, \tag{3.24}$$

 λ_p and Λ_p are the same as described in Section 3.1.1. The surface pressure coefficients can be expressed as:

$$C_P = 1 - \left(\cos\tau + \frac{u_t}{U_\infty}\right)^2 \tag{3.25}$$

$$= 1 - \frac{(1+u_t)^2}{1+g'(x)^2}. (3.26)$$

Using this equation the stagnation point at the leading edge is automatically satisfied.

3.2 Applications of the Spline Formulation for Aerofoils of Fixed Geometry

This section focuses on solutions for different types of aerofoils using the velocity singularity method. Comparisons are made on the present spline integration method to the similar polynomial method and the exact method based on conformal transformation. The spline formulation has the advantage of explicitly finding the coefficients (if the spline in Section C.1.2 is used).

3.2.1 Cambered Thin Aerofoils

Aerofoils with pointed leading edges are found on supersonic to transonic airplanes, and propellers (near the tip). Although this method does not pertain to compressible flow situations (as in the above mentioned situations), pressure distributions are still required for incompressible cases (i.e. for take off and landing situations). The method of velocity singularities is especially suitable for aerofoils with pointed leading edges because of the singularity at the leading edge created by the factor $\sqrt{\frac{1-x}{x}}$ in equation (3.14).

To start with, pressure distributions for circular arcs are shown in Figure 3.2. The best solution was found using the cubic spline as defined in Section C.1.2. Although this type of spline gives the highest accuracy it is important that the spline coefficients do not become very large with respect to unity. If this happens, the accuracy of the perturbation velocities decreases greatly and it is a sign that the spline has oscillations, instead of smoothly fitting between the camberline points.

It was found that ten points equally spaced along the chordline (giving 9 different

spline intervals) provided a reasonably good accuracy for the aerofoils with pointed leading edges. In Figure 3.2 the spline solution is in very close agreement with that of the polynomial method derived by Mateescu and Newman [17]. The relative difference between the two methods is within an order of six digits (10^{-6}) . The difference between the velocity singularity method compared to conformal transformation is within 3% error, except at the leading edge where it is larger. The method gives good accuracy even at higher angles of attack ($\alpha = 20^{\circ}$); however, in real flow situations at high angles of incidence, a flow separation would occur, which is not considered in this analysis. The next graph (Figure 3.3) shows how the accuracy is decreasing, compared to the exact solution, when the aerofoil camber increases. However an aerofoil of such camber magnitude is not very common. Only few low speed applications such as a STOL aircraft, flapped aerofoil (which would need to be treated differently) or a flexible membrane, such as a sail, would need such a high camber ratio.

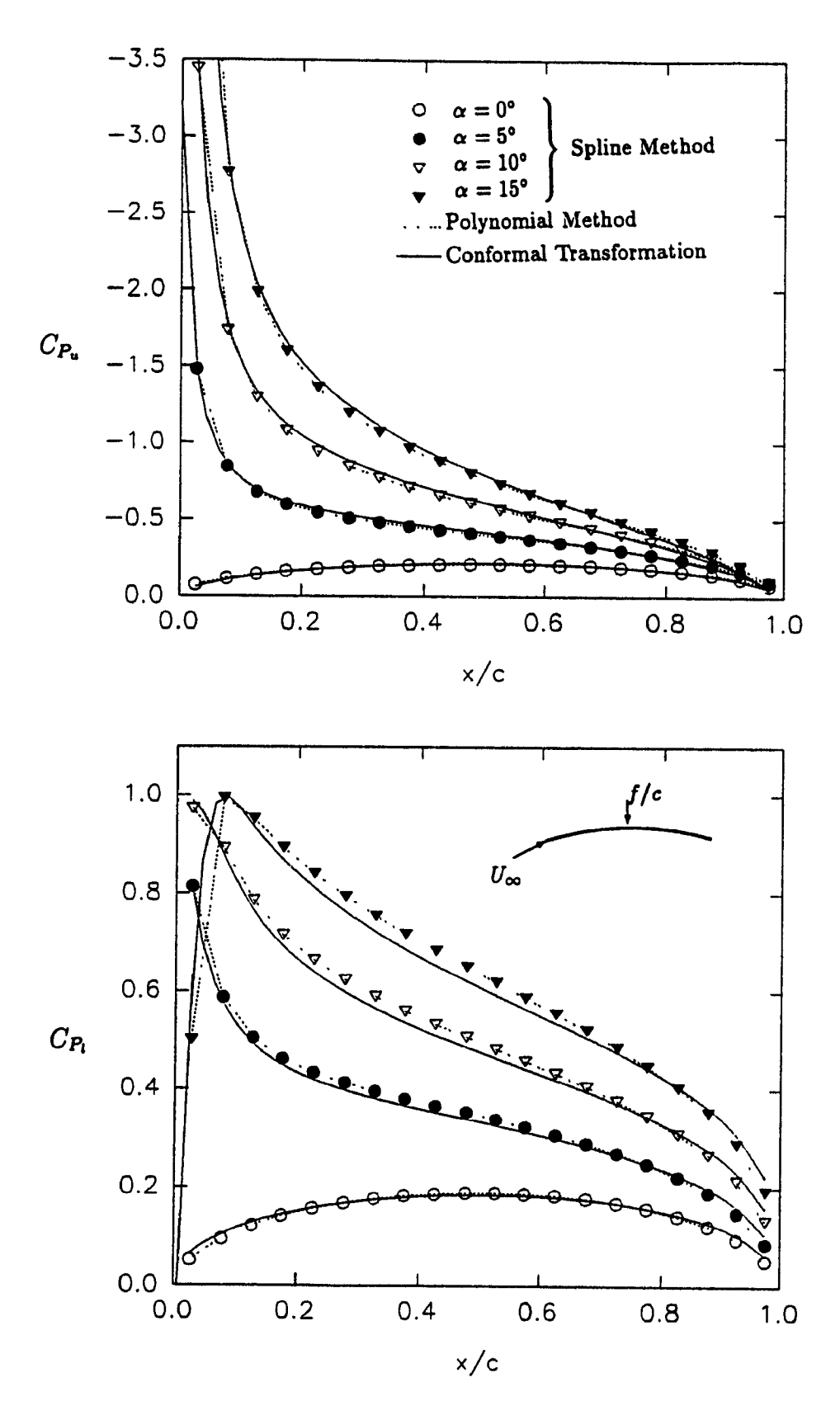


Figure 3.2: Pressure coefficients for circular arc aerofoil f/c=0.025 at various angles of attack.

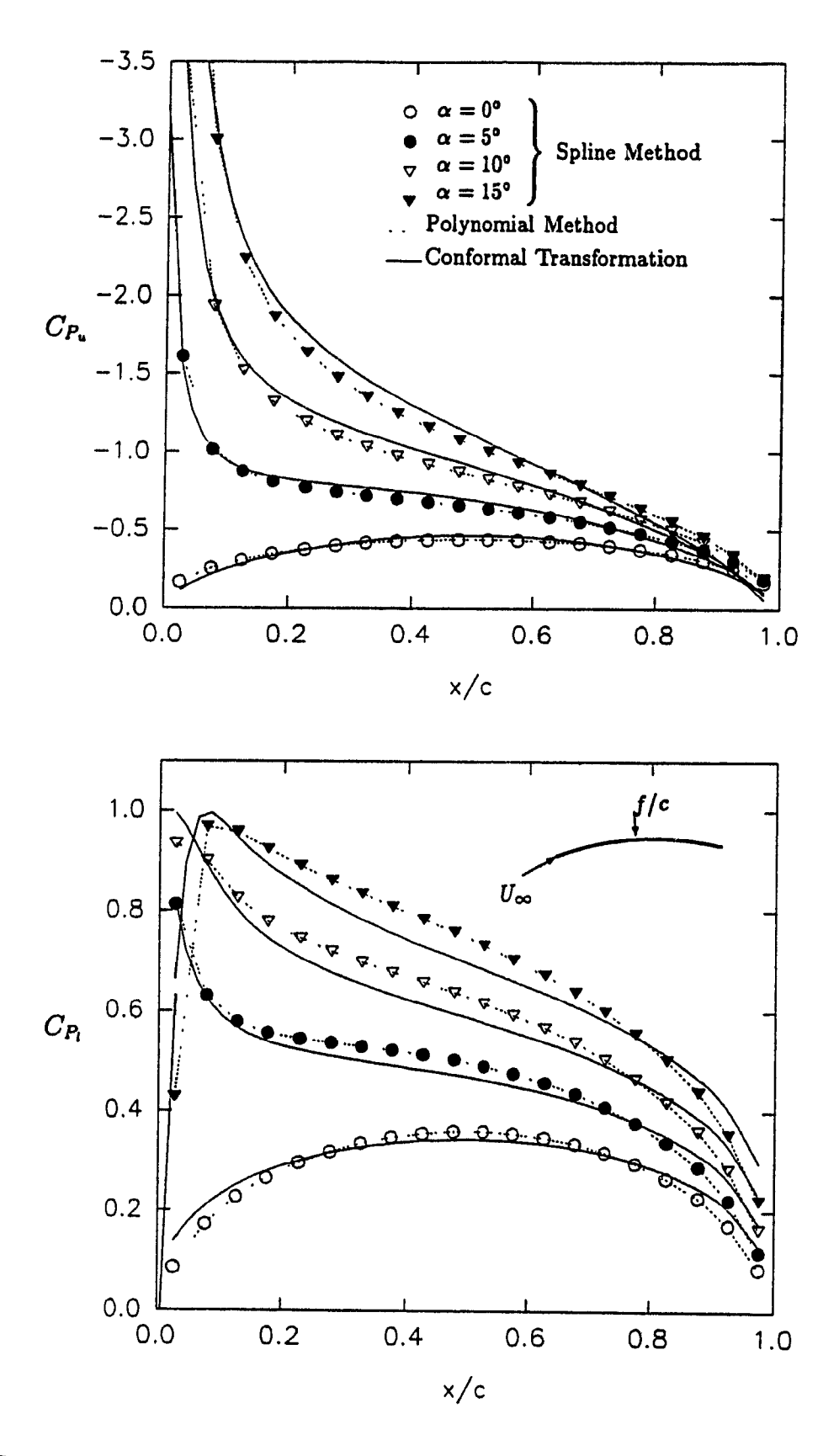


Figure 3.3: Pressure coefficients for circular arc aerofoil f/c=0.05 at various angles of attack.

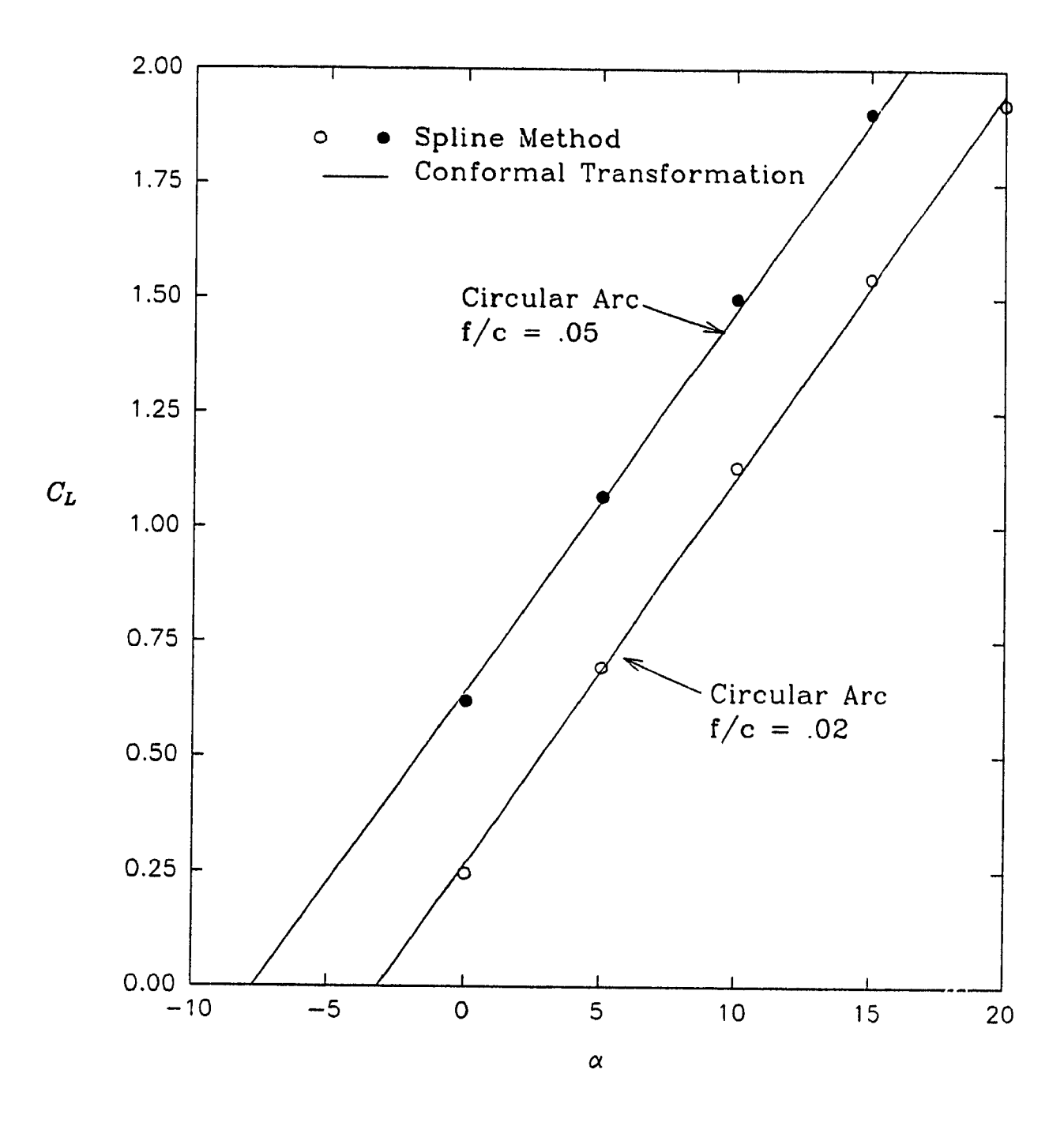


Figure 3.4: Lift coefficients for circular arcs with f/c = 0.02, and f/c = 0.05.

3.2.2 Aerofoils With Pointed Leading Edges

The pressure coefficient on aerofoils with pointed leading edges was treated in a similar manner, but in this case one has to consider both the solutions for the thin aerofoils and for the aerofoils of symmetrical thickness.

The lenticular aerofoil is the first symmetrical aerofoil which will be studied. This type of aerofoil is usually found on supersonic applications because of the pointed leading edge. These aerofoils usually have quite low thickness ratios ($\approx 2\%$ chord) because of the high speeds under which they operate. The first lenticular aerofoil investigated (Figure 3.5) has a thickness ratio of 5% (i.e. e/c = 0.05). The velocity singularity method gives very good accuracy on this type of aerofoil, except at the vicinity of the leading edge where, the leading edge singularity gives an infinite velocity. The next lenticular aerofoil shown (Figure 3.6) has a thickness ratio of 10% where the increasing thickness starts to deplete the accuracy of the method, but it still gives reasonably good results.

The crescent shaped aerofoil is the combination of a flat plate and a circular arc, symmetrical fore and aft of the mid chord point. Again an aerofoil of this type has supersonic applications under low thickness ratios. Nevertheless this type of aerofoil shows both the antisymmetrical and symmetrical perturbation velocities. This type of aerofoil shows how good the accuracy is on the lower surface. This is due to the flat plate nature of the lower surface which fits the boundary conditions underwhich the method was derived. The upper surface shows how the error increases as the thickness from the flat plate model aerofoil is increased. Figures 3.8 and 3.9 show the pressure distribution for two different crescent shaped aerofoils. The thicker crescent shaped aerofoil becomes to large in thickness and camber for the velocity singularity method to handle accurately.

Figure 3.10 shows a cambered aerofoil with a pointed leading edge. This aerofoil, like the crescent shaped aerofoil uses both the symmetrical and antisymmetrical solutions.

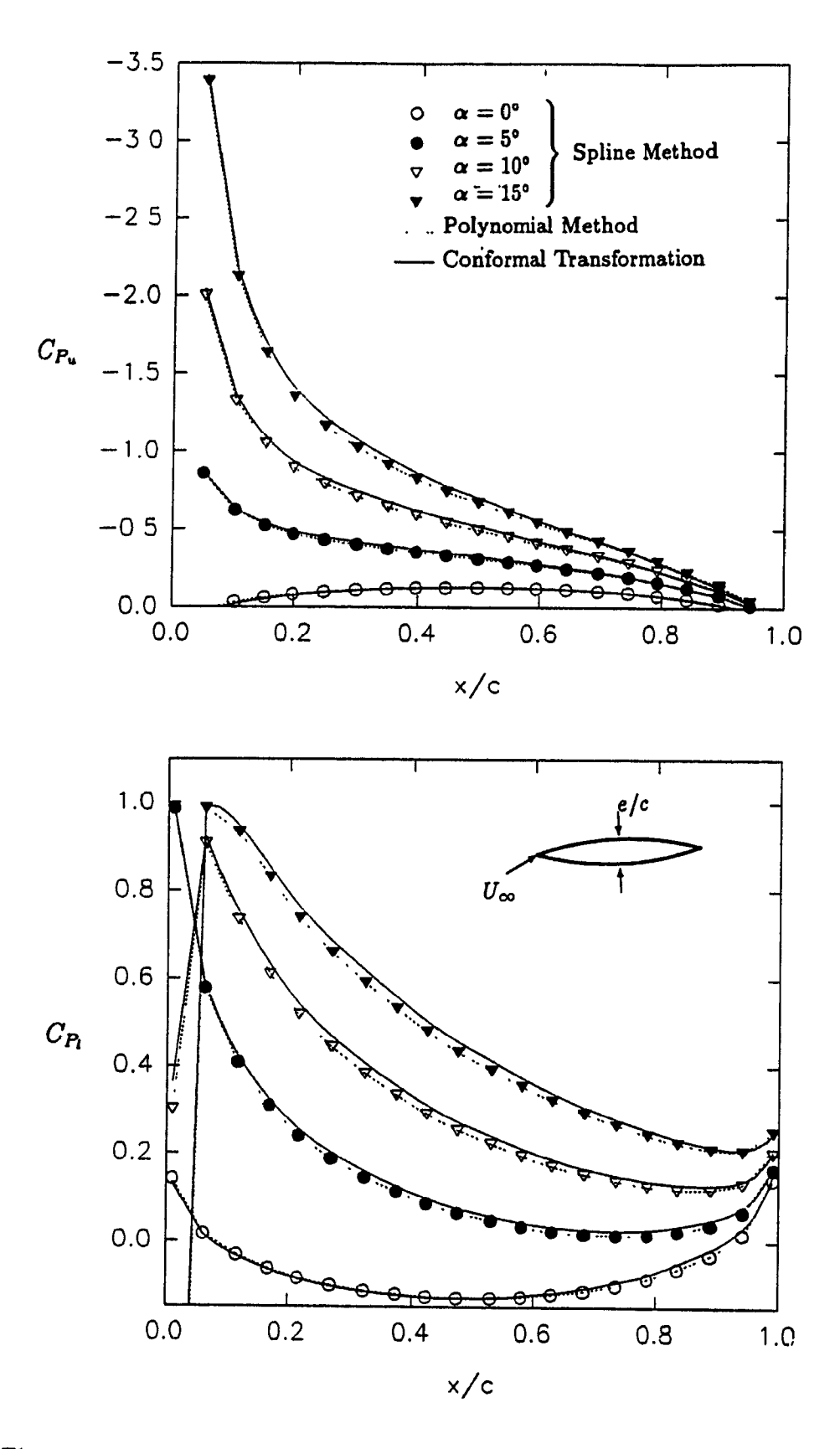


Figure 3.5: Pressure coefficients for symmetrical lenticular aerofoil e/c=0.05 at various angles of attack.

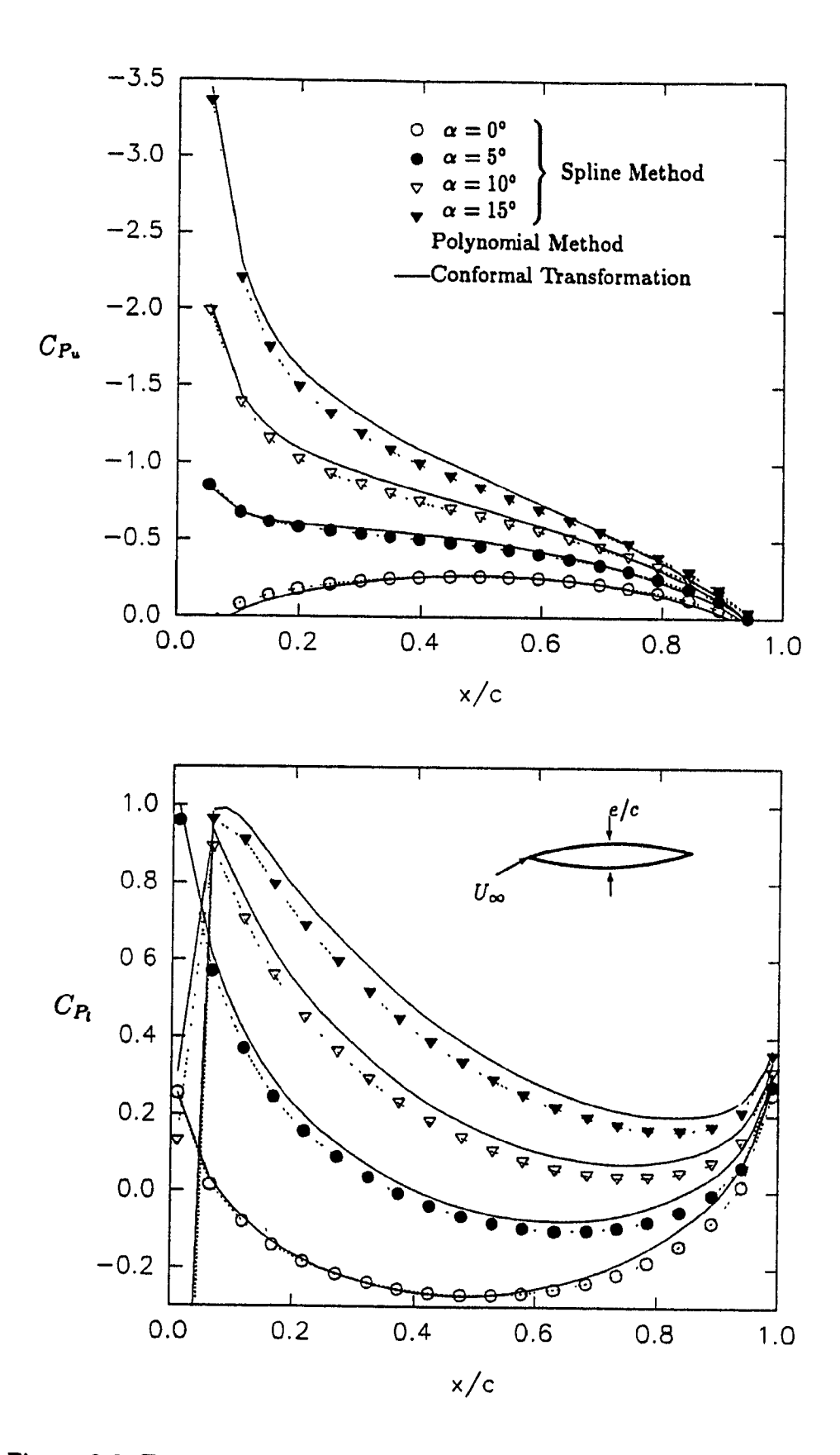


Figure 3.6: Pressure coefficients for symmetrical lenticular aerofoil $\epsilon/c=0.1$ at various angles of attack.

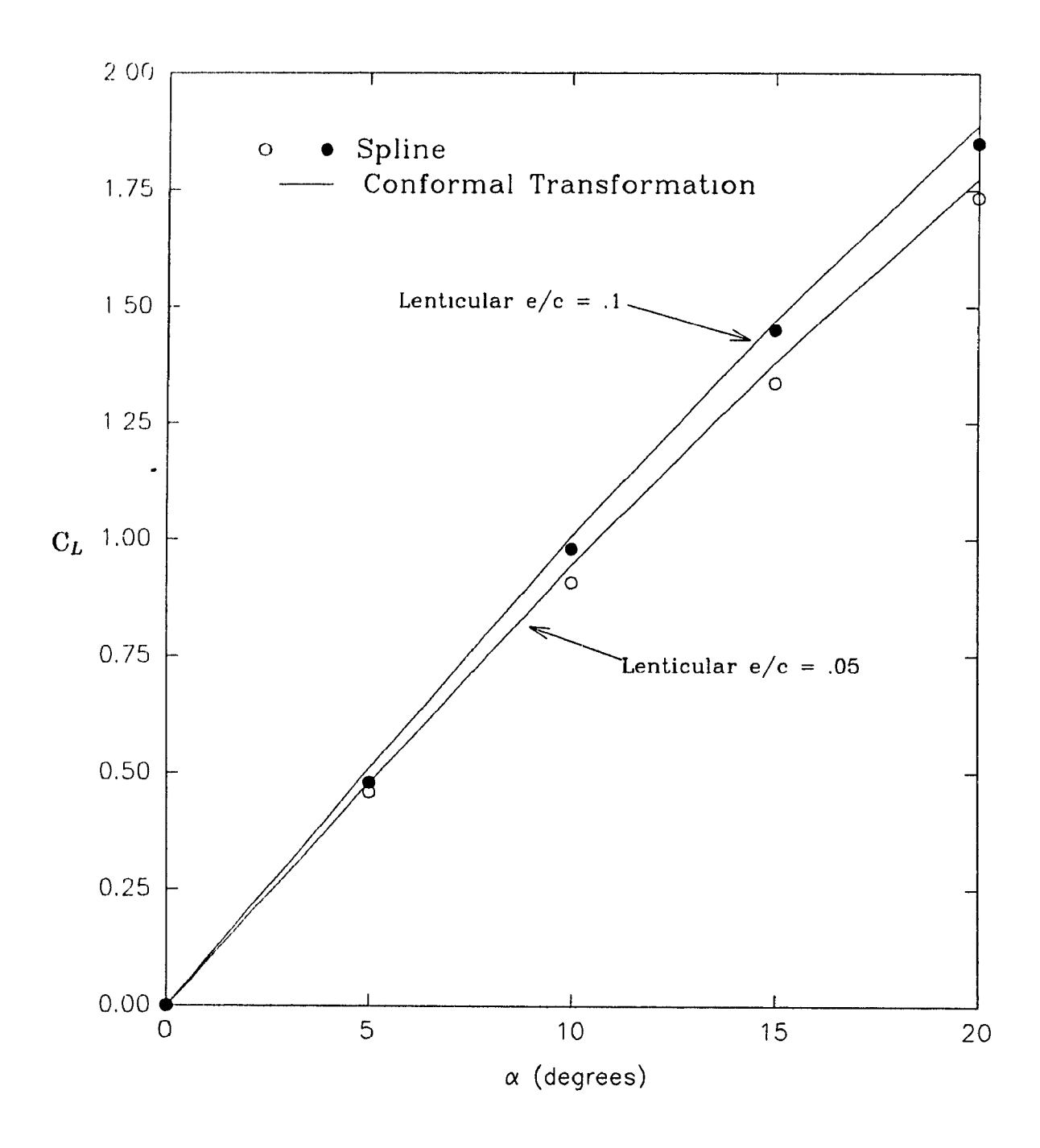


Figure 3.7: Lift Coefficients for symmetrical lenticular aerofoils with e/c=0.05, and e/c=0.1

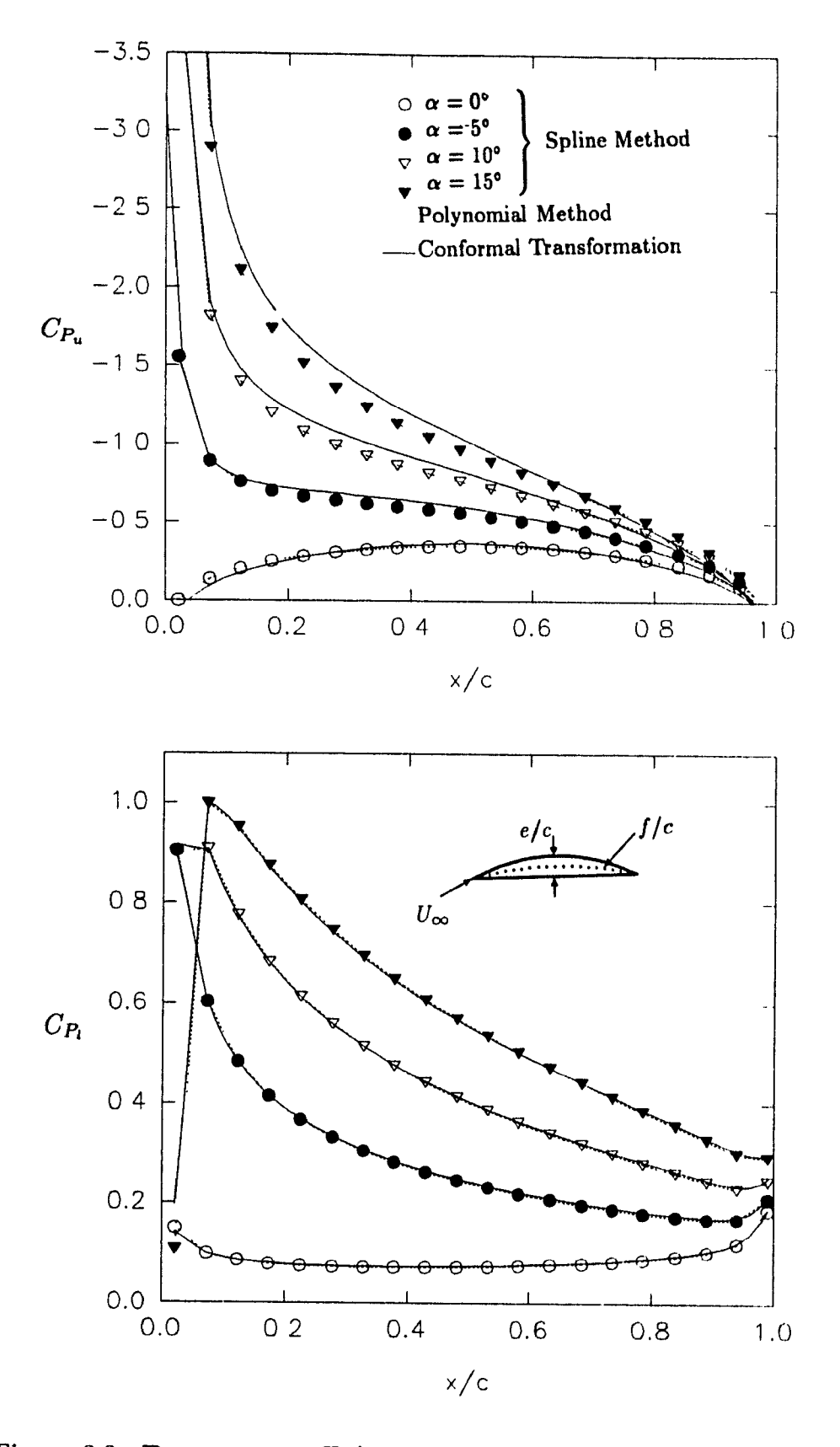


Figure 3.8: Pressure coefficients for crescent shaped aerofoil e/c=0.05 and f/c=0.025 at various angles of attack.

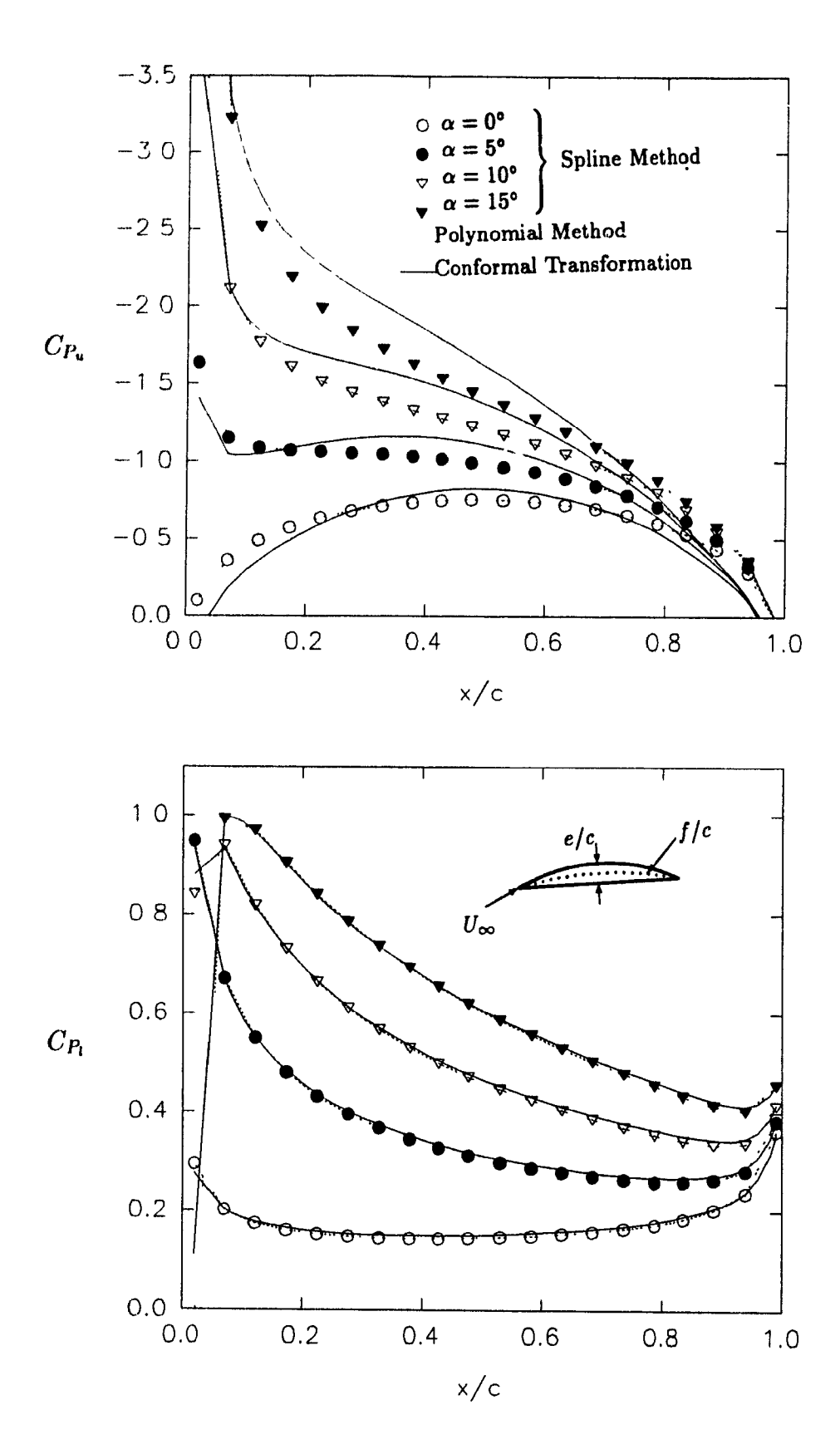


Figure 3.9: Pressure coefficients for crescent shaped aerofoil e/c=0.1 and f/c=0.05 at various angles of attack.

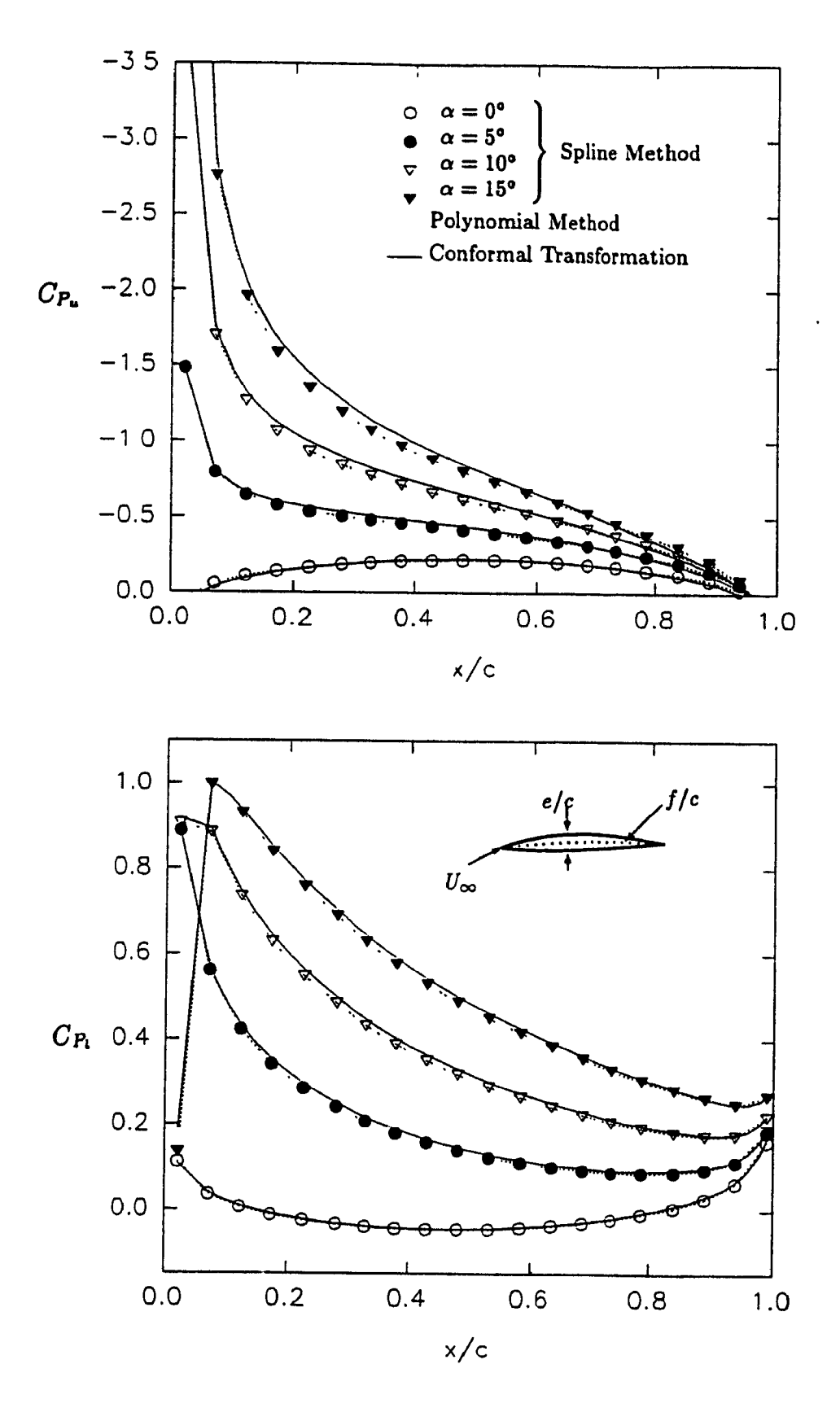


Figure 3.10: Pressure coefficients for cambered lenticular aerofoil e/c=0.05 and f/c=0.01 at various angles of attack.

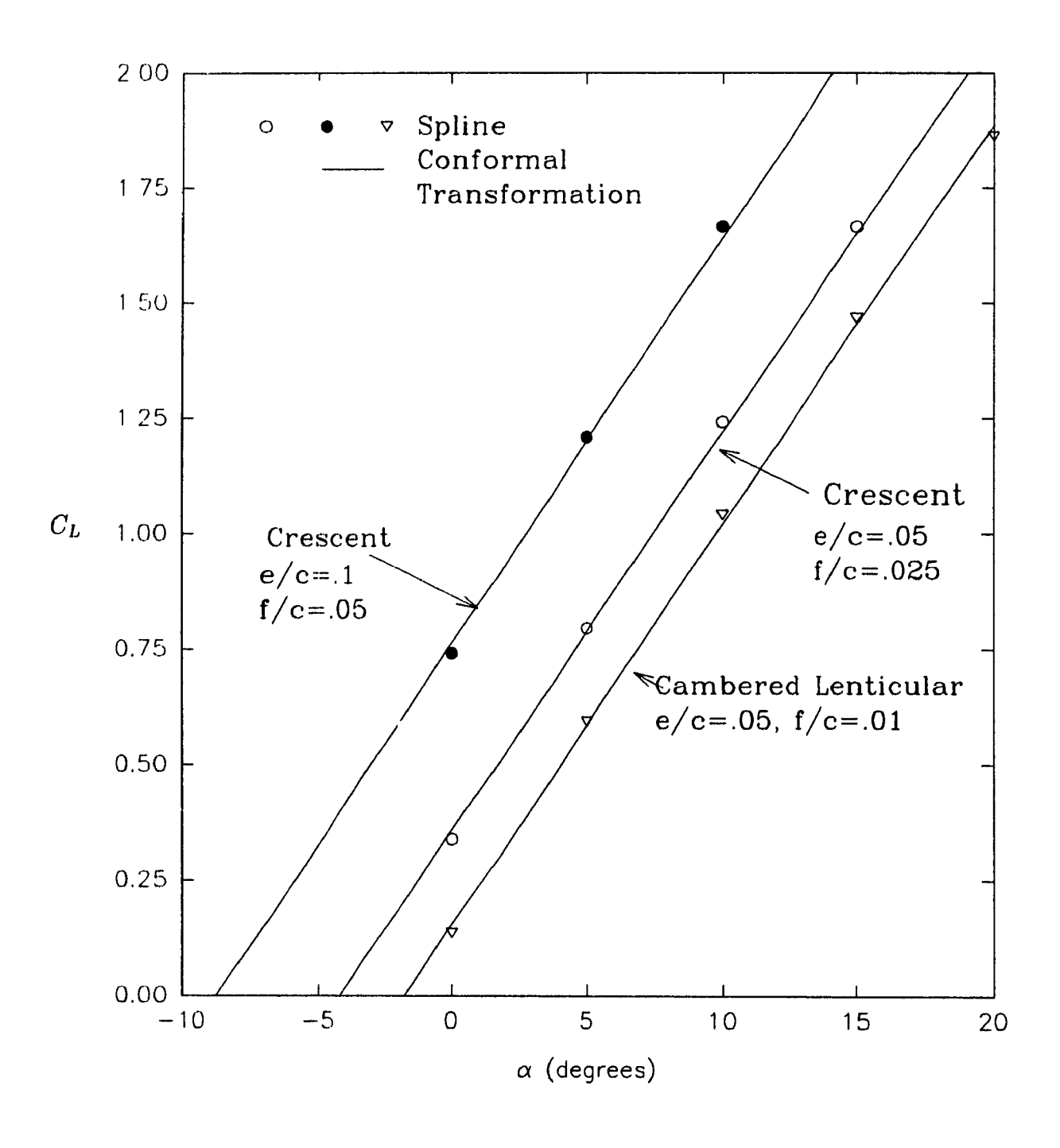


Figure 3.11: Lift coefficients for two crescent shaped and a cambered lenticular aerofoil.

3.2.3 Aerofoils with Rounded Leading Edges

Aerofoils with rounded leading edges are found in the case of subsonic applications. In practice these types of aerofoils usually have higher thickness ratios than that of aerofoils with pointed leading edges.

Joukowski Aerofoils at zero Incidence

The Joukowski aerofoil has the leading edge rounded, and will be used for discussion. This aerofoil also has a cusp at the trailing edge (i.e. $\tau = 0^{\circ}$) which satisfies the Kutta condition. For these types of aerofoil the velocity singularity method must be modified for a zero angle of attack ($\alpha = 0^{\circ}$). The first graph of an aerofoil with a rounded leading edge (Figure 3.12) shows error between the conformal transformation and the present method. This error was overcome by using the modified expansion described in Section 2.3.4 (non-linear spline) which is shown in Figure 3.13. Here the calculations were performed with $x_0 = 0.01$ and $x_N = 0.99$ and the relative error is shown by Table 3.1. If an even smaller value of difference was taken at the leading and trailing edge (such as $x_0 = 0.001$ and $x_N = 0.999$) the error difference was improved slightly which shows how stable this method is. For accurate solutions only seven chordwise points were required.

	Exact	Spline		Polynomial	
x/c	C_{P_u}	$C_{P_{\mathbf{u}}}$	% Error	$C_{P_{\mathbf{u}}}$	% Error
0.0100	-0.0782	-0.0784	+0.24	-0.0781	-0.13
0.1189	-0.2483	-0.2482	-0.04	-0.2482	-0.05
0.2278	-0.2087	-0.2086	-0.05	-0.2085	-0.06
0.3367	-0.1633	-0.1632	-0.06	-0.1632	-0.07
0.4456	-0.1179	-0.1178	-0.09	-0.1177	-0.10
0.5544	-0.0734	-0.0733	-0.13	-0.0733	-0.15
0.6633	-0.0304	-0.0303	-0.29	-0.0303	-0.36
0.7722	0.0112	0.0112	+0.21	0.0113	+0.96
0.8811	0.0511	0.0516	+0.86	0.0512	+0.21
0.9900	0.0895	0.0896	+0.08	0.0896	+0.12

Table 3.1: Accuracy of the present spline-velocity singularity method and polynomial method in comparison with the conformal transformation method for a symmetrical Joukowski aerofoil (e/c = 0.05, α = 0°).

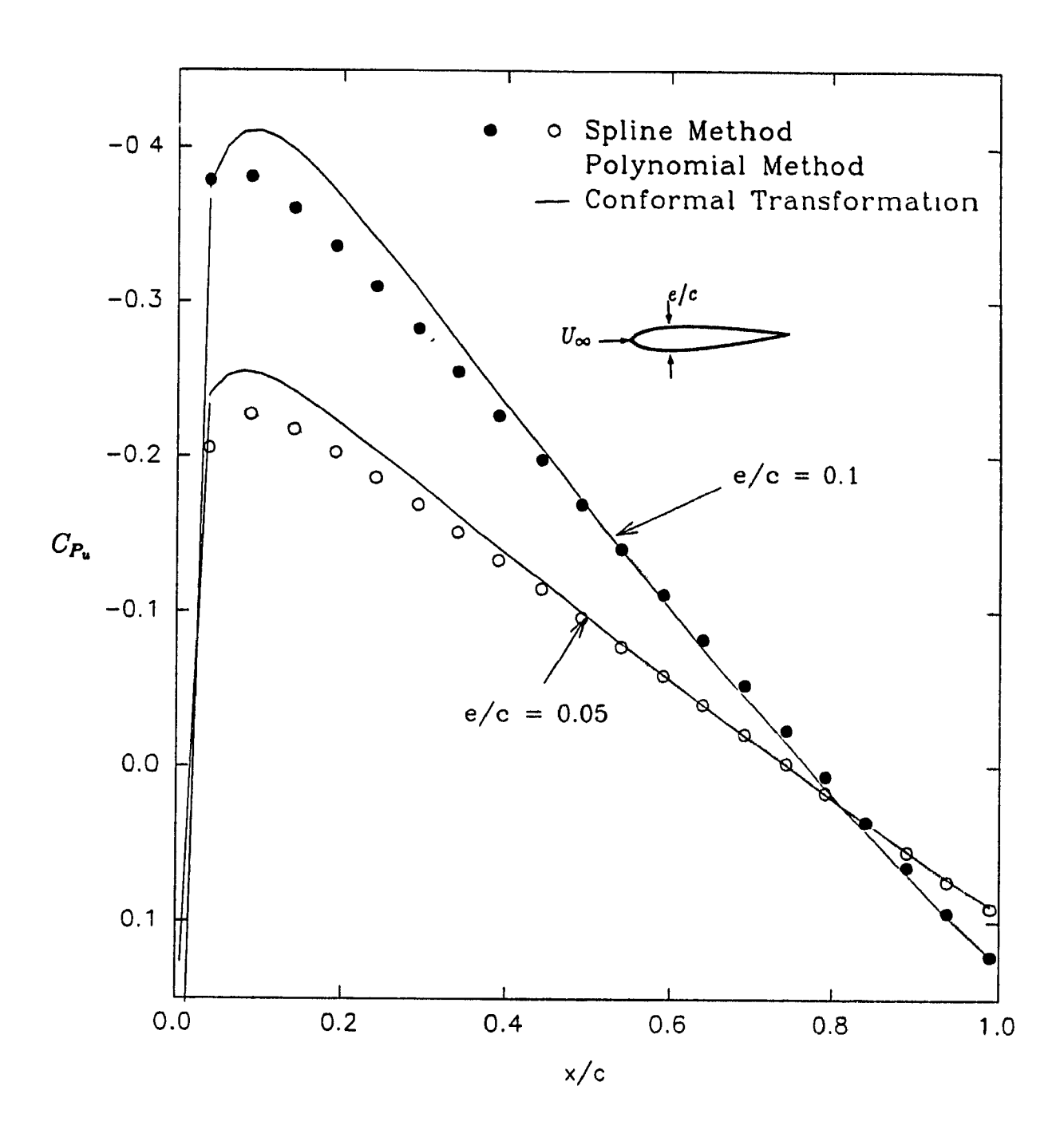


Figure 3.12: Pressure coefficients for symmetrical Joukowski aerofoil at $\alpha=0^{\circ}$ using regular expansion.

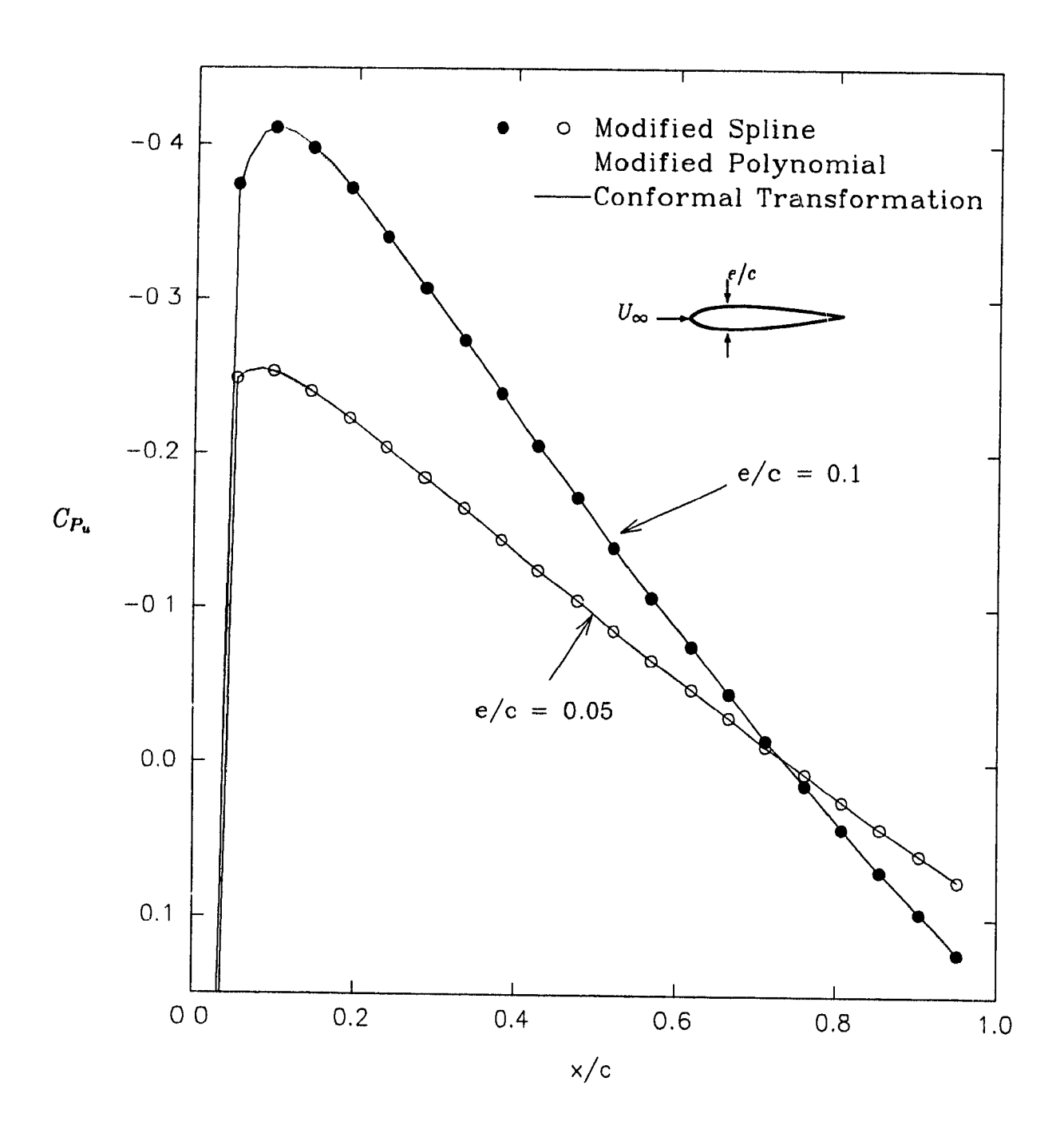


Figure 3.13: Pressure coefficients for symmetrical Joukowski aerofoil at $\alpha=0^{\circ}$ using modified expansion (non-linear spline).

Joukowski Aerofoils at Angles of Incidence

The symmetrical Joukowski aerofoil will first be analyzed. In analyzing the rounded leading edge it became evident that the further from the leading edge the first point was taken, the more stable the solutions became. This was due to the infinite slope at the leading edge which dissipated into a more realistic value at approximately x = 0.05 which the cubic spline could handle. On the aerofoil with the pointed leading edge this was not a problem because at the leading edge the slope had a finite value. For the spline to handle this problem without oscillations occuring, fifteen chordwise positions were taken. This, with the careful placement of the leading edge position obtained solutions within 5% error (except at the leading edge) for the first aerofoil analyzed, compared with the conformal transformation. This careful placement of the leading edge position was obtained by checking the spline coefficients. If the coefficients became large it was a sign that oscillations were present and the error increased significantly. In Figure 3.14 the leading edge position was taken at $x_0 = 0.04$. In Figure 3.15 the leading edge position was taken at the same position but the increasing thickness shows how the error is increased. The pressure coefficient variations on a cambered Joukowski aerofoil are shown, in Figure 3.16, in which one can notice again a good agreement between the present solution based on cubic spline and the exact solution obtained by conformal transformation.

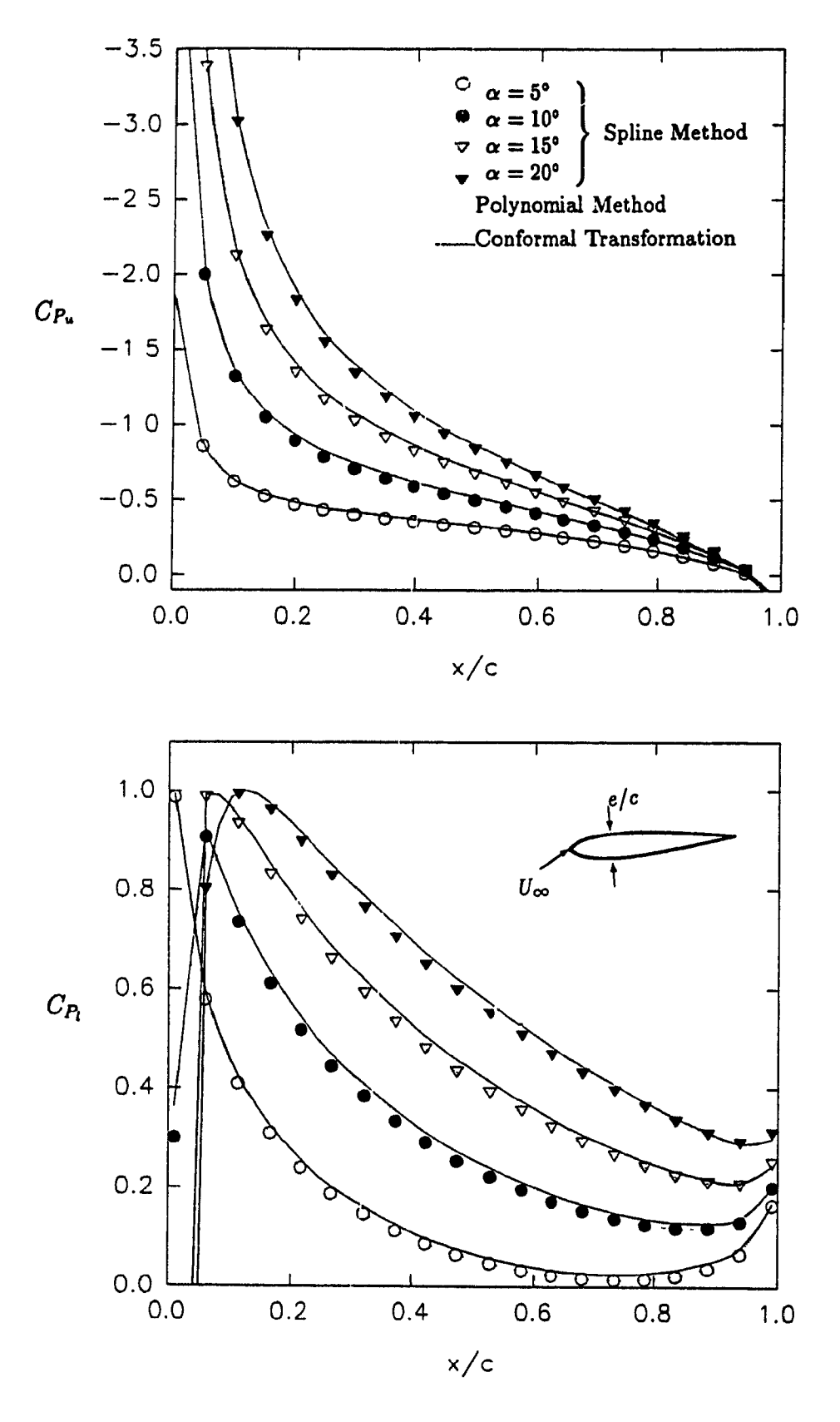


Figure 3.14: Pressure coefficients for symmetrical Joukowski aerofoil with e/c=0.05 at various angles of attack.

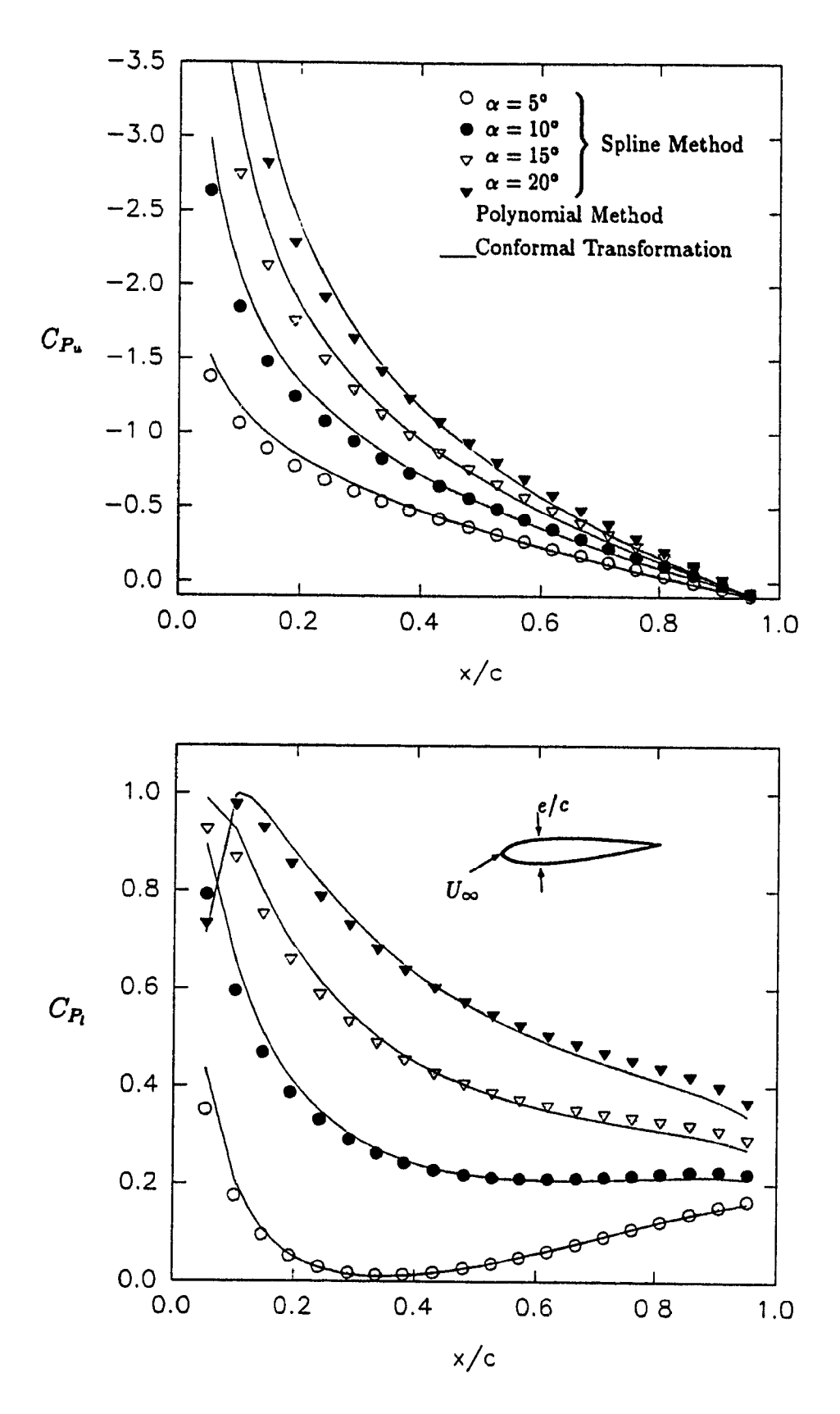


Figure 3.15: Pressure coefficients for symmetrical Joukowski aerofoil with e/c = 0.1 at various angles of attack.

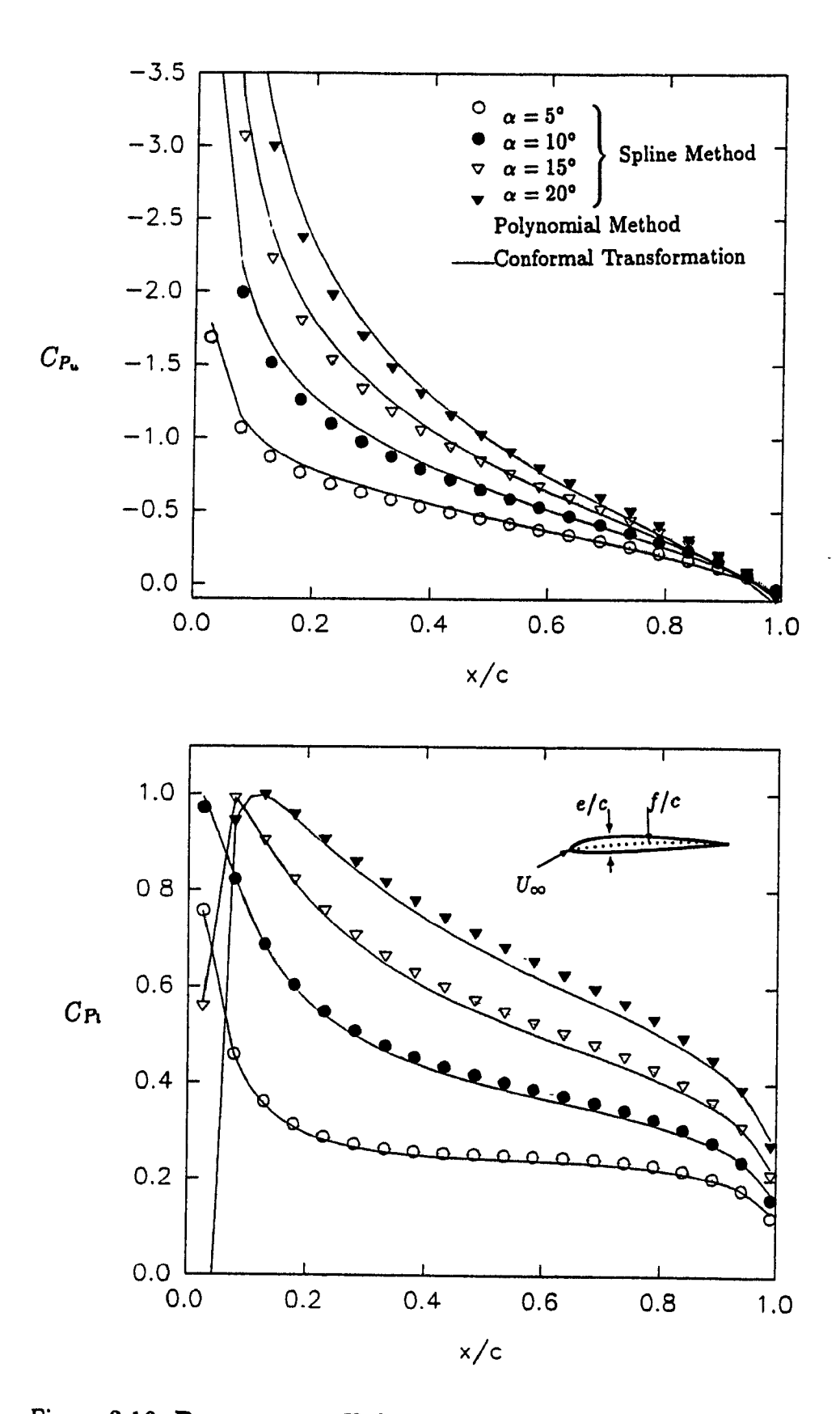


Figure 3.16: Pressure coefficients for a cambered Joukowski aerofoil with e/c=0.05 and f/c=0.025 at various angles of attack.

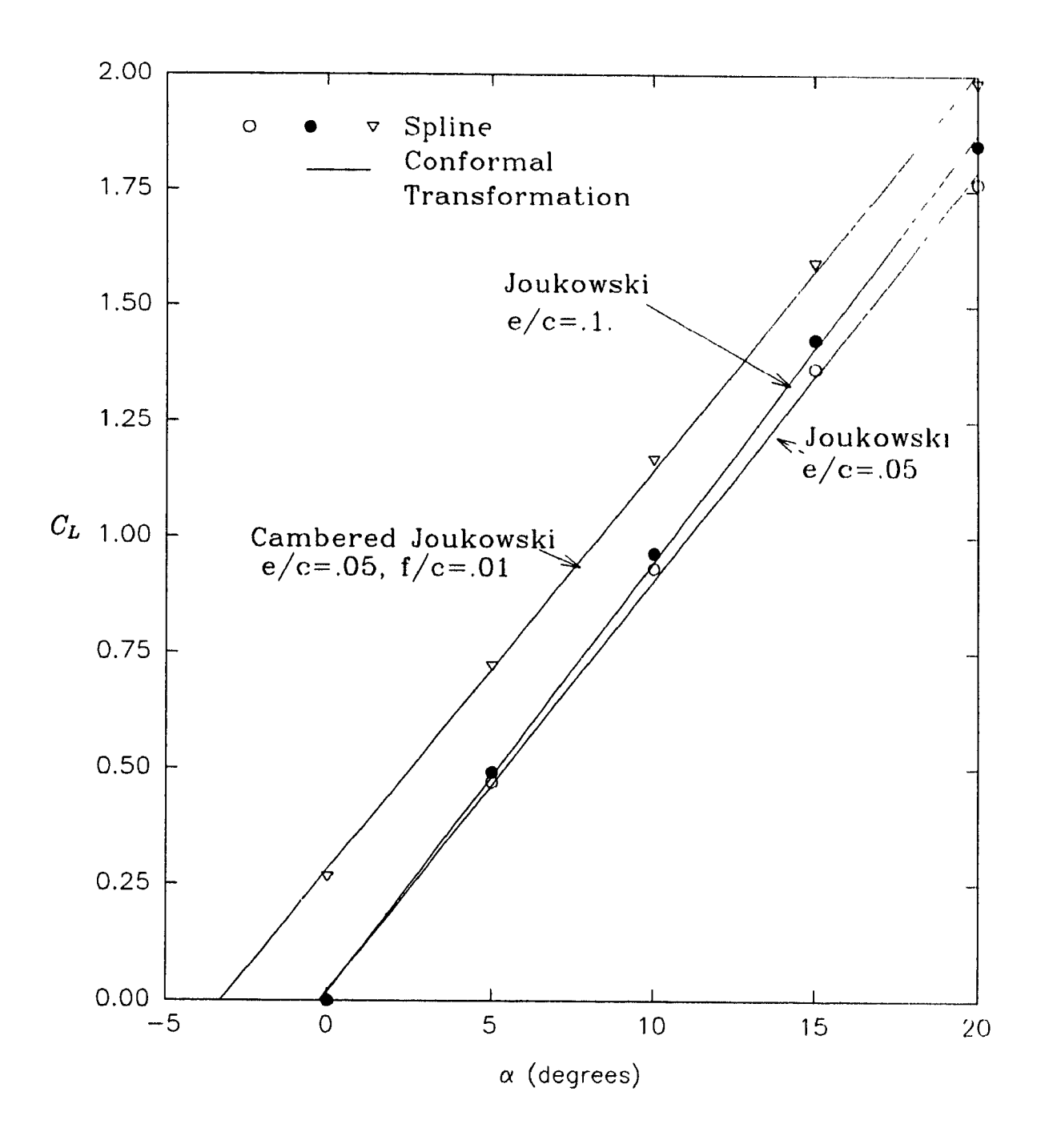


Figure 3.17: Lift coefficients for three Joukowski aerofoils.

Chapter 4

Analysis of Flexible Aerofoils

Membrane aerofoils can be thought of as thin flexible aerofoils. The material used to form this type of aerofoil is assumed to be inelastic. Some examples where flexible membranes are in use are the sails on sail boats, wings on ultralight aircraft, etc.. There have been several investigations on membrane aerofoils (Voelz). Thwaites [33] produced results using linearized thin aerofoil theory and applying it to an integro-differential equation. A couple of years after Thwaites's [33] publications, Nielsen [23] came up with a solution based on Fourier series treating two cases. One with a stagnation point at the leading edge of the aerofoil and another with a singular point at the leading edge (leading edge is referred to as a luff in nautical terms). Both Thwaites and Nielsen obtained solutions using an eigenvalue problem. Later there was research done on approximating these two methods [7]. Recently (1992) a paper by Mateescu and Newman [16,17] was published based on velocity singularities and using polynomial expansions. This seems to give the best overall accuracy in comparison with other methods. The present method of velocity singularities using cubic splines is primarily based on the work done by Mateescu and

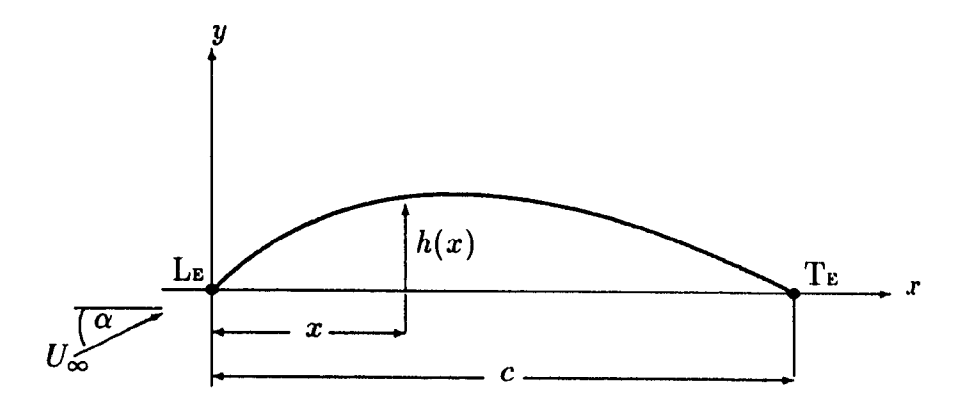


Figure 4.1: Typical side picture of two-dimensional flexible aerofoil

Newman [16,17].

4.1 General Theory of a Flexible Aerofoil

For two dimensional flow over a flexible inelastic membrane of very low porosity, (if porosity exists fluid will go from the high pressure side to the lower pressure side, thus decreasing the membrane lift) theory follows the lines of conventional linearized aerofoil theory. However, in the case of flexible aerofoils the geometrical shape is not known a priori, and it has to be determined by an equilibrium equation. Thwaites called this type of equation the sail equation. This means that the curvature of the sail (jib sail) must be in such a way that the sail tension counterbalances the aerodynamic forces.

The problem of calculating the aerodynamic characteristics of membranes, such as lift, pressure coefficients, the shape of the membrane and the excess length of the membrane material starts with an equilibrium equation. The shape of the sail is unknown but the tension may be specified. Neglecting the viscous shearing forces on the membrane (since this is an inviscid model) the tension on the sail is constant along the chordline. The

equilibrium equation can be expressed in the form

$$\Delta P = \frac{T}{R} \approx -Th''(x),\tag{4.1}$$

where $\frac{1}{R} = -h''(x)$ is an approximation for small slopes only, or in a more convenient form:

$$\Delta C_P = -cC_T h''(x), \tag{4.2}$$

where $\Delta C_P = \frac{\Delta P}{\frac{1}{2}\rho U_{\infty}^2}$ and $C_T = \frac{T}{\frac{1}{2}\rho U_{\infty}^2 c}$. Using thin aerofoil theory, the normal-to-chord velocity on the membrane can be approximated as

$$\frac{v(x)}{U_{\infty}} = -\alpha + h'(x), \tag{4.3}$$

where h'(x) is the camberline slope as defined in Section 3.1.1. Using this equation and noting that the difference in pressure can be written as

$$\Delta C_P = 4 \frac{u(x)}{U_{\infty}},\tag{4.4}$$

the equilibrium equation can be expressed in the form (C_T is used as an independent parameter for computational convenience)

$$\frac{u(x)}{U_{\infty}} = -c\frac{C_T}{4}\frac{v'(x)}{U_{\infty}}.\tag{4.5}$$

4.2 Spline Formulation For Flexible Aerofoils

Considering the equilibrium equation (4.4) the membrane shape can be approximated by cubic splines in the form

$$h''(x) = v'(x) = a(\frac{1}{2} - 2x)\sqrt{\frac{1-x}{x}} + H_1^i + 2H_2^i \Delta x_i + 3H_3^i \Delta x_i^2, \tag{4.6}$$

in which again the value of x is nondimensionalized by the chord, i.e. $\frac{x}{c}$, which puts the value of x between zero and one. The first term multiplied by the factor $\sqrt{\frac{1-x}{x}}$ is introduced to satisfy the equilibrium equation (4.5) at the leading edge, since u(x) contains the same factor. This factor sastisfies the Kutta condition at the trailing edge, x = 1, as well as the pointed leading edge singularity, $\sqrt{\frac{1-x}{x}}$. Integrating equation (4.6) once, gives the camberline slopes, and the camberline shape is found by integrating one more time.

$$h'(x) = \alpha + a\sqrt{x}(1-x)^{\frac{3}{2}} + \sum_{k=0}^{3} H_k^i \Delta x_i^k,$$
 (4.7)

$$h(x) = \alpha x + aJ_o + \sum_{k=0}^{3} \frac{H_k^i}{k+1} \Delta x_i^{k+1} + \varpi_i, \qquad (4.8)$$

where
$$J_o = \frac{1}{8} \cos^{-1} \sqrt{1-x} - \sqrt{(1-x)x} \left(\frac{1}{8} - \frac{7}{12}x + \frac{1}{3}x^2 \right)$$
. (4.9)

In equation (4.8) there is a constant of integration ϖ_i for every spline interval introduced (i.e. N constants for N splines). Knowing these camberline characteristics, the normal-to-chord perturbation velocity can be found in the form

$$v(x) = h'(x) - \alpha = a\sqrt{x}(1-x)^{\frac{3}{2}} + \sum_{k=0}^{3} H_k^i \Delta x_i^k, \tag{4.10}$$

Using the general solution formulated in Section 2.3.2, one obtains for u(x)

$$u(x) = \int_0^1 v(s) \sqrt{\frac{s}{1-s}} \frac{ds}{s-x}$$

$$= -\frac{1}{\pi} \sqrt{\frac{1-x}{x}} \left\{ \sum_{j=1}^N \sum_{k=0}^3 H_k^j K_k^j(x) + a \left[\frac{1}{2} - x + x(1-x) \ln \sqrt{\frac{1-x}{x}} \right] \right\}, (4.11)$$

where $K_k^j(x)$ is defined in Section 3.1.1 (or appendix B) and again H_k^j represents the spline coefficients A_i , B_i , C_i , and D_i as defined in Section C.1.2. Using this type of cubic spline, all the coefficients can be defined by the camberline coefficients h(x) and h'(x). This means that including the coefficient a there are 2N+3 unknowns over N+1 points.

The equilibrium equation (4.5) can be evaluated at points i = 1, 2, 3 ... N giving N cubic spline equations. This equation can also be evaluated at the midpoints $i = \frac{1}{2}, \frac{3}{2}, \frac{5}{2} ... N - \frac{1}{2}$ giving an overall 2N equations. Using the equilibrium equation (4.5) at x = 0 (the leading edge) leads to

$$\frac{a}{2}\left(\frac{1}{\pi} - \frac{C_T}{4}\right) + \frac{1}{\pi} \sum_{j=1}^{N} \sum_{k=1}^{3} k H_k^j K_k^j(x) = 0. \tag{4.12}$$

The Kutta condition is already satisfied in equation (4.5) because of the factor $\sqrt{\frac{1-x}{x}}$ at the trailing edge becomes zero. The final boundary condition left is to allow the membrane ends to be attached to the x axis. This means that the camberline height at the leading and trailing edges is zero:

$$h(1) = h(0) = 0. (4.13)$$

In using this boundary condition, it is required that the constants of integration ϖ_i are solved for. Knowing that h(0) = 0 the first constant ϖ_1 is solved as zero. The next ones can now be solved for as:

$$\varpi_2 = \sum_{k=0}^3 \frac{H_k^1}{k+1} \Delta x_1^{k+1},$$

$$\varpi_3 = \sum_{k=0}^3 \frac{H_k^1}{k+1} \Delta x_1^{k+1} + \sum_{k=0}^3 \frac{H_k^2}{k+1} \Delta x_2^{k+1}.$$

This keeps reoccuring right through the series of splines. If Δx_i is set to be the same throughout the chordline namely $\frac{1}{N}$, then a in equation (4.12) can be solved for as:

$$a = -\frac{16}{\pi} \left[\alpha + \sum_{i=1}^{N} \sum_{k=0}^{3} \frac{H_k^i}{k+1} \left(\frac{1}{N} \right)^{k+1} \right]. \tag{4.14}$$

Now there are 2N+2 equations with 2N+3 unknowns. To finish the system of equations the equilibrium equation is imposed once more at a small distance from the beginning of the first panel. This also helps the leading edge singularity and prevents the first spline from producing oscillations in the system of equations.

The lift coefficient can now be obtained in the form

$$C_{L} = \int_{0}^{1} \Delta C_{P} dx$$

$$= -\alpha C_{T} \left[\sum_{k=0}^{3} H_{k}^{N} \Delta x_{N}^{k} - H_{0}^{0} \right]. \tag{4.15}$$

The excess length of the membrane, defined as $\epsilon = \frac{l}{c} - 1$, can be calculated from the equation:

$$\epsilon = \int_0^1 \sqrt{1 + \left[\frac{v(x)}{U_\infty} + \alpha\right]^2} dx - 1$$

$$\approx \frac{\alpha^2}{2} \int_0^1 \left[1 + \frac{v(x)}{\alpha U_\infty}\right]^2 dx. \tag{4.16}$$

4.3 Solutions for Flexible Aerofoils and Discussion of Results

The following solution for flexible aerofoils (otherwise known as sails) is discussed as a function of α i.e. $\frac{Cl}{\alpha}$. It is important to note that these solutions are accurate for reasonable values of α (if α is large the solutions become inaccurate due to flow separation). The solution is given for $C_T > 1.727$ (the first eigenvalue solution); on a sailboat this would be the case of sailing straight into the wind or referred to having the sails in "irons". This may lead to an unsteady case, because the membrane may flap back and forth.

The solutions have good agreement with experimental tests for membranes with high tensions. For membranes with lower tension values the real flow separates at the trailing edge and a separation bubble forms at the leading edge due to the higher camber (as shown by Newman [22]).

To find the solutions, the cubic spline from Section C.1.2 was used. All the spline coefficients were broken into the two camberline coefficients h'(x) and h''(x) leaving 2N+3 unknowns. Good accuracy was found using ten equally spaced points along the chordline. This gave a 23 by 23 matrix which was easily solved with Guass-Jacobi elimination.

Table 4.1 shows how the present spline method compares with the polynomial method developed by Mateescu and Newman [16,17], and the eigenvalue methods by Thwaites [33] and Nielsen [23]. Of the two latter methods Thwaites is considered to be more accurate at higher values of C_T while Nielsen's method is better at lower values of C_T . The present spline method shows good agreement with the polynomial method, as well as, with the other two methods. As the tension in the membrane is increased the lift coefficient approaches $2\pi\alpha$ which is the theoretical value for a flat plate. This shows how a membrane would act if an infinite tension were applied to a membrane with zero porosity.

Table 4.2 shows how the camberline acts to different tension coefficients. It is interesting to note how the maximum camber position shifts from the mid chord position to a chord position of forty percent. These results compare well to the results found by Nielsen for lower tension coefficients ($2 < C_T < 15$). Another point of interest is the fact that at the lower tension where the maximum camber is at mid chordline, the camberline is not symmetrical. This table is also shown as a graph (Figure 4.2) where the comparison is made to the polynomial method by Mateescu and Newman. This also shows the flat plate tendencies as the tension in increased.

Flat plate tendencies are also shown in Figure 4.4 where lift coefficients are graphed against tension coefficients. As the tension approaches infinite values the well known lift coefficient of $2\pi\alpha$ for a flat plate (which is determined by thin aerofoil theory) is approached. This is also shown in Figure 4.5 where the centers of pressure are graphed

against various values C_T . As the tension is increased the center of pressure approaches the quarter chordline position. Again this is the position obtained for a flat plate using thin aerofoil theory.

	[\ [- 4] _]	1 /	01
C_T	Method	$\alpha/\sqrt{\epsilon}$	C_L/α
	Spline Method (present)	0.322	28.252
2	Polynomial Method (Mateescu & Newman)	0.322	28.250
	Nielsen	0.322	28.148
	Thwaites	0.340	24.989
	Spline Method (present)	2.434	8.952
4	Polynomial Method (Mateescu & Newman)	2.434	8.952
	Nielsen	2.411	8.821
	Thwaites	2.480	8.848
	Spline Method (present)	6.427	7.256
8	Polynomial Method (Mateescu & Newman)	6.424	7.255
	Nielsen	6.329	7.120
	Thwaites	6.400	7.277
	Spline Method (present)	8.404	7.022
10	Polynomial Method (Mateescu & Newman)	8.400	7.021
	Nielsen	8.266	6.884
	Thwaites	8.371	7.120
	Spline Method (present)	13.33	6.744
15	Polynomial Method (Mateescu & Newman)	13.33	6.744
	Nielsen	13.10	6.605
	Thwaites	13.29	6.762
	Spline Method (present)	96.94	6.345
100	Polynomial Method (Mateescu & Newman)	96.88	6.345
	Nielsen		
	Thwaites	96.86	6.349
	Spline Method (present)	391.93	6.298
400	Polynomial Method (Mateescu & Newman)	391.88	6.298
	Nielsen		
	Thwaites	391.83	6.299

Table 4.1: Comparison of lift coefficients and excess membrane length for various tension coefficients C_T .

	C_T						
x/c	2	4	8	10	15	100	400
0.00	0.0000	0.0000	0.0000	0.0000	0.0000	0.0000	0.0000
0.05	0.3666	0.0621	0.0254	0.0197	0.0126	0.0018	0.0004
0.10	0.6974	0.1114	0.0446	0.0344	0.0220	0.0031	0.0008
0.15	0.9930	0.1515	0.0597	0.0460	0.0292	0.0041	0.0010
0.20	1.2516	0.1837	0.0715	0.0549	0.0348	0.0048	0.0012
0.25	1.4710	0.2088	0.0803	0.0615	0.0388	0.0054	0.0013
0.30	1.6495	0.2273	0.0865	0.0661	0.0417	0.0057	0.0014
0.35	1.7857	0.2397	0.0903	0.0690	0.0434	0.0059	0.0015
0.40	1.8788	0.2463	0.0921	0.0702	0.0441	0.0060	0.0015
0.45	1.9283	0.2475	0.0918	0.0699	0.0438	0.0060	0.0015
0.50	1.9344	0.2436	0.0898	0.0683	0.0427	0.0058	0.0014
0.55	1.8978	0.2349	0.0860	0.0654	0.0408	0.0055	0.0014
0.60	1.8194	0.2218	0.0808	0.0613	0.0383	0.0052	0.0013
0.65	1.7010	0.2046	0.0742	0.0563	0.0351	0.0047	0.0012
0.70	1.5447	0.1836	0.0663	0.0502	0.0313	0.0042	0.0010
0.75	1.3532	0.1593	0.0573	0.0434	0.0270	0.0036	0.0009
0.80	1.1297	0.1318	0.0473	0.0358	0.0223	0.0030	0.0007
0.85	0.8779	0.1017	0.0364	0.0275	0.0171	0.0023	0.0006
0.90	0.6021	0.0694	0.0248	0.0187	0.0116	0.0016	0.0004
0.95	0.3073	0.0353	0.0126	0.0095	0.0059	0.0008	0.0002
1.00	0.0000	0.0000	0.0000	0.0000	0.0000	0.0000	0.0000

Table 4.2: Comparison of $h(x)/\alpha$ for various tension coefficients C_T . The position of maximum camber is outlined.

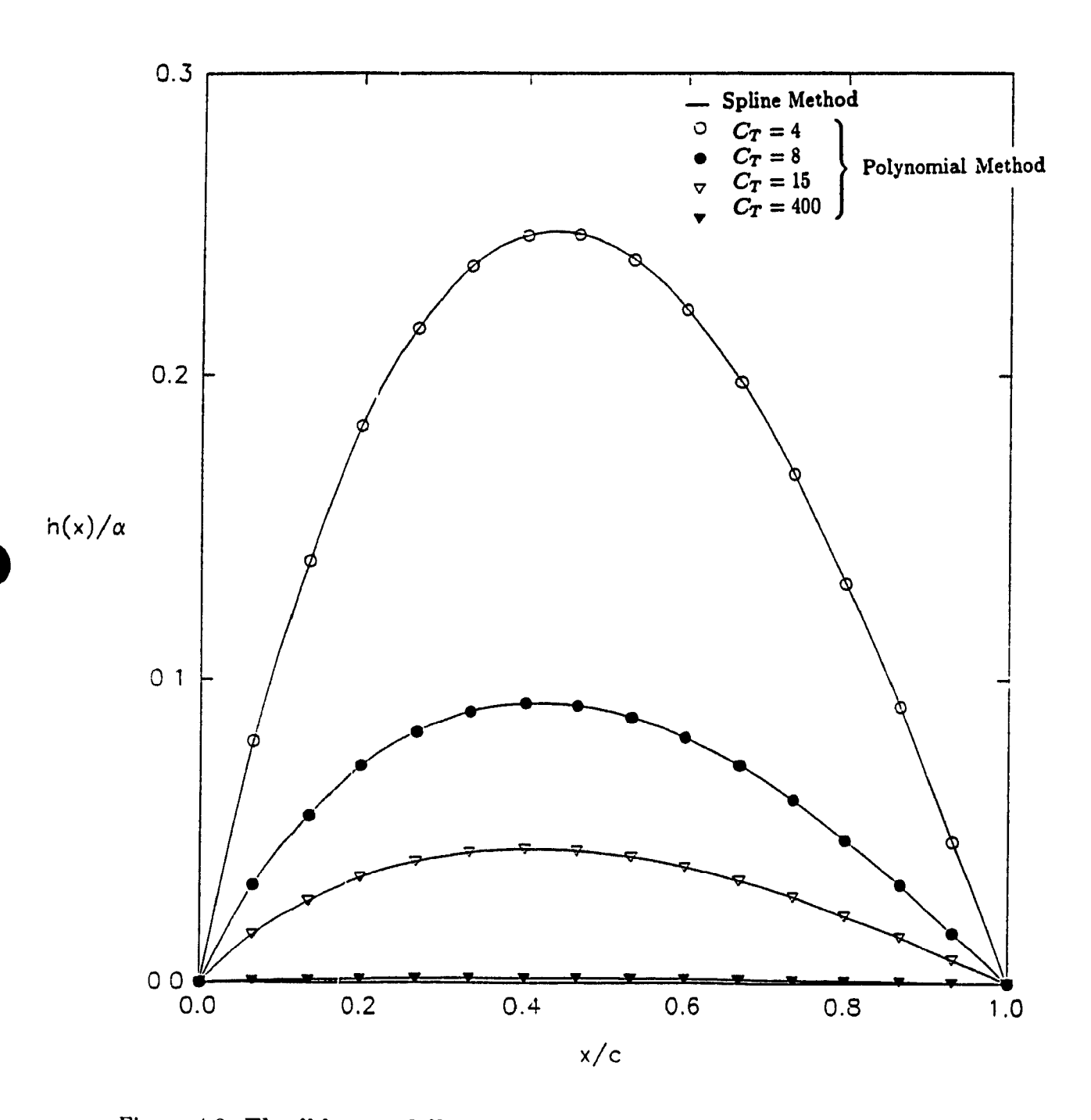


Figure 4.2: Flexible-aerofoil geometry for various tension coefficients C_T compared with Mateescu and Newman.

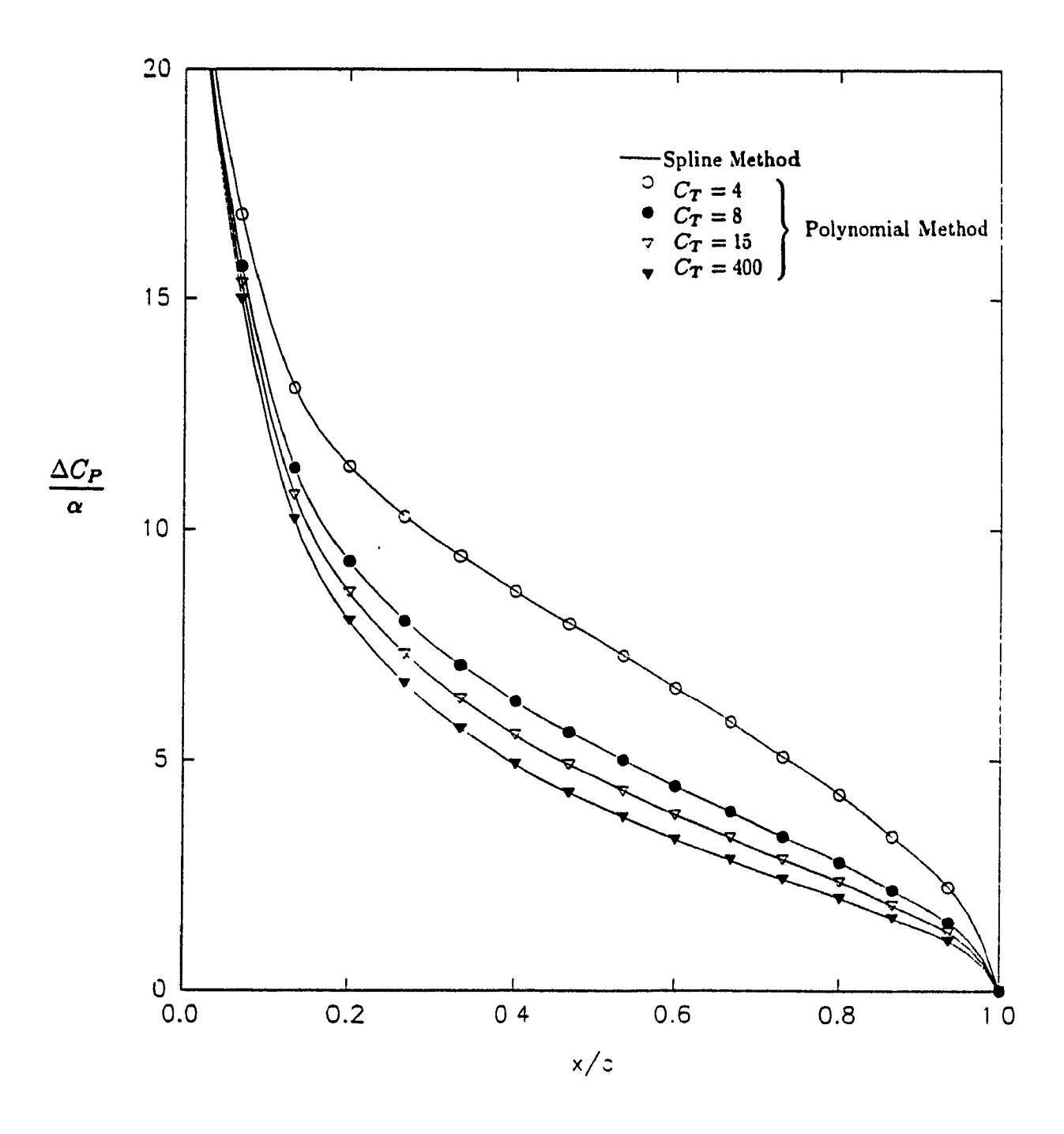


Figure 4.3: Pressure coefficients vs chordwise position for various tension coefficients C_T .

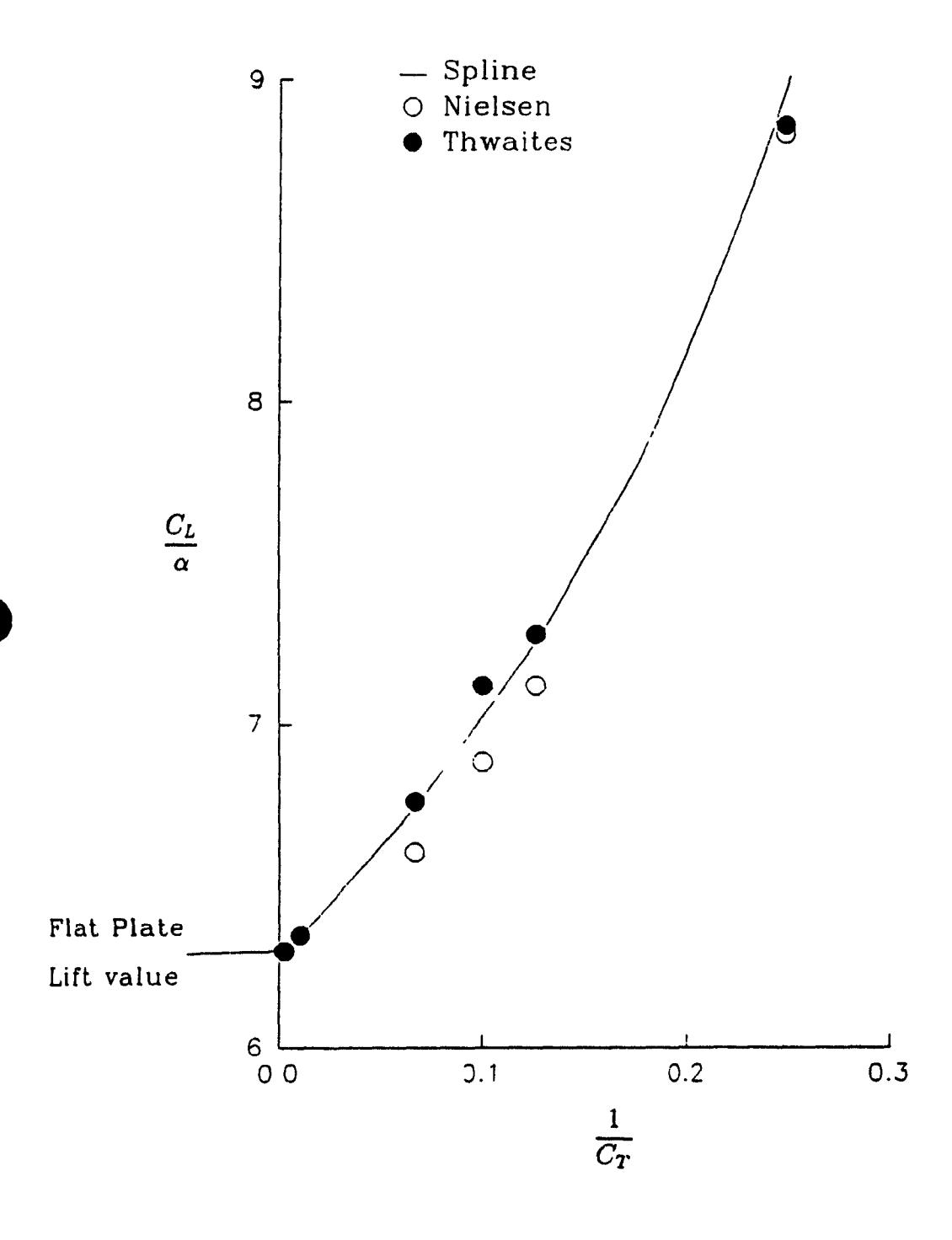


Figure 4.4: Lift coefficients vs various tension coefficients C_T .

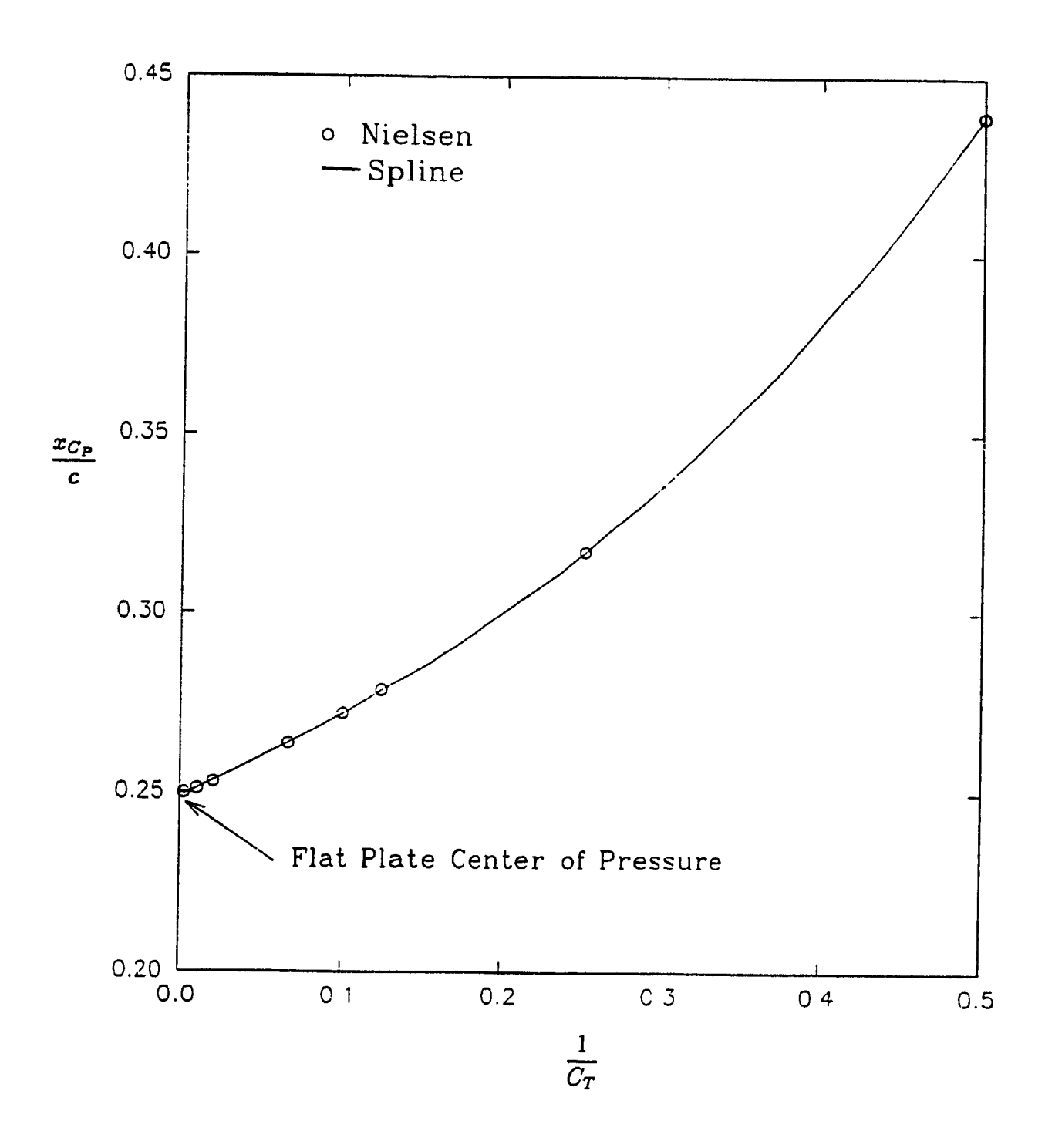


Figure 4.5: Centers of pressure for various tension coefficients C_T .

Chapter 5

Analysis of Jet Flapped Aerofoils

It seems to be common knowledge that a flapped aerofoil gives a much higher lift coefficient than an aerofoil without a flap. A jet flap is an arrangement where a thin sheet of fluid (air in this case) is ejected from the trailing edge of an aerofoil at specific angle, β (see Figure 5.1). This jet sheet gives thrust in both the horizontal and vertical directions, while increasing the circulation around the aerofoil (hence increasing lift). This type of arrangement was tried on a British trainer during World War II without much success (the jet flap would sometimes alter the flow so much that separation would occur, sometimes only on one wing, creating thus undesirable landing or takeoff conditions). There has been much research on suction and blowing around the aerofoil; this section will concentrate on blowing near the trailing edge.

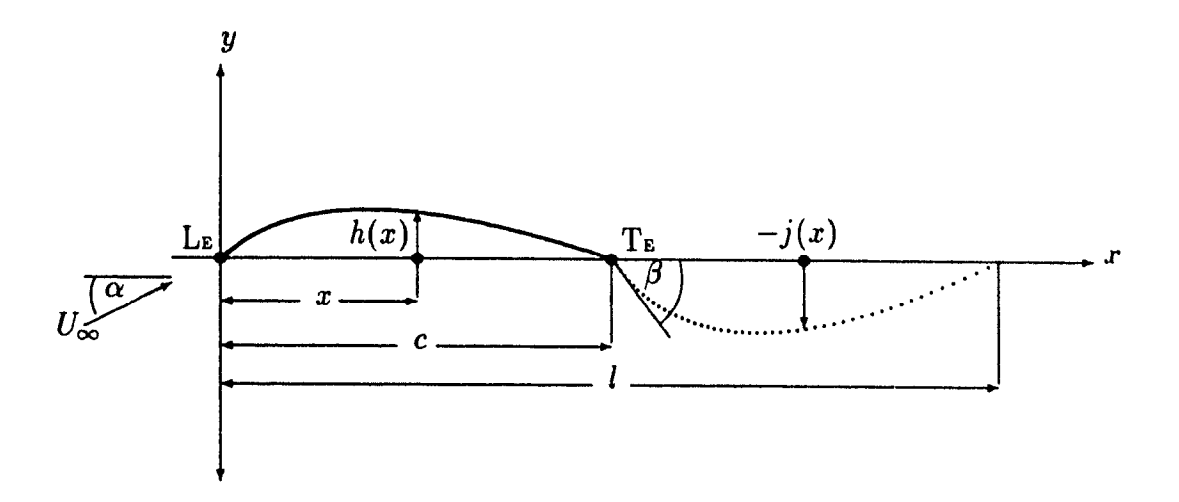


Figure 5.1: Geometry of a jet flapped aerofoil

5.1 General Theory of a Jet Flapped Aerofoil

Let us consider the momentum flux of the jet defined as (Spence [27,28,29])

$$J = \rho V^2 \delta, \tag{5.1}$$

where δ represents the thickness of the jet, which is assumed very small, and V is the velocity of the jet stream, assumed very large. The jet is confined between two vortex sheets which become streamlines. One may define the nondimensional jet momentum coefficient, C_J , in the form

$$C_J = \frac{\rho V^2 \delta}{\frac{1}{2} \rho U_{\infty}^2 c} = \frac{2J}{\rho U_{\infty}^2 c}.$$
 (5.2)

Like the flexible membrane, the jet sheet shape is defined by an equilibrium equation over the jet, relating the jet sheet curvature with the pressure difference across the jet flap:

$$\Delta P = \frac{J}{R}.\tag{5.3}$$

Using the relationship of the jet sheet curvature $\frac{1}{R} \approx j''(x)$, where j(x) represents the coordinate of the jet flap, one obtains

$$\Delta C_P = C_J j''(x), \tag{5.4}$$

where $\Delta C_P = 4 \frac{u(x)}{U_\infty}$ represents the nondimensional pressure difference across the jet sheet. Using linear theory from Section 3.1.1, the normal-to-chord perturbation velocity can be expressed on the jet flap as

$$v(x) = [-\alpha + j'(x)]U_{\infty}, \qquad (5.5)$$

$$v'(x) = j''(x)U_{\infty}. \tag{5.6}$$

The curvature of the jet flap shape, which is a priori unknown, has to be determined using the equilibrium equation:

$$u(x) = \frac{C_J}{4}v'(x), \tag{5.7}$$

where $\Delta C_P = 4 \frac{u(x)}{U_{\infty}}$ has been introduced in equation (5.4). The jet flap angle β at which the fluid is ejected at the trailing edge must be specified:

$$j'(c) = -\tan\beta \approx -\beta. \tag{5.8}$$

The Kutta condition in this case must be satisfied at the end of the jet flap. Since the length of the jet flap is unknown, a value l is specified to be as a very large distance (theoretically infinite), from the trailing edge of the aerofoil; this distance l is usually taken as 2 or 3 chordlengths, depending on the value of the jet coefficient C_J . At this distance l, the perturbation velocities become zero:

$$v(l) = u(l) = 0,$$
 (5.9)

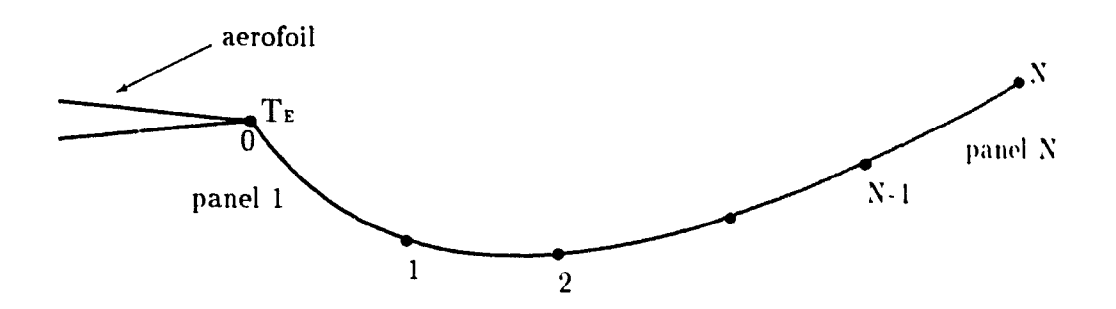


Figure 5.2: Jet flap panel arrangement

and the curvature of the jet stream becomes also zero, the jet stream becoming straight and parallel with the undisturbed flow U_{∞} :

$$j'(l) = \alpha, (5.10)$$

$$j''(l) = 0. (5.11)$$

5.2 Spline Formulation for Jet Flapped Aerofoils

Using cubic splines to approximate perturbation velocities on jet flaps has a great advantage over using large polynomials. In the polynomial formulation the normal-to-chord perturbation velocity on the jet is represented by:

$$\frac{v(x)}{U_{\infty}} + \alpha = \sum_{k=0}^{N} \frac{c_k}{x^k} + a \cdot F(x), \tag{5.12}$$

where e_k represented the polynomial coefficients on the jet and the extra function $a \cdot F(x)$, (as defined in Reference 17) helped to approximate the large singularity created by the jet flap at the trailing edge of the aerofoil; in this method large coefficients for the polynomial are obtained which can create problems when trying to calculate pressure coefficients on the aerofoil. With the spline formulation these large coefficients are avoided. The perturbation velocities can be approximated by two different sets of splines, one set for the aerofoil and the other set for the jet flap. On the aerofoil, the normal-to-chord

perturbation velocity on the aerofoil, is represented, as explained in Section 2.3.2. by:

$$v_a(x) = -\alpha + \sum_{k=0}^{3} H_k^i(x - x_{i-1})^k.$$
 (5.13)

The subscript a denotes the aerofoil and subscript J will be used to denote the jet flap.

First Jet Panel

On the jet there is a singularity at the flap beginning and the end of the aerofoil. The problem of approximating this singularity can be accomplished by using a special function on the first panel of the jet. This function is related to the integration of u(x) whereby the perturbation velocity is approximated by:

$$v_J'(x) = j''(x) = \sum_{k=1}^3 k E_k^1 (x - x_0)^{k-1} + a \frac{2}{\pi} \sinh^{-1} \sqrt{\frac{x_1 - x}{x_1(x - 1)}}.$$
 (5.14)

The extra function is designed to disappear at the end of the first panel and presents a singular behaviour at the trailing edge of the aerofoil, where the slope of the jet-flapped aerofoil has a sudden jump. Integrating this equation results in:

$$v_J(x) + \alpha = j'(x) = \sum_{k=0}^{3} E_k^1(x - x_0)^k + a \cdot f(x),$$
 (5.15)

where
$$f(x) = \frac{2}{\pi} \left[(x-1)\sinh^{-1}\sqrt{\frac{x_1 - x}{x_1(x-1)}} - \sqrt{x_1 - 1}\cos^{-1}\sqrt{\frac{x}{x_1}} \right].$$
 (5.16)

For simplicity in approximating the chordwise perturbation velocity, this extra function is also approximated by a spline

$$v_J'(x) = \sum_{k=1}^3 k \left(E_k^1 + a \cdot F_k \right) (x - x_0)^{k-1}, \tag{5.17}$$

$$v_J(x) = -\alpha + \sum_{k=0}^{3} \left(E_k^1 + a \cdot F_k \right) (x - x_0)^k.$$
 (5.18)

The Remaining Jet Panels

On the rest of the jet panels the extra function is not required, which leaves:

$$v_J'(x) = \sum_{k=1}^3 k E_k^i (x - x_{i-1})^{k-1}, \qquad (5.19)$$

$$v_J(x) = -\alpha + \sum_{k=0}^{3} E_k^i (x - x_{i-1})^k.$$
 (5.20)

Finding the chordwise perturbation velocities u(x) is similar to that of Section 3.1.1, where the limits of integration are changed from 0 and 1 to 0 and $L = \frac{l}{c}$.

$$u(x) = \int_{0}^{L} v(s) \sqrt{\frac{s}{L - s}} \frac{ds}{s - x}$$

$$= \sqrt{\frac{L - x}{x}} \left\{ \alpha - \frac{1}{\pi} \left[\sum_{k=0}^{3} \left(E_{k}^{1} + a F_{k}^{1} \right) K_{J_{k}}^{1}(x) + \sum_{i=2}^{N} \sum_{k=0}^{3} E_{k}^{i} K_{J_{k}}^{i}(x) + \sum_{i=1}^{N} \sum_{k=0}^{3} H_{k}^{i} K_{a_{k}}^{i}(x) \right] \right\},$$
(5.21)

where the $K_{J_k}^i(x)$ represents the integration over the jet and the integration over the aerofoil is represented by $K_{a_k}^i(x)$. The integration is found in appendix B where c must be replaced by L which gives:

$$K_{k}^{i}(x) = \sum_{q=0}^{k} C_{k}^{q} x_{i}^{q} \left\{ \sum_{l=0}^{k-q} x^{l} \Lambda_{k-q-l} + \lambda_{k-q} \right\},$$
 (5.22)

$$\lambda_{p} = \frac{-2x^{p+1}}{\sqrt{x(L-x)}} \begin{cases} \cosh^{-1}\sqrt{\frac{s(L-x)}{L(s-x)}} & \text{for } s > x \\ \sinh^{-1}\sqrt{\frac{s(L-x)}{L(x-s)}} & \text{for } x > s, \end{cases}$$
(5.23)

$$\Lambda_p = \int_{x_{i-1}}^{x_i} \frac{s^p ds}{\sqrt{s(L-s)}},\tag{5.24}$$

where the integrals for Λ_p are:

 \bullet p=0

$$\Lambda_0 = \int_{x_{i-1}}^{x_i} \frac{ds}{\sqrt{s(L-s)}} = \left[\cos^{-1}\left(\frac{L-2s}{L}\right)\right]_{x_{i-1}}^{x_i},$$

•
$$p = 1$$

$$\Lambda_1 = \int_{x_{i-1}}^{x_i} \frac{sds}{\sqrt{s(L-s)}} = \left[\frac{L}{2}\cos^{-1}\left(\frac{L-2s}{L}\right) - \sqrt{s(L-s)}\right]_{x_{i-1}}^{x_i},$$

• p = 2

$$\Lambda_2 = \int_{x_{i-1}}^{x_i} \frac{s^2 ds}{\sqrt{s(L-s)}} = \left[\frac{3L^2}{8} \cos^{-1} \left(\frac{L-2s}{L} \right) - \left(\frac{s}{2} + \frac{3L}{4} \right) \sqrt{s(L-s)} \right]_{x_{i-1}}^{x_i},$$

• p = 3

$$\Lambda_3 = \int_{x_{1-1}}^{x_1} \frac{s^3 ds}{\sqrt{s(L-s)}} = \left[\frac{5L^3}{16} \cos^{-1} \left(\frac{L-2s}{L} \right) - \left(\frac{s^2}{3} + \frac{5Ls}{12} + \frac{5L^2}{8} \right) \sqrt{s(L-s)} \right]_{x_{1-1}}^{x_1}.$$

Putting the perturbation velocities into the jet momentum equilibrium equation (5.4), a solution can be obtained in a similar manner as in the case of flexible membranes, where the spline coefficients are broken into their respective derivatives. This needs to be done for the spline approximating the jet flap (E_k^i) . The spline coefficients on the aerofoil H_i^k can be found using linear aerfoil theory found in Section 3.1.1. The spline coefficients for F_k^i are found by evaluating equation (5.16) at the beginning and the end of the first panel. After this has been done, there are 2N + 3 unknowns to be solved for, by using the boundary conditions previously discribed in Section 5.1:

$$j'(c) + a \cdot f(c) = -\tan \beta, \qquad (5.25)$$

$$j'(l) = \alpha, (5.26)$$

$$j''(l) = 0. (5.27)$$

The last condition also represents the Kutta condition where the perturbation velocities become zero at the end of the jet.

C_{J}	L	$C_{L_{spline}}$	$C_{L_{Spence}}$
0.25	2.5	1.02	1.02
0.50	2.77	1.48	1.49
0.75	3.25	1.87	1.87
1.00	3.75	2.20	2.20
1.25	4.36	2.53	2.52
1.50	4.97	2.80	2.81

Table 5.1: Coefficients of lift for a jet-flapped aerofoil with $\beta=31.4^{\circ}$, compared to Spence's solution.

5.3 Solutions for Jet Flapped Aerofoils and Discussion of Results

The spline formulation becomes especially advantageous over the polynomial method for the solution of the jet-flapped aerofoils. In finding the solution it became apparent that a value of 0.1 for Δx_i (i.e. $x_i - x_{i-1} \approx 0.1$) produced accurate enough results. The problem of choosing the variational parameter L proved to become rather difficult. This parameter changed with the angle of the jet and the value of the jet coefficient. A graph for different values of C_J against L were compiled (see Figure 5.5) using $\Delta x_i = 0.1$. These values were attained by checking the overall lift coefficient from the jet, with the values attained by Spence [27,28,29]. On the first panel a special function was added to take into account for the singularity produced by the jet. It was found that for the best results the first jet panel point was taken at c + 0.01. If a value closer to the chordlength was taken, the singularity became to large and produced oscillations within the spline formulation. Typical values for L are shown in Table 5.1 for various values of C_J for a jet-flapped aerofoil ($\alpha = 0^{\circ}$, $\beta = 31.4^{\circ}$). Figure 5.3 shows the pressure difference across a typical jet

flapped aerofoil at zero incidence. This shows the good agreement with Dimmock's [32] experimental results. In Figure 5.4 lift slopes of the jet-flap are compared to Spence's solution [27,28,29].

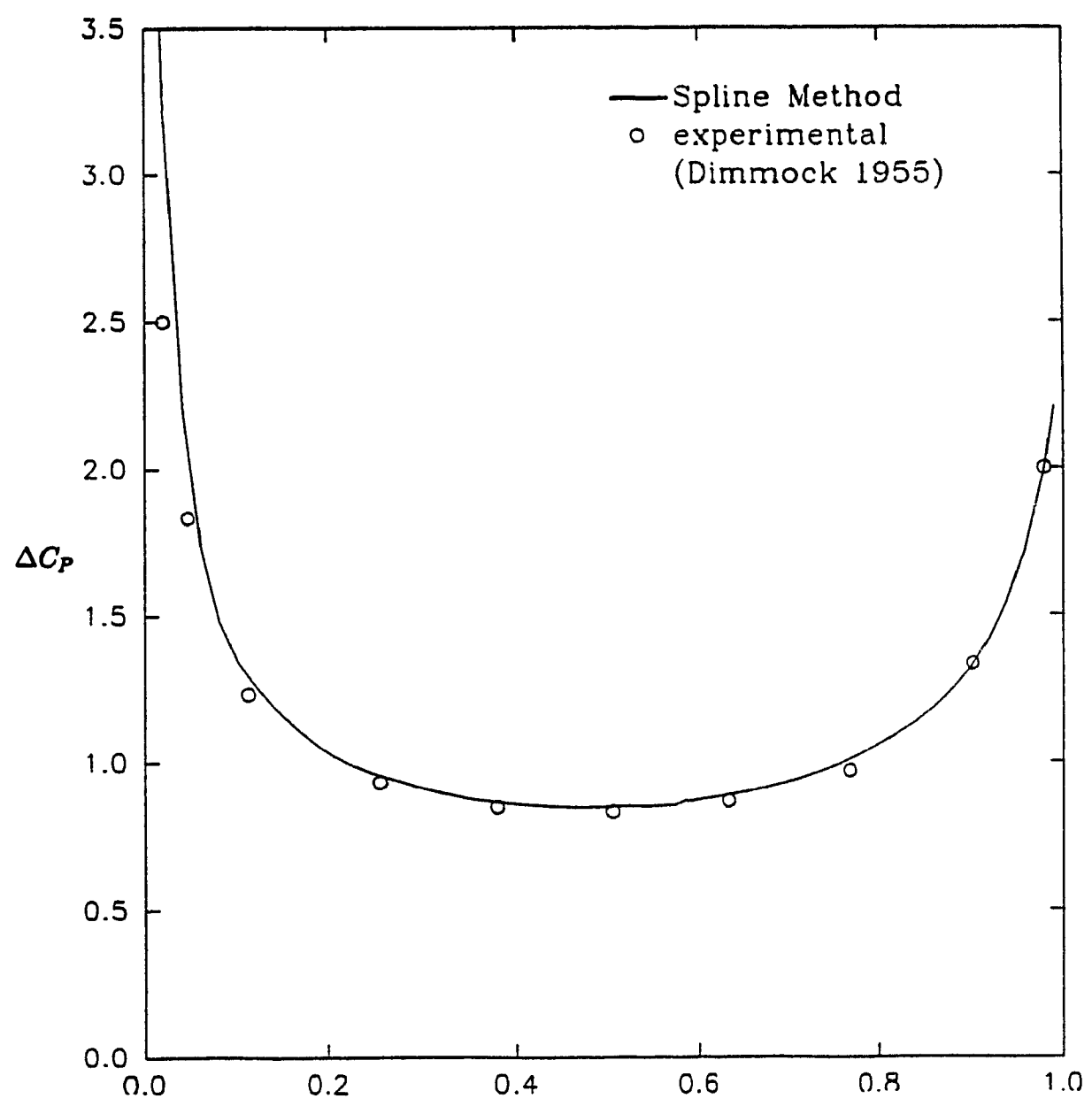


Figure 5.3: Nondimensional pressure difference ΔC_P across a jet flapped symmetrical aerofoil at zero incidence compared to Dimmock's, experimental results ($\alpha = 0^{\circ}$, $\beta = 31^{\circ}$, $C_J = 0.3$).

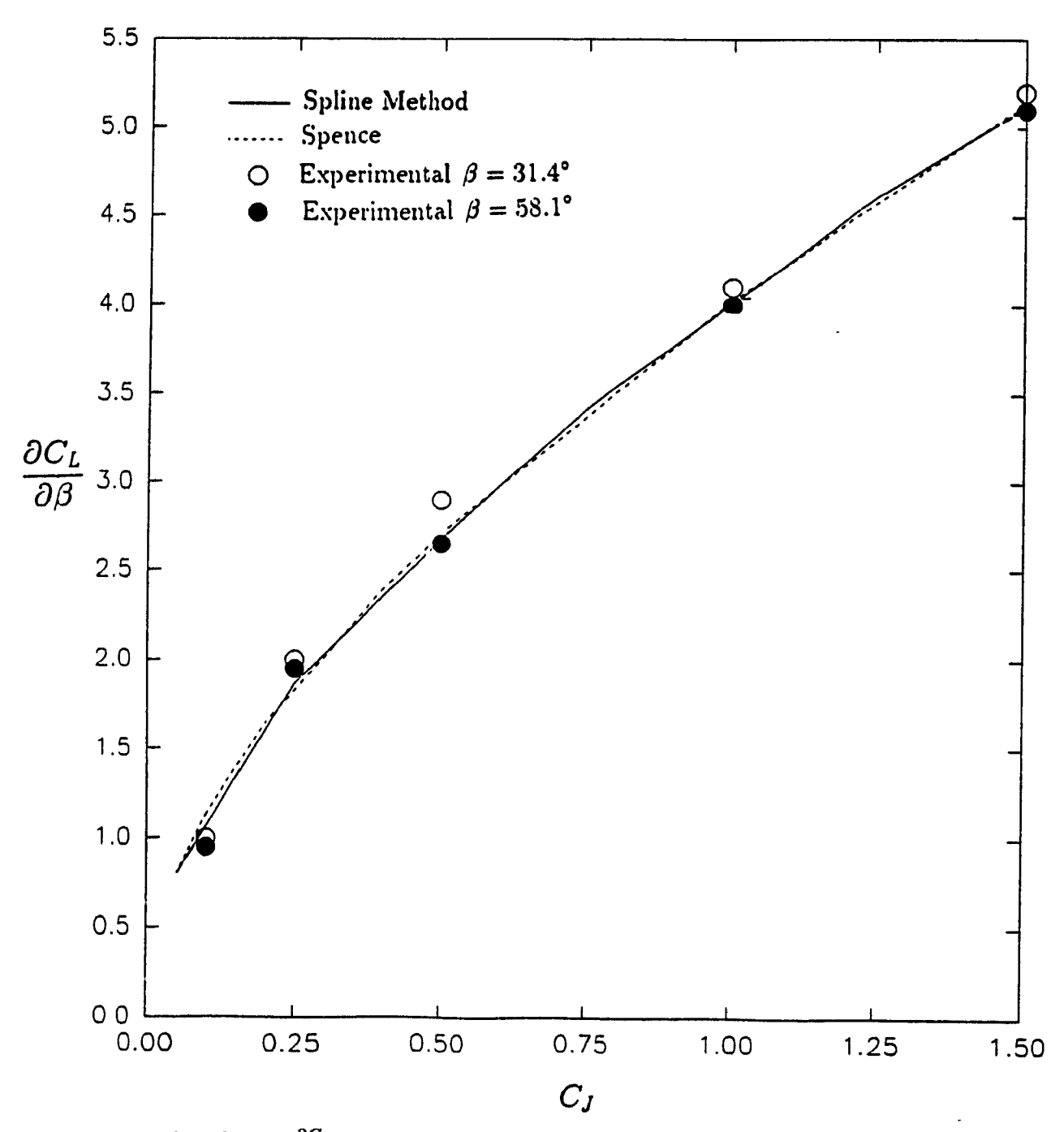


Figure 5.4: Lift slope, $\frac{\partial C_L}{\partial \beta}$, compared to Spence's solution and Spence's experimental values.

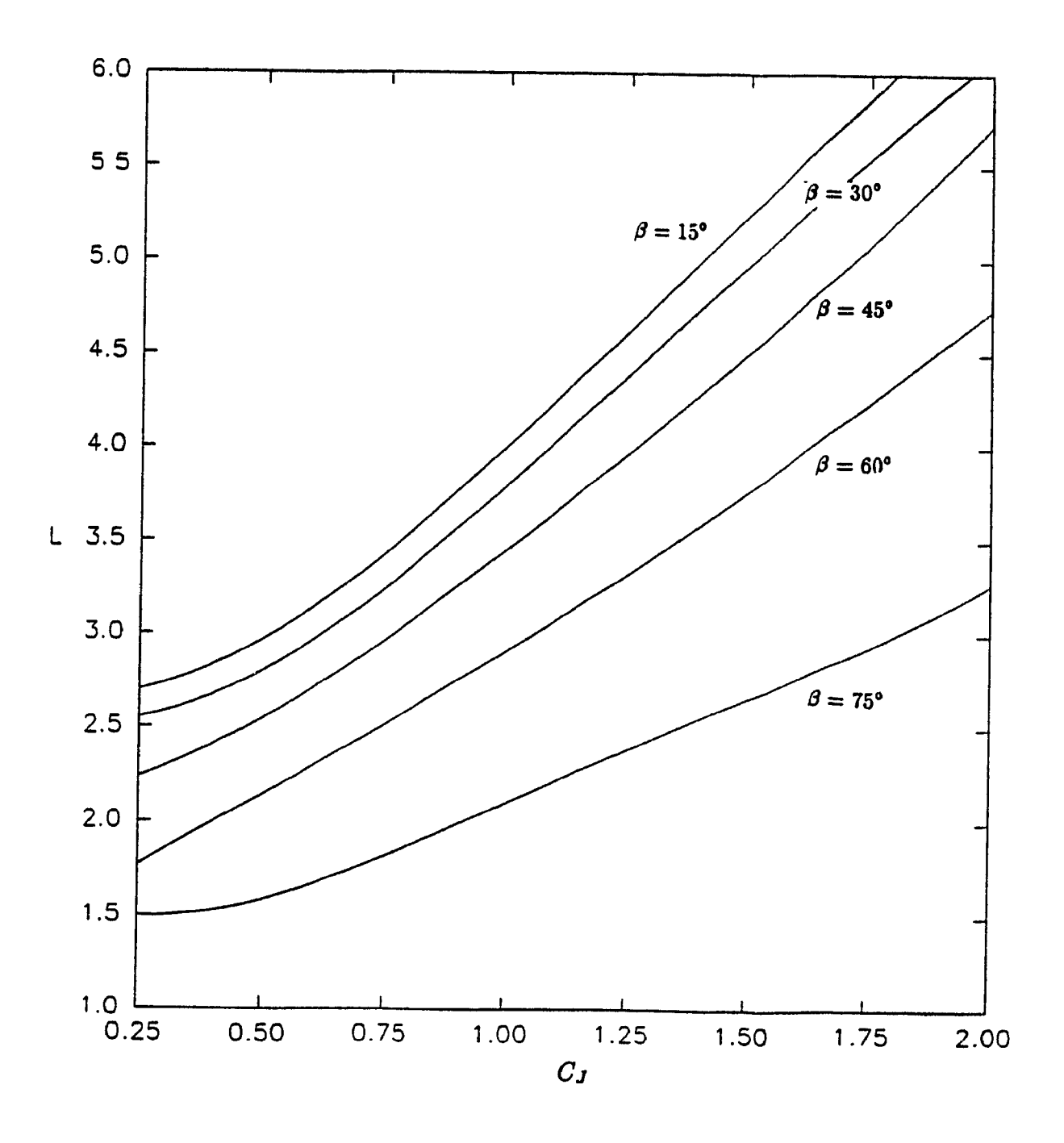


Figure 5.5: Plot of the jet-flap length L against jet coefficients C_J .

Chapter 6

Analysis of Multi-Element Aerofoils

Multi-element aerofoils are used on almost all airplanes in operation today, which need high lift devices such as leading and trailing edge flaps in order to take off and land within reasonable runway distances. It is interesting to adapt the method of velocity singularities for these special types of aerofoils.

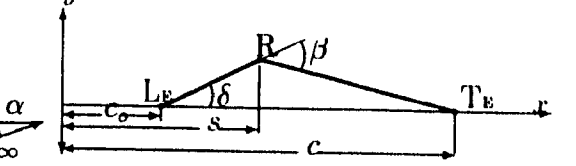
6.1 Flow Field Solution outside the Aerofoil Contour by the Method of Velocity Singularities

In the linear analysis of single element aerofoils it was assumed that the aerofoil was in steady unperturbed air flow, and the calculations have been made to determine the pressure distribution on the aerofoil contour. In the case of the multi-element aerofoils, there are perturbation velocities generated by one aerofoil section which affect the other aerofoil section. To find these perturbation velocities, an analysis of the complex functions appearing in the expression of the complex conjugate perturbation velocity, has to be

Part	$-\infty < z = x < c_o$	$c \infty < z = x < c_o$ $c_o < z = x < s$ $s < z = x < s$		$c < z = x < \infty$
Real	0	$\cosh^{-1}\sqrt{\frac{(c-z)(s-c_o)}{(c-c_o)(s-z)}}$	$\sinh^{-1}\sqrt{\frac{(c-z)(s-c_o)}{(c-c_o)(z-s)}}$	0
Imag	$\cos^{-1}\sqrt{\frac{(c-z)(s-c_o)}{(c-c_o)(s-z)}}$	0	$\frac{\pi}{2}$	$\cos^{-1}\sqrt{\frac{(c-z)(s-c_o)}{(c-c_o)(s-z)}}$

Table 6.1: Real and imaginary parts of the ridge function found in the complex conjugate perturbation function.

done for the domain outside of the aerofoil contour.



6.1.1 Thin Aerofoil Solutions

In analyzing the domain outside of a thin flapped aerofoil (as shown in figure above), the complex perturbation velocity function from Section 2.3.2 must be evaluated. This function is written for a thin flapped aerofoil as:

$$W(z) = A\sqrt{\frac{c-z}{z-c_o}} - \Delta v \frac{2}{\pi} \cosh^{-1} \sqrt{\frac{(c-z)(s-c_o)}{(c-c_o)(s-z)}}.$$
 (6.1)

Here c_o defines the position of the leading edge of the aerofoil and c defines the trailing edge position. This function does not present any problems while z is inside the limits of the aerofoil (i.e. $c_o < z = x < c$). While outside the limits of the aerofoil at the chordline, (i.e. y = 0, z = x > c, and $z = x < c_o$), the function $\sqrt{\frac{c-z}{z-c_o}}$ becomes imaginary, and the second function $\cosh^{-1}\sqrt{\frac{(c-z)(s-c_o)}{(c-c_o)(s-z)}}$ changes as shown in Table 6.1. The constant A remains the same as in Section 2.3.2:

$$A = -\left[v_{c_o} + \frac{2}{\pi} \Delta v \cos^{-1} \sqrt{\frac{s - c_o}{c - c_o}}\right]. \tag{6.2}$$

Putting this into the disturbance function yields:

$$W(z) = i \sqrt{\frac{z-c}{z-c_o}} \left[-v_{c_o} - \Delta v \frac{2}{\pi} \cos^{-1} \sqrt{\frac{s-c_o}{c-c_o}} \right] - i \Delta v \frac{2}{\pi} \cos^{-1} \sqrt{\frac{(c-z)(s-c_o)}{(c-c_o)(s-z)}}.$$
 (6.3)

Modelling the aerofoil as a continuous distribution of ridges gives:

$$W_{A}(z) = i\sqrt{\frac{z-c}{z-c_{o}}} \left\{ -v_{A}(c_{o}) - \frac{2}{\pi} \int_{c_{o}}^{c} \left(\frac{dv_{A}}{dx}\right)_{x=s} \cos^{-1} \sqrt{\frac{s-c_{o}}{c-c_{o}}} ds \right\}$$

$$-i\frac{2}{\pi} \int_{c_{o}}^{c} \left(\frac{dv_{A}}{dx}\right)_{x=s} \cos^{-1} \sqrt{\frac{(c-z)(s-c_{o})}{(c-c_{o})(s-z)}} ds; \qquad (6.4)$$

one obtains after integrating by parts

$$W_A(z) = -\frac{i}{\pi} \sqrt{\frac{z-c}{z-c_o}} \int_{c_o}^c v_A(s) \sqrt{\frac{s-c_o}{c-s}} \frac{ds}{s-z} + i v_{c_o}.$$
 (6.5)

Evaluating the imaginary part on the x-axis (y = 0), the vertical perturbation velocity induced upstream or downstream of the aerofoil $(z = x > c, z = x < c_o)$ is

$$v_A(x) = -\frac{1}{\pi} \sqrt{\frac{x-c}{x-c_o}} \int_{c_o}^c v_A(s) \sqrt{\frac{s-c_o}{c-s}} \frac{ds}{s-x}.$$
 (6.6)

Hence, in the case of a two-element aerofoil, it is necessary to take into account the vertical velocity induced by one of the aerofoils, on the other aerofoil, which will be evaluated using equation (6.6).

Considering a cubic spline representation for the vertical velocity on the aerofoil in the form

$$v_A(x)|_{x_{i-1} < x < x_i} = \sum_{k=0}^3 V_k^i (x - x_{i-1})^k,$$
 (6.7)

the vertical perturbation velocity induced upstream and downstream of the aerofoil (z = x > c, $z = x < c_o$) is obtained from equation (6.6) in the form:

$$v_A(x) = -\frac{1}{\pi} \sqrt{\frac{x-c}{x-c_o}} \sum_{i=1}^{N} \sum_{k=0}^{3} V_k^i Q_k^i(x), \qquad (6.8)$$

where $Q_k^i(x)$ are expressed as

$$Q_{k}^{l}(x) = \sum_{q=0}^{k} C_{k}^{q} x_{1}^{q} \left\{ \sum_{l=0}^{k-q} x^{l} T_{k-q-l} - c_{o} \sum_{l=0}^{k-q-1} x^{l} T_{k-q-l-1} - 2x^{k-q} \sqrt{\frac{x-c_{o}}{x-c}} \cos^{-1} \sqrt{\frac{(c-x)(s-c_{o})}{(c-c_{o})(s-x)}} \right\},$$
(6.9)

in which

$$T_p = \int_{x_{i-1}}^{x_i} \frac{s^p ds}{\sqrt{(s - c_o)(c - s)}}. (6.10)$$

For the various p, the expressions of T_p are:

$$T_{0} = \left[\cos^{-1}\left(\frac{c+c_{o}-2s}{c-c_{o}}\right)\right]_{x_{i-1}}^{x_{i}},$$

$$T_{1} = \left[\left(\frac{c+c_{o}}{2}\right)\cos^{-1}\left(\frac{c+c_{o}-2s}{c-c_{o}}\right) - \sqrt{(s-c_{o})(c-s)}\right]_{x_{i-1}}^{x_{i}},$$

$$T_{2} = \left[\frac{3}{8}\left(c^{2}+6cc_{o}+c_{o}^{2}\right)\cos^{-1}\left(\frac{c+c_{o}-2s}{c-c_{o}}\right) - \left[\frac{s}{2}+\frac{3}{4}\left(c+c_{o}\right)\right]\sqrt{(s-c_{o})(c-s)}\right]_{x_{i-1}}^{x_{i}},$$

$$T_{3} = \left[\frac{1}{16}\left(-13c_{o}^{3}+21c_{o}^{2}c-15c^{2}c_{o}+5c^{3}+18c_{o}c\right)\cos^{-1}\left(\frac{c+c_{o}-2s}{c-c_{o}}\right) - \left(\frac{s^{2}}{3}+\frac{5sc}{12}+\frac{5c^{2}}{8}+\frac{c_{o}c}{12}+\frac{5c_{o}s}{12}+\frac{3c_{o}^{2}}{4}\right)\sqrt{(s-c_{o})(c-s)}\right]_{x_{i-1}}^{x_{i}}.$$

The integration value s is varied between x_{i-1} and x_i situated on the studied aerofoil, $x_i \in [c_o, c]$ for any i, and C_k^q represents the coefficients of the binomial expansion $(x-x_{i-1})^k$, [i.e. $C_k^q = (-1)^q \frac{k!}{q!(k-q)!}$] The integration and algebra to find these velocities can be found in Appendix D.

As concerns the axial perturbation velocity, u_A , on the aerofoil itself (outside of the aerofoil $u_A|_{y=0}=0$), this can be obtained, in the same manner as in Section 2.3.2, from the equation

$$u_A(x) = -\frac{1}{\pi} \sqrt{\frac{c-x}{x-c_o}} \int_{c_o}^c v_A(s) \sqrt{\frac{s-c_o}{c-s}} \frac{ds}{s-x}.$$
 (6.11)

which leads to the following expression for the cubic spline representation:

$$u_A(x) = -\frac{1}{\pi} \sqrt{\frac{c-x}{x-c_o}} \sum_{i=1}^{N} \sum_{k=0}^{3} V_k^i R_k^i(x), \tag{6.12}$$

where $R_k^i(x)$ are expressed as

$$R_{k}^{i}(x) = \sum_{q=0}^{k} C_{k}^{q} x_{i}^{q} \left\{ \sum_{l=0}^{k-q} x^{l} T_{k-q-l} - c_{o} \sum_{l=0}^{k-q-1} x^{l} T_{k-q-l-1} - 2x^{k-q} \sqrt{\frac{x-c_{o}}{c-x}} \Gamma(c_{o}, c, s, x) \right\},$$
(6.13)

in which T_p is the same as previously expressed and

$$\Gamma(c_o, c, s, x) = \begin{cases} \cosh^{-1} \sqrt{\frac{(c-x)(s-c_o)}{(c-c_o)(s-x)}} & c_o < x < s \\ \sinh^{-1} \sqrt{\frac{(c-x)(s-c_o)}{(c-c_o)(x-s)}} & s < x < c \\ 0 & x < c_o, x > c. \end{cases}$$
(6.14)

6.1.2 Aerofoils of Symmetrical Thickness

A similar evaluation of the perturbation velocity must be done for aerofoils of symmetrical thicknesses. The corresponding complex velocity function for a typical symmetrical aerofoil is defined as

$$W_{S}(z) = \frac{1}{\pi} \left[v_{c_{o}} \ln(z - c_{o}) + \int_{c_{o}}^{c} \left(\frac{dv}{dx} \right)_{x=s} \ln(z - s) ds - v_{c} \ln(z - c) \right]$$

$$= \frac{1}{\pi} \int_{c_{o}}^{c} v_{S}(s) \frac{ds}{z - s}. \tag{6.15}$$

As already known, for y = 0 outside the symmetrical aerofoil $(z = x < c_o \text{ and } z = x > c)$, the vertical perturbation velocity calculated with the above equation is zero, $v_S(x) = 0$. Hence, by contrast with the antisymmetrical part of the solution, there is no vertical velocity induced by the symmetrical thickness of one aerofoil on the second aerofoil contour.

To calculate the axial velocity $u_S(x)$, the symmetrical vertical velocity on the aerofoil $v_S(x)$, will be put into the form of a cubic spline representation

$$v_S(x)|_{x_{i-1} < x < x_i} = \sum_{k=0}^{3} G_k^i (x - x_{i-1})^k.$$
 (6.16)

Putting this spline representation into equation (6.15) the axial velocity can be found similarly to that of Section 2.3.3 where:

$$u_S(x) = -\frac{1}{\pi} \sum_{i=1}^{N} \sum_{k=0}^{3} G_k^i J_k^i(x), \tag{6.17}$$



Figure 6.1: Flapped aerofoil at incidence α and flap incidence β . where $J_k^i(x)$ are the same as previously expressed in Section 2.3.3.

6.2 Analysis of Two-Element Aerofoils

The analyzed two-element aerofoil is shown in Figure 6.2, in which c_1 represents the chordlength of the first aerofoil and c_2 the chordlength of the flap, which will be denoted in the following as the *second* aerofoil. The distance between the two aerofoils is Δc (i.e. the distance from the trailing edge of aerofoil one and the leading edge of aerofoil two). The angle of incidence of the first aerofoil is α and β represents the deflection angle of the second aerofoil (the flap) with respect to the chord of the first aerofoil.

Table 6.2 shows the definition of the chordlengths according to the notations used in Sections 6.2.1 and 6.2.2. In order to analyze the flow past the two-element aerofoil, the problem will be decomposed into two separate flow fields, namely the antisymmetrical

Aerofoil	С	c _o	
1	c_1	0	
2	$c_1 + \Delta c + c_2$	$c_1 + \Delta c$	

Table 6.2: Definitions for c and c_o for aerofoil 1 and aerofoil 2.

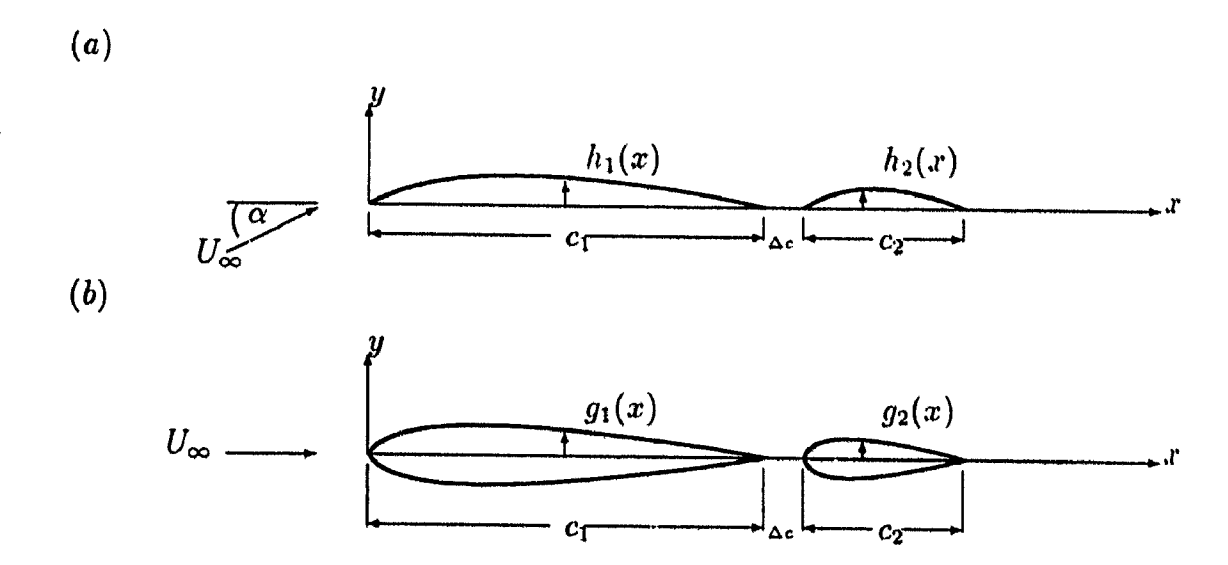


Figure 6.2: Decomposition of (a) antisymmetrical and (b) symmetrical parts of a two-element aerofoil.

and symmetrical velocity flow fields:

$$u = u_A + u_S, (6.18)$$

$$v = v_A + v_S, (6.19)$$

where u and v define the perturbation velocity in the x and y directions, and where the subscripts A and S stand for the antisymmetrical and symmetrical flow fields, respectively. As shown in Figure 6.2a, the antisymmetrical velocity field takes into account the effect of the aerofoil camber and angle of attack, and in Figure 6.2b, the symmetrical velocity field takes into account the effect of the symmetrical thickness of the aerofoil. The antisymmetrical and symmetrical flow fields are defined by the following boundary conditions:

$$v_{A}(x) = \begin{cases} [-\alpha + h'_{1}(x)] U_{\infty}, & \text{for } 0 < x < c_{1} \\ [-(\alpha + \beta) + h'_{2}(x)] U_{\infty}, & \text{for } c_{1} + \Delta c < x < c_{1} + \Delta c + c_{2} \end{cases}$$

$$u_{A}(x) = 0, & \text{for } x < 0, c_{1} < x < c_{1} + \Delta c, x > c_{1} + \Delta c + c_{2}$$

$$(6.20)$$

$$u_A(x) = 0,$$
 for $x < 0, c_1 < x < c_1 + \Delta c, x > c_1 + \Delta c + c_2$ (6.21)

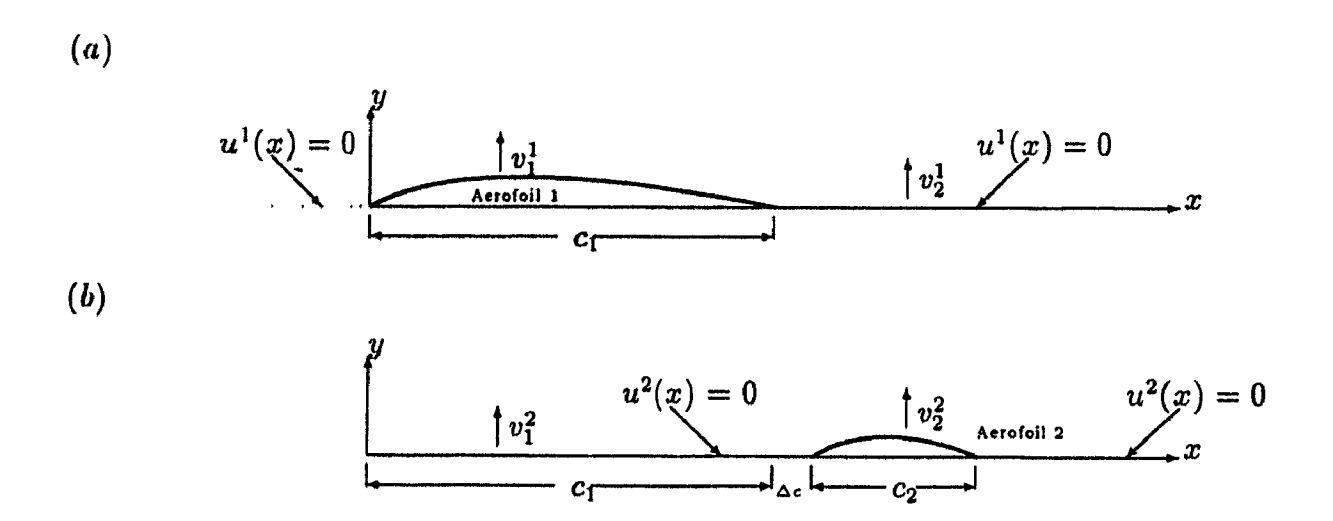


Figure 6.3: Two thin cambered aerofoils to determine the antisymmetrical velocity flow field.

$$v_{S}(x) = \begin{cases} g'_{1}(x)U_{\infty}, & \text{for } 0 < x < c_{1} \\ g'_{2}(x)U_{\infty}, & \text{for } c_{1} + \Delta c < x < c_{1} + \Delta c + c_{2} \\ 0, & \text{for } x < 0, c_{1} < x < c_{1} + \Delta c, x > c_{1} + \Delta c + c_{2}. \end{cases}$$
(6.22)

6.2.1 Antisymmetrical Part of the Solution

The antisymmetrical part of the flow field is decomposed into two separated antisymmetrical flow fields past two isolated thin aerofoils represented by the camberlines of the first and second aerofoils, as shown in Figure 6.3:

$$v_A(x) = v_A^1(x) + v_A^2(x),$$
 (6.23)

$$u_A(x) = u_A^1(x) + u_A^2(x).$$
 (6.24)

The superscripts 1 and 2 are used in the above equations to denote the corresponding antisymmetrical flows past the first and the second aerofoils, which are defined by the

following spline distributions of the vertical velocities:

$$v_{A_1}^1(x)|_{x_{i-1} < x < x_i} = \sum_{k=0}^3 V_k^{1,i} (x - x_{i-1})^k, \qquad 0 < x < c_1, \qquad (6.25)$$

$$v_{A_2}^2(x)|_{x_{j-1} < x < x_i} = \sum_{k=0}^3 V_k^{2,i} (x - x_{i-1})^k, \qquad c_1 + \Delta c < x < c_1 + \Delta c + c_2. \tag{6.26}$$

where the spline coefficients $V_k^{1,i}$ and $V_k^{2,i}$ are unknown a priori and will be determined later; the subscripts 1 and 2 indicate the aerofoils on which the vertical velocity is formulated.

Using equation (6.18), the following expressions are obtained for the axial perturbation velocities, $u_A^1(x)$ and $u_A^2(x)$:

$$u_A^1(x) = -\frac{1}{\pi} \sqrt{\frac{c_1 - x}{x}} \sum_{i=1}^{N} \sum_{k=0}^{3} V_k^{1,i} R_k^i(x), \qquad 0 < x < c_1$$
 (6.27)

$$u_A^2(x) = -\frac{1}{\pi} \sqrt{\frac{c_1 + \Delta c + c_2 - x}{x - (c_1 + \Delta c)}} \sum_{i=1}^{N} \sum_{k=0}^{3} V_k^{2,i} R_k^i(x), c_1 + \Delta c < x < c_1 + \Delta c + c_2. (6.28)$$

The vertical velocity induced by the aerofoil 1 on the aerofoil 2, $v_{A_2}^1(x)$, and the vertical velocity induced by the aerofoil 2 on the aerofoil 1, $v_{A_1}^2(x)$, are obtained from equation (6.8) in the form:

$$v_{A_2}^1(x) = -\frac{1}{\pi} \sqrt{\frac{x-c_1}{x}} \sum_{i=1}^N \sum_{k=0}^3 V_k^{1,i} Q_k^i(x), \qquad c_1 + \Delta c < x < c_1 + \Delta c + c_2, \quad (6.29)$$

$$v_{A_1}^2(x) = -\frac{1}{\pi} \sqrt{\frac{x - (c_1 + \Delta c + c_2)}{x - (c_1 + \Delta c)}} \sum_{i=1}^{N} \sum_{k=0}^{3} V_k^{2,i} Q_k^i(x), \qquad 0 < x < c_1. \quad (6.30)$$

The a priori unknown coefficients $V_k^{1,i}$ and $V_k^{2,i}$ can now be determined using the boundary conditions (equation (6.20)) in the form

$$v_{A_1}^1(x) + v_{A_1}^2(x) = \left[-\alpha + h_1'(x) \right] U_{\infty}, \tag{6.31}$$

$$v_{A_2}^1(x) + v_{A_2}^2(x) = [-(\alpha + \beta) + h_2'(x)] U_{\infty}, \tag{6.32}$$

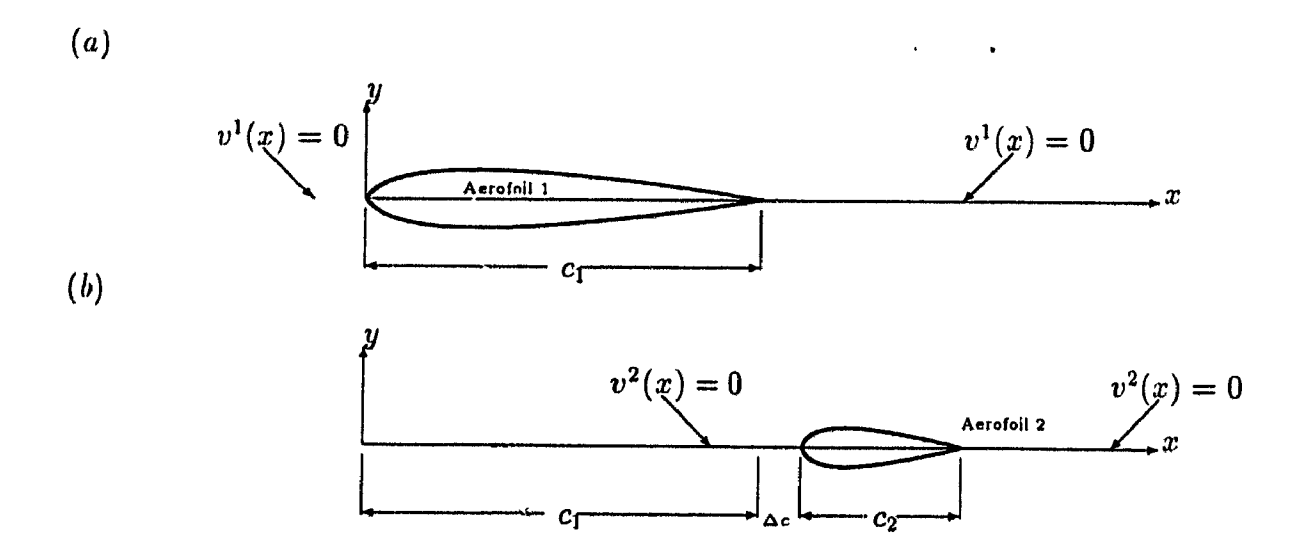


Figure 6.4: Two symmetrical aemofoils to determine the symmetrical velocity flow field.

which lead to a linear system of equations. To make the system of equations simpler, the spline coefficients were broken into the two main components (as described in Appendix C.1.2) of v(x) and v'(x) for both the aemofoils. Then the components for v'(x) can be broken down further into functions of v(x) using second order differencing techniques. This produces a matrix with a dominent diagonal which reduces any possibilities of ill-conditioning. Solving the problem by this method leaves 2N+2 unknowns. Once the spline coefficients $V_k^{1,i}$ and $V_k^{2,i}$ are solved for, the axial components from equation (6.27) and equation (6.28) can be determined.

6.2.2 Symmetrical Part of the Solution

The analysis of the symmetrical velocity field is also decomposed into two separate symmetrical flow fields past two isolated aerofoils of symmetrical thickness (Figure 6.4):

$$v_S(x) = v_S^1(x) + v_S^2(x),$$
 (6.33)

$$u_S(x) = u_S^1(x) + u_S^2(x). (6.34)$$

Where the superscripts 1 and 2 denote the corresponding symmetrical flow fields defined by the following boundary conditions:

$$v_S^1(x) = \begin{cases} g_1'(x)U_{\infty}, & \text{for } 0 < x < c_1 \\ 0, & \text{for } x < 0, \ x > c_1 \end{cases}$$
 (6.35)

$$v_S^2(x) = \begin{cases} g_2'(x)U_{\infty}, & \text{for } c_1 + \Delta c < x < c_1 + \Delta c + c_2 \\ 0, & \text{for } x < c_1 + \Delta c, \ x > c_1 + \Delta c + c_2 \end{cases}$$
(6.36)

Cubic spline representations for the vertical velocities on the two aerofoils in the form

$$v_{S_1}^1(x)|_{x_{i-1} < x < x_i} = g_1'(x)U_{\infty} = \sum_{k=0}^3 G_k^{1,i} (x - x_{i-1})^k, \qquad 0 < x < c_1, \qquad (6.37)$$

$$v_{S_2}^2(x)|_{x_{i-1} < x < x_i} = g_2'(x)U_{\infty} = \sum_{k=0}^3 G_k^{2,i} (x - x_{i-1})^k,$$

for
$$c_1 + \Delta c < x < c_1 + \Delta c + c_2$$
. (6.38)

The axial perturbation velocities on the first aerofoil, $u_{S_1}^1(x)$ and $u_{S_1}^2(x)$, and those on the second aerofoil, $u_{S_2}^1(x)$ and $u_{S_2}^2(x)$, are obtained as

$$u_{S_1}^1(x) = -\frac{1}{\pi} \sum_{i=1}^N \sum_{k=0}^3 G_k^{1,i} J_k^i(x), \qquad 0 < x < c_1, \qquad (6.39)$$

$$u_{S_1}^2(x) = -\frac{1}{\pi} \sum_{i=1}^N \sum_{k=0}^3 G_k^{2,i} J_k^i(x), \qquad 0 < x < c_1, \qquad (6.40)$$

$$u_{S_2}^1(x) = -\frac{1}{\pi} \sum_{i=1}^N \sum_{k=0}^3 G_k^{1,i} J_k^i(x), \qquad c_1 + \Delta c < x < c_1 + \Delta c + c_2, \qquad (6.41)$$

$$u_{S_2}^2(x) = -\frac{1}{\pi} \sum_{i=1}^N \sum_{k=0}^3 G_k^{2,i} J_k^i(x), \qquad c_1 + \Delta c < x < c_1 + \Delta c + c_2, \qquad (6.42)$$

where $J_k^i(x)$ are defined by equation (3.20) in Section 3.1.2. The symmetrical part of the solution for the axial perturbation velocities on each aerofoil can hence be calculated as

$$u_S(x)|_{1} = u_{S_1}^1(x) + u_{S_1}^2(x), \qquad 0 < x < c_1,$$
 (6.43)

$$u_S(x)|_2 = u_{S_2}^1(x) + u_{S_2}^2(x), \qquad c_1 + \Delta c < x < c_1 + \Delta c + c_2.$$
 (6.44)

			Karman-Trefftz Characteristics		
Aerofoil	e/c	f/c	ε	n	γ
A	0.05	0.02	0.024	1.97	2.32°
В	0.05	0.00	0.040	2.00	0.00°

Table 6.3: Definitions of two types of aerofoil.

where $u_S(x)|_1$ and $u_S(x)|_2$ define the total axial velocity due to symmetrical thickness. All of the symmetrical velocities can be found explicitly if the cubic spline of Appendix C.1.2 is used.

6.3 Results and Comparisons for Two-Element Aerofoils

To determine the accuracy of the present method, comparisons were performed for the case of two-element aerofoils, with the results obtained by Seebohm and Newman [26] using a surface vortex method.

These comparisons have been made for the case when the main aerofoil section (aerofoil 1) and the flapped section (aerofoil 2) are both Karman-Trefftz aerofoils with the same characteristics f/c, e/c, ϵ , n and γ . The results have been obtained for two different aerofoils indicated by A and B in Table 6.3 (in fact the aerofoil B is a Joukowski aerofoil, which represents a particular type of Karman-Trefftz aerofoil with n=2 and the trailing edge angle $\gamma=0$).

The antisymmetrical and the symmetrical parts of the solution were determined for these two-element aerofoils in the manner indicated in Sections 6.2.1 and 6.2.2, and then the pressure coefficients are calculated based on these solutions as indicated by equations (3.8) and (3.9) in Section 3.1.

The pressure coefficients distributions obtained for these two-element aerofoils are shown in Figures 6.5- 6.8 for the following geometrical characteristics: $c_1 = 1$, $c_2 = 0.35$, and $\Delta c = 0.05$.

The results obtained for the two-element aerofoil based on the Karman-Trefftz aerofoil of type A (see Table 6.3) are shown in Figure 6.5 for $\alpha=0^{\circ}$ and $\beta=15^{\circ}$ and in Figure 6.6 for $\alpha=10^{\circ}$ and $\beta=15^{\circ}$. The results for the two-element aerofoils based on the Joukowski aerofoil of type B (see Table 6.3) are shown in Figure 6.7 for $\alpha=0^{\circ}$ and $\beta=20^{\circ}$ and in Figure 6.8 for $\alpha=10^{\circ}$ and $\beta=20^{\circ}$.

In all these figures, the solutions obtained with the present method, using 25 equally spaced points on each aerofoil, have been compared with the results obtained by Scebohm and Newman ^[26] using a vortex panel method. A reasonable good agreement has been found between the results obtained with these two methods.

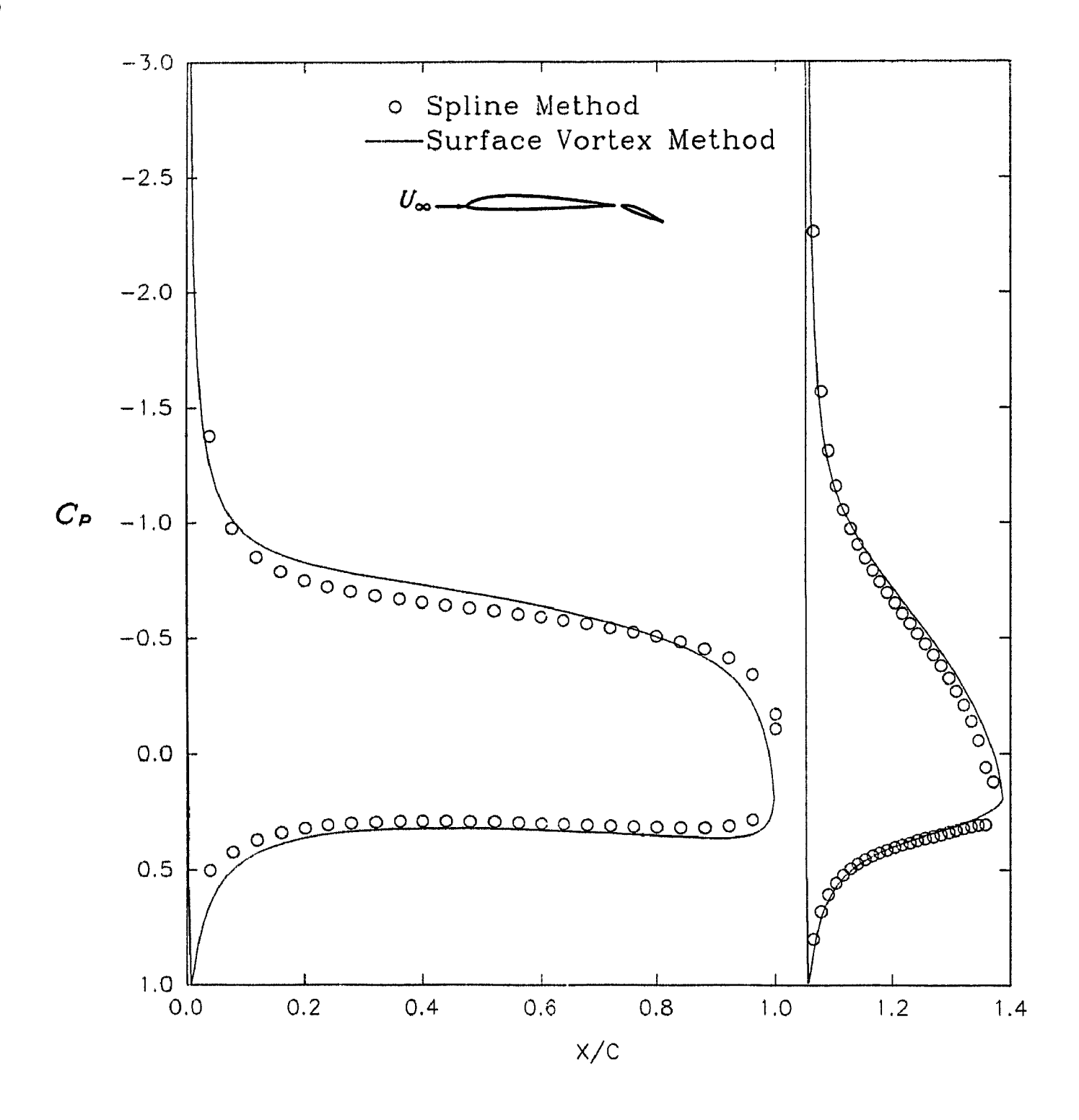


Figure 6.6: Pressure coefficients for an aerofoil with a rounded leading edge $(e/c=0.05,\ f/c=0.02)$ and a 35% flap $(\alpha=0^{\circ},\ \beta=15^{\circ})$.

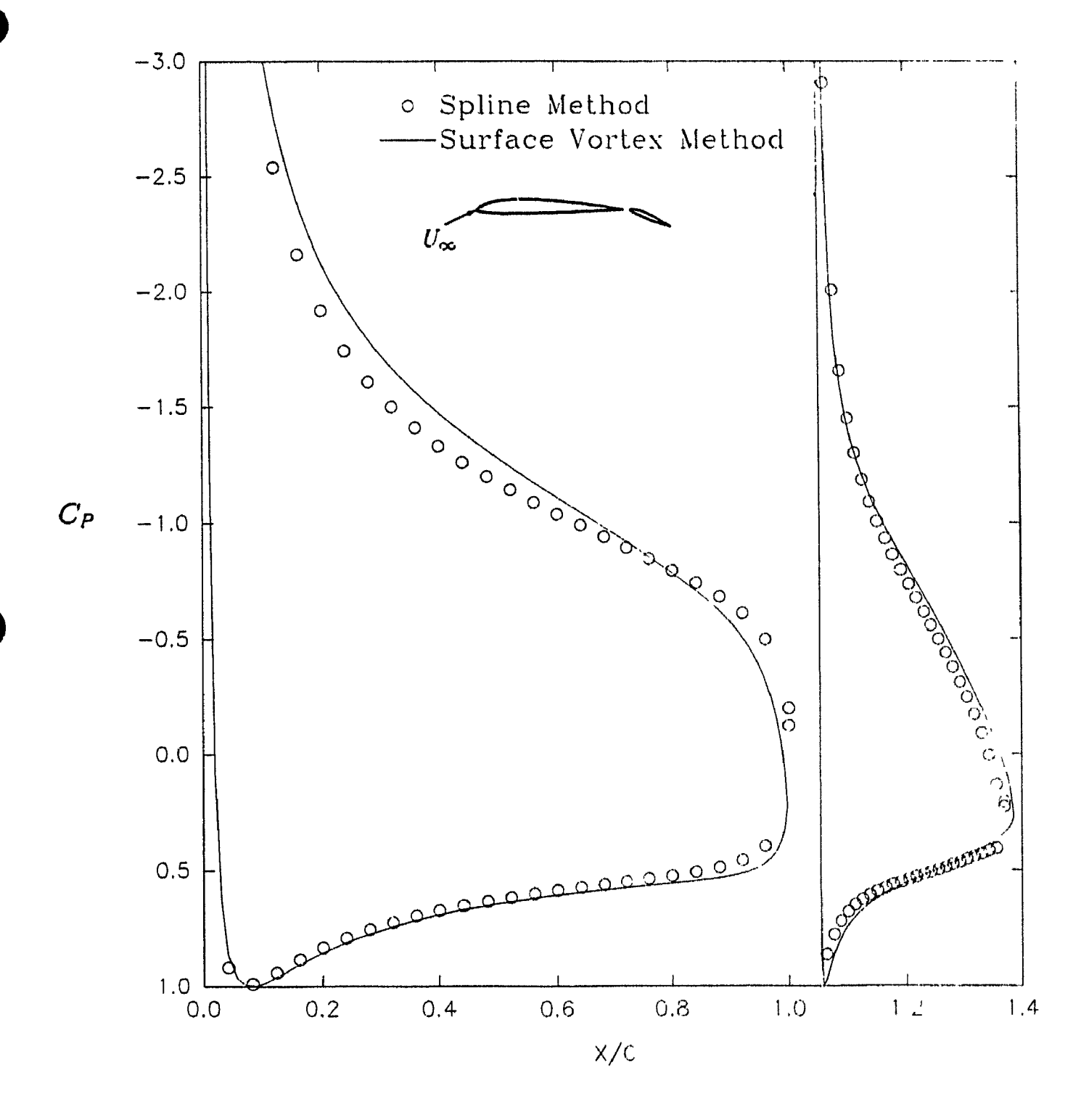


Figure 6.7: Pressure coefficients for an aerofoil with a rounded leading edge (e/c = 0.05, f/c = 0.02) and a 35% flap $(\alpha = 10^{\circ}, \beta = 15^{\circ})$.

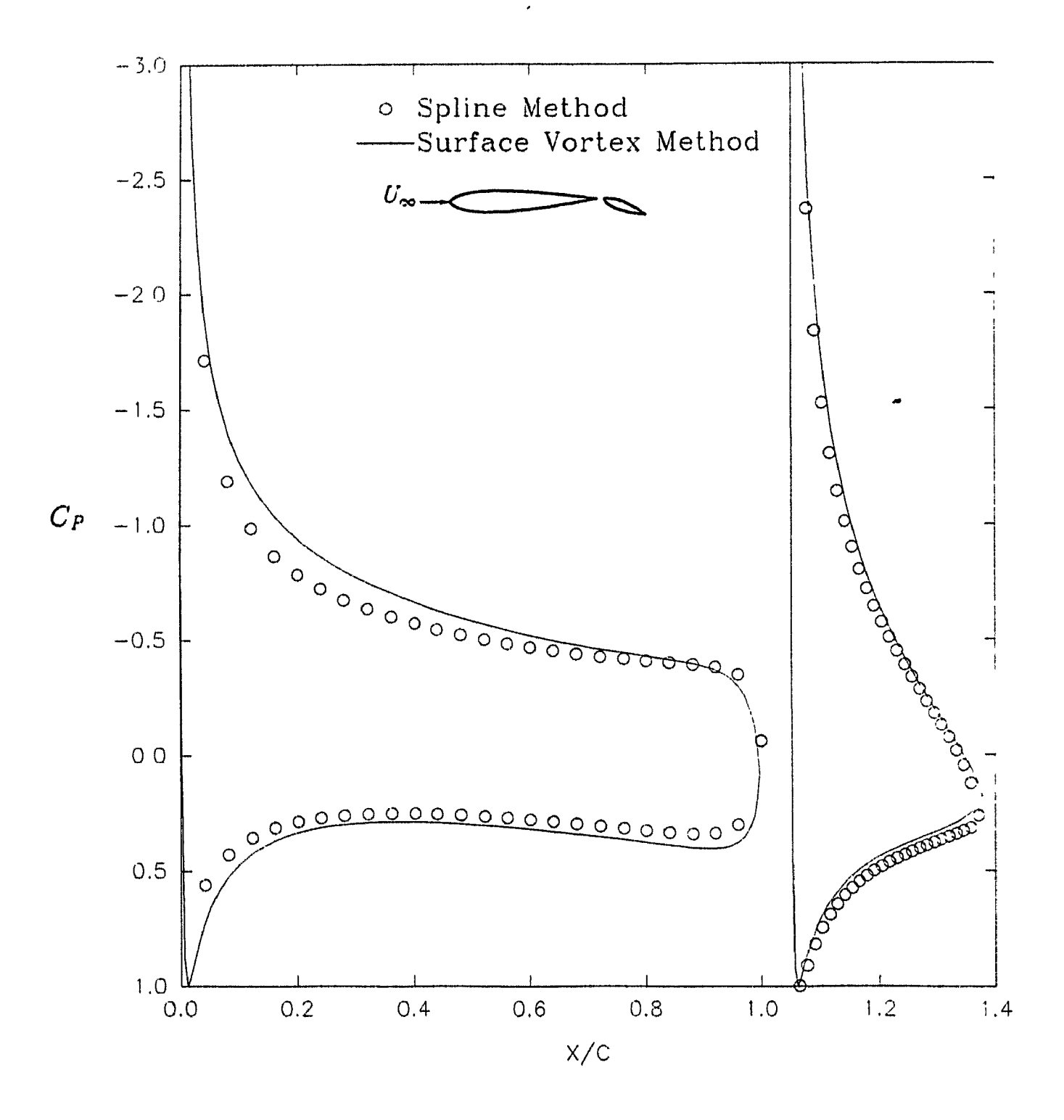


Figure 6.8: Pressure coefficients for a symmetrical Joukowski aerofoil (e/c = 0.05) with 35% flap ($\alpha = 0^{\circ}$, $\beta = 20^{\circ}$).

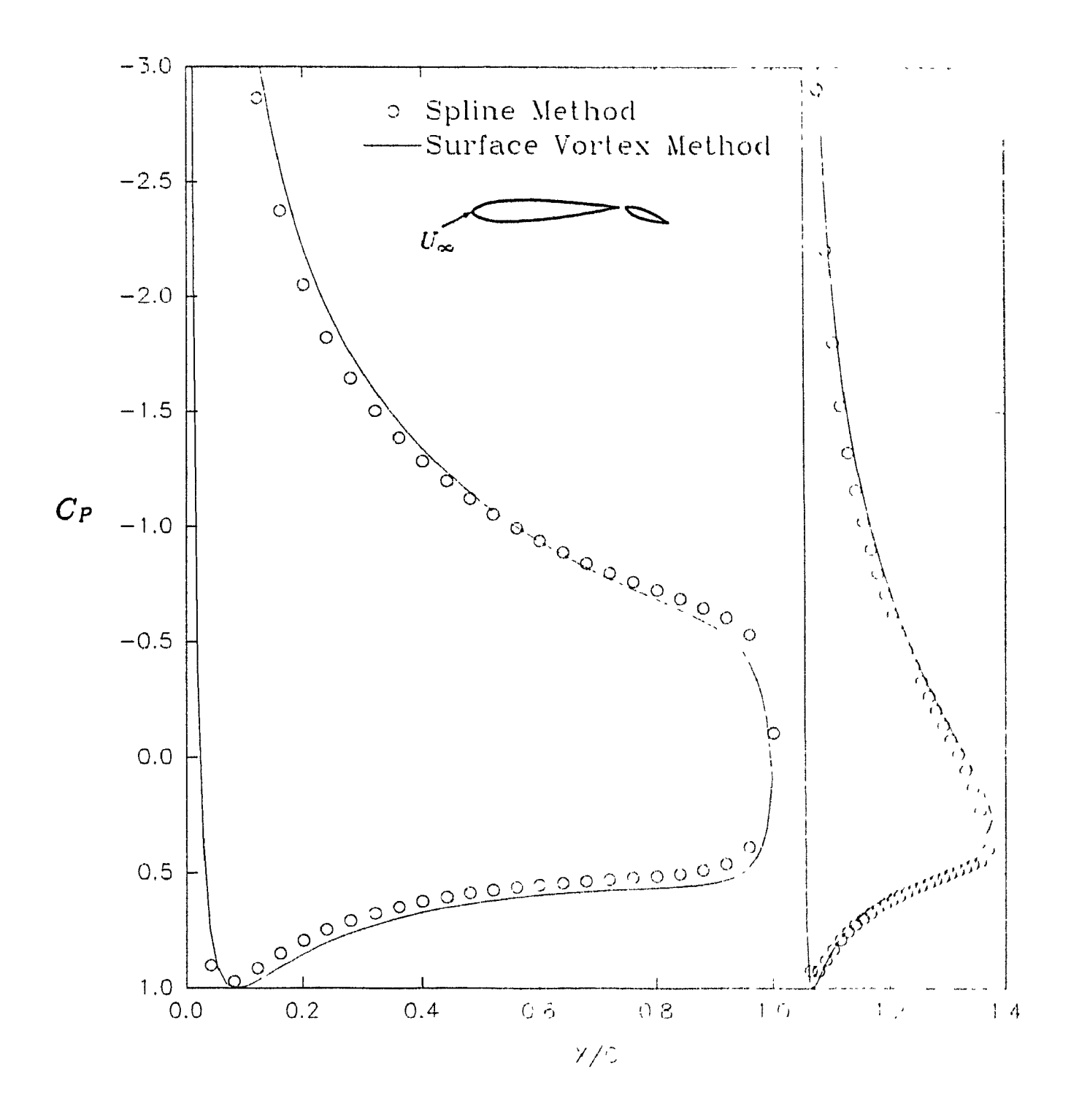


Figure 6.9: Pressure coefficients for a symmetrical Joukowski aerofoil (e/c = 0.05) with 35% flap ($\alpha = 10^{\circ}$, $\beta = 20^{\circ}$).

Chapter 7

Conclusions

In this thesis, the method of velocity singularities has been developed in conjunction with a cubic spline representation of the aerofoil contour slope. This spline representation has improved substantially the accuracy and stability of the solution in special problems such as the jet-flapped aerofoils; in these cases, the polynomial representation previously used can lead to high-order polynomials with large coefficients, which can have adverse effects on the accuracy of the solution. The spline-velocity singularity method developed in this respect has proven to lead to accurate solutions, computationally efficient, in all studied problems.

This method has been first validated for the cases of rigid and flexible aerofoils, in comparison with the previous solutions based on conformal transformations, or obtained by Thwaites [33] and Nielsen [23]. A very good argeement has been obtained between the present spline-velocity singularity solutions and the previous results, as well as with the results based on the polynomial representation [15,16,17].

The method has then been used to solve the flow past jet-flapped aerofoils, in which

case it has been characterized by a better accuracy and an enhanced stability of the solution in comparison with the polynomial representation used previously in conjunction with the same method of velocity singularities. The solutions obtained for the jet-flapped aerofoils have been compared with the theoretical solution obtained by Spence [27,28,29] and the experimental results obtained by Dimmock [32]; a good agreement has been found between these results.

The spline-velocity singularity method has also been extended to the problem of multi-element aerofoils. The solutions obtained for two-element aerofoils, represented by an aerofoil with a flap, have been compared with the results obtained by Seebohm and Newman [26] using a surface vortex method. A good agreement has been obtained for both cases of Karman-Trefftz and Joukowski aerofoils,

In all problems treated in this thesis, the spline-velocity singularity method has proven to have a definite advantage in comparison with the polynomial formulation, displaying a better accuracy and stability of the solution; this was found especially in the problems in which the aerofoil geometry is not known a priori and depends on the pressure distribution, as in the cases of the flexible or jet-flapped aerofoils.

Bibliography

- [1] Abbott, II. and Von Doenhoff, A.E., Theory of Wing Sections., Dover, New York, 1959.
- [2] Burden, R.L., Faires, D.J., *Numerical Analysis*, third ed., Prindle, Weber & Schmidt Publishers 1985.
- [3] Carafoli E., Mateescu D., and Nastase A., Wing Theory in Supersonic Flow., Pergamon Press, 1969, pp. 1-591.
- [4] Durand, W.F., Aerodynamic Theory., Vol II, Division E, Berlin, Julius Springer, 1935.
- [5] Glauert, H., The elements of aerofoil and airscrew theory, Cambridge University Press, second edition., 1926.
- [6] Goldstein, S., "Approximate Two-dimensional Aerofoil Theory," Curr. pap. A.R.C., Lond. 68-73, 1952.
- [7] Greenhalgh, S., Curtiss, H.C., and Smith, B., "Aerodynamic Properties of a Two Dimensional Inextensible Flexible Airfoil," AIAA Journal, Vol. 22, No. 7, 1984, pp. 865-870.

- [8] Halsey, N.D., "Potential flow analysis of multielement airfoils using conformal mapping." AIAA Journal, vol. 17, no. 12, 1979, pp. 1281-1288
- [9] Hess, J.L., Smith, A.M., "Calculation of Potential Flow about Arbitrary Bodies." Progress in Aeronautical Sciences, vol. 8, edited by D. Küchemann, Pergamon Press, 1967
- [10] Hunt, B., "The Panel method for subsonic aerodynamic flows." VKI. Lecture Scries, 1978, March 13-17.
- [11] Kuethe, A.M., and Chow, C.Y., Foundations of Aerodynamics, 4th ed., Wiley, New York, 1986, pp. 122-124.
- [12] Lancaster, P., Salkauskas, K., Curve and Surface Fitting Academic Press, 1986.
- [13] Mateescu, D., "A Hybrid Panel Method for Aerofoil Aerodynamics". Boundary Elements XII, Vol. 2, Applications in Fluid Mechanics and Field Problems, edited by M. Tanaka, C.A. Brebia, and T. Honma, Computational Mechanics Publications, Southampton, England, UK, and Springer-Verlag, Berlin, 1990, pp. 3-14.
- [14] Mateescu, D., "Wing and Conical Body of Arbitrary Cross-Section in Supersonic Flow", Journal of Aircraft., Vol. 24, No. 4, 1987, pp 239-247.
- [15] Mateescu, D. and Newman, B.G., "A New potential flow theory for thin aerofoils based on velocity singularities". Aerodynamics symposium of CASI, 1985.
- [16] Mateescu, D. and Newman, B.G., "Analysis of flexible-membrane aerofoils by a method of velocity singularities". Proc. of Tenth Canadian Congress of Applied Mechanics, 1985, pp B-187-88.

- [17] Mateescu, D. and Newman, B.G., "The analysis of flexible-membrane and jet-flapped aerofoils using a method of velocity singularities.", AIAA Journal, vol. 28, 1992, pp. 789-795.
- [18] Mateescu, D. and Nadeau, Y., "A Nonlinear Analytical Solution for Aerofoils in Irrotational Flow.", Proceedings of the Third International Congress of Fluid Mechanics, Cairo, Egypt, Vol. IV, 1990, pp. 1421-1432.
- [19] Milne-Thomson, L.M., Theoretical Aerodynamics. Dover Publications Inc., New York, 1958.
- [20] Nadeau, Y., "A Comparative Non-Linear Analytical and Numerical Irrotational Analysis of Aerofoils at High Angle of Attack", Masters Thesis, Department of Mechanical Engineering, McGill University, 1989.
- [21] Newman, B.G., "The Aerodynamics of Flexible Membranes.", Proceedings of the Indian Academy of Sciences, Vol. 5, 1982, pp. 107-129.
- [22] Newman, B.G., "Aerodynamic Theory for Membranes and Sails.", Progressive Aerospace Science, Vol. 24, 1987, pp. 1-27.
- [23] Nielsen, J.N., "Theory of Flexible Aerodynamic Surfaces", Journal of Applied Mechanics, Vol. 30, No. 9, 1963, pp.435-442.
- [24] O'Mahoney, R., and Smith, F.T., "On the Calculation of the Incompressible Flow Past an Aerofoil with a Jet Flap", Aeronautical Quarterly, Vol. 29, 1978, pp.44-59.
- [25] Seebohm, T., "The Prediction of Viscous Flow round Multiple-section Aerofoils.", PhD Thesis, Department of Mechanical Engineering, McGill University, 1972.

- [26] Seebohm, T., Newman, B.G., "A Numerical Method for Calculating Viscous Flow Round Multiple-Section Aerofoils.", Proc Royal Aeronautical Soc., January 1975 pp 176-188.
- [27] Spence, D.A., "The Lift Coefficient of a Thin Jet-Flapped Wing", Proceedings of the Royal Society, Series A, Vol. 238, 1956, pp.46-68.
- [28] Spence, D.A., "The Lift of a Thin Aerofoil with a Jet-Augmented Flap", Aeronautical Quarterly, Vol. 9, Nov. 1958, pp.287-299.
- [29] Spence, D.A., "Some Simple Results for Two-Dimensional Jet-Flapped Aerofoils", Aeronautical Quarterly, Vol. 9, Nov. 1958, pp.395-406.
- [30] Stewart, H.J., "A Simplified Two-Dimensional Theory of Thin Airfoils", Journal of Aeronautical Sciences, Vol. 9, No. 12, 1942, pp.452-456.
- [31] Theodorsen, T., "Theory of Wing Sections of Arbitrary Shape", N.A.C.A., Report 411, 1932.
- [32] Thwaites, B., Incompressible aerodynamics, Clarendon Press, Oxford, 1960.
- [33] Thwaites, B., "The Aerodynamic Theory of Sails: Two-Dimensional Sails", Proceedings of the Royal Society, Series A, Vol. 261, 1961, pp.402-422.
- [34] White, F., Fluid Mechanics, McGraw-Hill Book Company, University of Rhode Island, 2nd ed, 1986.
- [35] Bach, C.G., "Numerical Analysis I" Lecture Notes, McGill University, fall 1990.
- [36] Bach, C.G., "Numerical Analysis II" Lecture Notes, McGill University, winter 1991.

- [37] Mateescu, D., "Computational Aerodynamics" Lecture Notes, McGill University, winter 1991.
- [38] Mateescu, D., "Unsteady Aerodynamics" Lecture Notes, McGill University, fall 1990.
- [39] Mateescu, D., "Supersonic Aerodynamics" Lecture Notes, McGill University, fall 1990.
- [40] Newman, B.G., "Subsonic Aerodynamics" Lecture Notes, McGill University, fall 1991.

Appendix A

Conformal Transformation

A.1 Karman-Trefftz Transformation

Here the Karman-Trefftz transformation is explained. This transformation is defined by equation (2.13)

$$\frac{z - nb}{z + nb} = \left(\frac{\zeta - b}{\zeta + b}\right)^n. \tag{A.1}$$

If we let:

$$Me^{i\phi} = \left(\frac{\zeta - b}{\zeta + b}\right)^n,$$
 (A.2)

we can get an equation to solve for z (note: do not confuse ϕ with the velocity potential described in chapter 2):

$$z = -nb\left(\frac{Me^{i\phi} + 1}{Me^{i\phi} - 1}\right). \tag{A.3}$$

Breaking z into real and imaginary parts:

$$x = -nb\left(\frac{M^2 - 1}{M^2 - 2M\cos\phi + 1}\right),\tag{A.4}$$

$$y = \left(\frac{2nbM\sin\phi}{M^2 - 2M\cos\phi + 1}\right). \tag{A.5}$$

On the circle, M and ϕ are written as functions of θ ,

$$Me^{i\phi} = \left(\frac{\zeta - b}{\zeta + b}\right)^n = \left(\frac{r_1 e^{i\theta_1}}{r_2 e^{i\theta_2}}\right)^n,$$
 (A.6)

where

$$M = \left(\frac{r_1}{r_2}\right)^n, \quad \phi = n(\theta_1 - \theta_2). \tag{A.7}$$

At a point (P) on the circle r_1, r_2, θ_1 and θ_2 are obtained using the cosine law:

$$r_1^2 = b^2 + r^2 - 2rb\cos\theta, (A.8)$$

$$\theta_1 = \pi - \cos^{-1}\left(\frac{b^2 + r_1^2 - r^2}{2r_1b}\right),\tag{A.9}$$

$$r_2^2 = b^2 + r^2 - 2rb\cos(\pi - \theta), \tag{A.10}$$

$$\theta_2 = \cos^{-1}\left(\frac{b^2 + r_2^2 - r^2}{2r_2b}\right). \tag{A.11}$$

Now r and θ are the only unknowns. r can be obtained using

$$r = b(G(\theta) + H(\theta)), \tag{A.12}$$

where

$$G(\theta) = -\epsilon \cos \theta + (1 + \epsilon) \tan \gamma \sin \theta,$$
 (A.13)

$$H(\theta) = \sqrt{\frac{(1+\epsilon)^2}{\cos^2 \gamma} - F^2(\theta)}, \tag{A.14}$$

$$F(\theta) = -\epsilon \sin \theta - (1 + \epsilon) \tan \gamma \cos \theta. \tag{A.15}$$

Iteration for a y coordinate on the aerofoil at position x can be obtained by guessing θ using

$$\theta = \cos^{-1}\left(\frac{x}{2b}\right),\tag{A.16}$$

as an approximation. Now numerical analysis can be applied (i.e. using a secant method). To find a value for the unknown constant b, the chordlength is set to unity and b can be

Karman-Trefftz Aerofoil							
Aerofoil	Parameters			Characterisitics			
Type	ϵ	n	γ°	e/c	% chord	f/c	% chord
Circular Arc	0.000000	2.00	2.865	0.00		0.025	50
Circular Arc	0.000000	2.00	5.711	0.00		0.050	50
Lenticular	0.002931	1.94	0.000	0.05	50	0.000	
Lenticular	0.005807	1.88	0.000	0.10	50	0.000	
Cambered Lenticular	0.002911	1.94	1.178	0.05	50	0.010	50
Cresent Shaped	0.002806	1.94	2.944	0.05	50	0.025	50
Cresent Shaped	0.004788	1.88	6.028	0.10	50	0.050	50
Symmetrical Joukowski	0.040226	2.00	0.000	0.05	22	0.000	
Symmetrical Joukowski	0.083915	2.00	0.000	0.10	22	0.000	
Cambered Joukowski	0.040200	2.00	2.292	0.05	22	0.025	50

Table A.1: Summary of aerofoil parameters used in Karman-Trefftz transformation.

evaluated using

$$c = 2nb\frac{\chi}{1-\chi}, \tag{A.17}$$

where
$$\chi = \left(\frac{\epsilon}{1+\epsilon}\right)^n$$
. (A.18)

A summary of the different aerofoils used in this thesis are given by table A.1.

A.2 Flow Around A Circle With Circulation

To find the velocity components we need to define the flow around the circle by a complex potential:

$$F(z) = U_{\infty} \left(\zeta^* + \frac{b^2}{\zeta^*} \right) - \frac{i \Gamma \ln(\zeta^*)}{2\pi}, \tag{A.19}$$

where $\zeta^* = re^{i\theta^*}$, r is the radius at which flow is to be defined, $\theta^* = \theta - \alpha$, and Γ is the circulation around the aerofoil. Taking the derivative of the complex potential gives the

complex conjugate function of the circle:

$$F'(\zeta^*) = U_{\infty} \left(1 - \frac{a^2}{\zeta^{*2}} - \frac{i\Gamma}{2\pi U_{\infty} \zeta^*} \right). \tag{A.20}$$

Using the Kutta condition by imposing the perturbation velocities to be zero at the trailing edge, the circulation around the aerofoil can be determined as

$$\Gamma = -4\pi a U_{\infty} \sin(\alpha + \gamma). \tag{A.21}$$

Taking the modulus of the complex velocity potential

$$|F'(\zeta^*)| = 2U_{\infty}(\sin(\theta - \alpha) + \sin(\alpha + \gamma)), \tag{A.22}$$

the flow field around the aerofoil is obtained by:

$$V = |F'(z)| = \frac{|F'(\zeta^*)|}{\left|\frac{d\zeta}{dz}\right|}.$$
 (A.23)

Now pressure coefficients can be solved for using equation 2.10.

Appendix B

Perturbation Velocity Formulation

B.1 The Antisymmetrical Velocity field

B.1.1 Complex Conjugate Disturbance Velocity Function

As wrote in Section 2.3.2 the complex conjugate perturbation velocity function:

$$W(z) = \left\{ -v(0) - \frac{2}{\pi} \underbrace{\int_0^c v'(s) \cos^{-1} \sqrt{s} ds}_{I_0} \right\} \sqrt{\frac{c-x}{x}} - \frac{2}{\pi} \underbrace{\int_0^c v'(s) \cosh^{-1} \sqrt{\frac{s(c-x)}{c(s-x)}} ds}_{I_1}.$$

Breaking the complex conjugate perturbation velocity into smaller integrals and doing the integration by parts:

• Integral I₀:

$$\int_0^c v'(s)\cos^{-1}\sqrt{s}ds = \left[v(s)\cos^{-1}\sqrt{s}\right]_0^c + \frac{1}{2}\int_0^c \frac{v(s)}{\sqrt{s(c-s)}}ds,$$
$$= -\frac{\pi}{2}v(0) + \frac{1}{2}\int_0^c \frac{v(s)}{\sqrt{s(c-s)}}ds.$$

• Integral I₁:

$$\int_0^c v'(s) \cosh^{-1} \sqrt{\frac{s(c-x)}{c(s-x)}} ds$$

$$= \lim_{\epsilon \to 0} \left\{ \underbrace{\int_0^{x-\epsilon} v'(s) \cosh^{-1} \sqrt{\frac{s(c-x)}{c(s-x)}} ds}_{I_2} + \underbrace{\int_{x+\epsilon}^c v'(s) \cosh^{-1} \sqrt{\frac{s(c-x)}{c(s-x)}} ds}_{I_3} \right\}.$$

• Integral I2:

$$\int_0^{x-\epsilon} v'(s) \cosh^{-1} \sqrt{\frac{s(c-x)}{c(s-x)}} ds = \left[i \frac{\pi}{2} v(s)\right]_0^{x-\epsilon} + \int_0^{x-\epsilon} v(s) \sinh^{-1} \sqrt{\frac{s(c-x)}{c(s-x)}} ds.$$

• Integral I_3 :

$$\int_{x+\epsilon}^{c} v'(s) \cosh^{-1} \sqrt{\frac{s(c-x)}{c(s-x)}} ds = \left[v(s) \cosh^{-1} \sqrt{\frac{s(c-x)}{c(s-x)}} \right]_{x+\epsilon}^{c} + \frac{1}{2} \int_{x+\epsilon}^{c} v(s) \sqrt{\frac{x(c-x)}{c(s-x)}} \frac{ds}{s-x}.$$

• From integrals I_2 and I_3 :

$$\lim_{\epsilon \to 0} \left\{ v(x - \epsilon) \sinh^{-1} \sqrt{\frac{(x - \epsilon)(c - x)}{c \cdot \epsilon}} - v(x + \epsilon) \cosh^{-1} \sqrt{\frac{(x + \epsilon)(c - x)}{c \cdot \epsilon}} \right\} = 0.$$

Putting these integrals into the complex conjugate perturbation velocity equation:

$$W(x) = \sqrt{\frac{c-x}{x}} \left\{ -v(0) - \frac{2}{\pi} \left(-\frac{\pi}{2} v(0) + \frac{1}{2} \int_0^c \frac{v(s) ds}{\sqrt{s(c-s)}} \right) \right\} - \frac{2}{\pi} \left\{ \frac{1}{2} \int_0^c v(s) \sqrt{\frac{x(c-x)}{c(s-x)}} \frac{ds}{s-x} + i \frac{\pi}{2} (v(s) - v(0)) \right\}.$$

Taking real parts for $u_A(x)$ where the A subscript stands for antisymmetrical velocities:

$$u_A(x) = -\frac{1}{\pi} \sqrt{\frac{c-x}{x}} \int_0^c v_A(s) \sqrt{\frac{s}{c-s}} \frac{ds}{s-x}.$$
 (B.1)

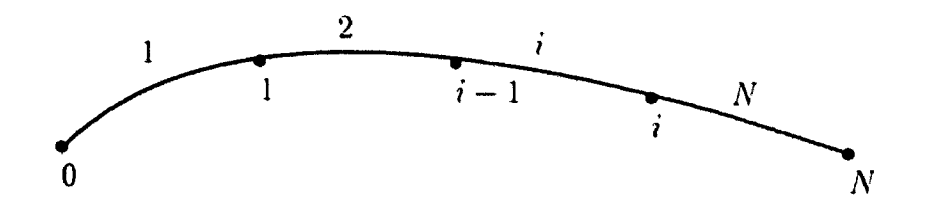


Figure B.1: Geometric notations of camberline panels used for the cubic spline representation of the aerofoil camberline

B.1.2 Spline Formulation

Using linear theory as defined in Section 3.1.1 a cubic spline approximation is used to find the velocity $u_A(x)$:

$$h'(x) = H_0^i + H_1^i \Delta x_i + H_2^i (\Delta x_i)^2 + H_3^i (\Delta x_i)^3,$$
 (B.2)

$$= \sum_{k=0}^{3} H_k^i (\Delta x_i)^k, \tag{B.3}$$

where
$$\Delta x_i = x_i - x_{i-1}$$
. (B.4)

 H_k^i are spline coefficients as defined in Appendix C. Now $v_A(x)$ can be written using equation (B.3) and linear theory:

$$v_A(x) = -\alpha + \sum_{k=0}^{3} H_k^i(\Delta x_i)^k.$$
 (B.5)

This can now be used to solve for $u_A(x)$:

$$u_{A}(x) = -\frac{1}{\pi} \sqrt{\frac{c-x}{x}} \int_{0}^{c} \left(-\alpha + \sum_{i=1}^{N} \sum_{k=0}^{3} H_{k}^{i} (\Delta x_{i})^{k}\right)_{x=s} \sqrt{\frac{s}{c-s}} \frac{ds}{s-x},$$

$$= \underbrace{\frac{\alpha}{\pi} \sqrt{\frac{c-x}{x}} \int_{0}^{c} \sqrt{\frac{s}{c-s}} \frac{ds}{s-x}}_{I_{4}} - \underbrace{\frac{1}{\pi} \sqrt{\frac{c-x}{x}} \sum_{i=1}^{N} \sum_{k=0}^{3} H_{k}^{i} \int_{x_{i-1}}^{x_{i}} (s-x_{i-1})^{k} \sqrt{\frac{s}{c-s}} \frac{ds}{s-x}}_{I_{5}},$$

$$I_4 = \frac{\alpha}{\pi} \sqrt{\frac{c-x}{x}} \int_0^c \sqrt{\frac{s}{c-s}} \frac{ds}{s-x},$$

$$= \frac{\alpha}{\pi} \sqrt{\frac{c-x}{x}} \left\{ \int_{0}^{c} \frac{ds}{\sqrt{s(c-s)}} + x \int_{0}^{c} \frac{ds}{\sqrt{s(c-s)(s-x)}} \right\},$$

$$= \frac{\alpha}{\pi} \sqrt{\frac{c-x}{x}} \left\{ \left[\cos^{-1} \left(\frac{c-2s}{c} \right) \right]_{0}^{c} - \frac{2x}{\sqrt{x(c-x)}} \int_{0}^{c} -\frac{1}{2} \sqrt{\frac{x(c-x)}{s(c-x)}} \frac{ds}{s-x} \right\},$$

$$= \alpha \sqrt{\frac{c-x}{x}},$$

$$I_{5} = \frac{1}{\pi} \sqrt{\frac{c-x}{x}} \sum_{i=1}^{N} \sum_{k=0}^{3} H_{k}^{i} K_{k}^{i}(x),$$

$$\text{where } K_{k}^{i}(x) = \int_{x_{i-1}}^{x_{i}} (s-x_{i-1})^{k} \sqrt{\frac{s}{c-s}} \frac{ds}{s-x}.$$

Now the perturbation velocity in the x direction can be written:

$$u_A(x) = \sqrt{\frac{c-x}{x}} \left(\alpha - \frac{1}{\pi} \sum_{i=1}^{N} \sum_{k=0}^{3} H_k^i K_k^i(x) \right).$$
 (B.6)

B.1.3 Derivation of Integral $K_k^i(x)$

The integral for $K_k^i(x)$ becomes quite tedious, long and difficult. This is probably the largest downfall to using the spline velocity method.

$$K_{k}^{i}(x) = \int_{x_{i-1}}^{x_{i}} (s - x_{i-1})^{k} \sqrt{\frac{s}{c - s} \frac{ds}{s - x}},$$

$$\det (s - x_{i-1})^{k} = \sum_{q=0}^{k} C_{q}^{k} s^{k-q} x_{i-1}^{q},$$

$$K_{k}^{i}(x) = \sum_{q=0}^{k} C_{q}^{k} x_{i-1}^{q} \int_{x_{i-1}}^{x_{i}} \frac{s^{k-q+1}}{\sqrt{s(c-s)}} \frac{ds}{s - x},$$

$$\det (s^{k-q+1} - x^{k-q+1}) = (s - x) \sum_{l=0}^{k-q} s^{k-q-l} x^{l},$$

$$K_{k}^{i}(x) = \sum_{q=0}^{k} C_{q}^{k} x_{i-1}^{q} \left\{ \sum_{l=0}^{k-q} x^{l} \int_{x_{i-1}}^{x_{i}} \frac{s^{k-q-l} ds}{\sqrt{s(c-s)}} + x^{k-q+1} \int_{x_{i-1}}^{x_{i}} \frac{ds}{\sqrt{s(c-s)(s-x)}} \right\},$$

$$I_{7} = x^{k-q+1} \int_{x_{i-1}}^{x_{i}} \frac{ds}{\sqrt{s(c-s)(s-x)}},$$

$$= \frac{-2x^{k-q+1}}{\sqrt{x(c-x)}} \int_{x_{i-1}}^{x_{i}} -\frac{1}{2} \sqrt{\frac{x(c-x)}{s(c-s)}} \frac{ds}{s-x},$$

$$= \frac{-2x^{k-q+1}}{\sqrt{x(c-x)}} \begin{cases} \cosh^{-1} \sqrt{\frac{s(c-x)}{c(s-x)}} & \text{for } s > x \\ \sinh^{-1} \sqrt{\frac{s(c-x)}{c(x-s)}} & \text{for } x > s \end{cases}.$$

Integral number I_7 will be identified by λ_p . Integral number I_6 must be integrated separately as k is changed, and will be identified by Λ_p :

$$p = 0$$

$$\Lambda_0 = \int_{x_{i-1}}^{x_i} \frac{ds}{\sqrt{s(c-s)}} = \left[\cos^{-1}\left(\frac{c-2s}{c}\right)\right]_{x_{i-1}}^{x_i}.$$

•
$$p = 1$$

$$\Lambda_1 = \int_{x_{i-1}}^{x_i} \frac{sds}{\sqrt{s(c-s)}} = \left[\frac{c}{2} \cos^{-1} \left(\frac{c-2s}{c} \right) - \sqrt{s(c-s)} \right]_{x_{i-1}}^{x_i}.$$

•
$$p = 2$$

$$\Lambda_2 = \int_{x_{i-1}}^{x_i} \frac{s^2 ds}{\sqrt{s(c-s)}} = \left[\frac{3c^2}{8} \cos^{-1} \left(\frac{c-2s}{c} \right) - \left(\frac{s}{2} + \frac{3c}{4} \right) \sqrt{s(c-s)} \right]_{x_{i-1}}^{x_i}.$$

$$p = 3$$

$$\Lambda_3 = \int_{x_{i-1}}^{x_i} \frac{s^3 ds}{\sqrt{s(c-s)}} = \left[\frac{5c^3}{16} \cos^{-1} \left(\frac{c-2s}{c} \right) - \left(\frac{s^2}{3} + \frac{5cs}{12} + \frac{5c^2}{8} \right) \sqrt{s(c-s)} \right]_{x_{i-1}}^{x_i}.$$

Now $K_k^i(x)$ can be written:

$$K_k^i(x) = \sum_{q=0}^k C_k^q x_{i-1}^q \left\{ \sum_{l=0}^{k-q} x^l \Lambda_{k-q-l} + \lambda_{k-q} \right\}.$$
 (B.7)

The C_k^q represents the coefficients of the binomial expression of $(s-x_{i-1})^k$,

$$C_k^q = (-1)^q \frac{k!}{q!(k-q)!},$$
 (B.8)

Putting this into $K_k^i(x)$, written out in long form:

$$K_0^{i}(x) = \Lambda_0 + \lambda_0$$

$$K_1^{i}(x) = \Lambda_1 + x\Lambda_0 + \lambda_1 - x_{i-1}(\Lambda_0 + \lambda_0)$$

$$K_2^{i}(x) = \Lambda_2 + x\Lambda_1 + x^2\Lambda_0 + \lambda_2 - 2x_{i-1}(\Lambda_1 + x\Lambda_0 + \lambda_1) + x_{i-1}^2(\Lambda_0 + \lambda_0)$$

$$K_3^{i}(x) = \Lambda_3 + x\Lambda_2 + x^2\Lambda_1 + x^3\Lambda_0 + \lambda_3 - 3x_{i-1}(\Lambda_2 + x\Lambda_1 + x^2\Lambda_0 + \lambda_2) + 3x_{i-1}^2(\Lambda_1 + x\Lambda_0 + \lambda_1) - x_{i-1}^3(\Lambda_0 + \lambda_0).$$

B.2 The Symmetrical Velocity Field

B.2.1 Complex Conjugate Disturbance Velocity Function

The symmetrical velocity field described in Section 2.3.3 leads us to:

$$W_S(z) = \frac{1}{\pi} \left\{ v(0) \ln z + \int_0^c \left(\frac{dv}{dx} \right)_{x=s} \ln(z-s) ds - v(c) \ln(z-c) \right\}.$$
 (B.9)

Because we are dealing with the symmetrical velocity field the chordlength can be set to unity (the chordlength changes only when using the jet flapped antisymmetrical velocities):

$$\int_0^1 \left(\frac{dv}{dx}\right)_{x=s} \ln(x-s) ds = [v(s)\ln(x-s)]_0^1 + \int_0^1 v(s) \frac{ds}{s-x}.$$
 (B.10)

Putting the relation $v(s) \ln(x-s) = v(s)(i\pi + \ln(s-x))$ for s > x, and the results from equation (B.10) into equation (B.9):

$$= \lim_{\epsilon \to 0} \left\{ \left[v(s) \ln(x-s) \right]_0^{x-\epsilon} + \left[v(s) (i\pi + \ln(s-x)) \right]_{x+\epsilon}^1 \right\} + \int_0^1 v(s) \frac{ds}{s-x}$$

$$= v(1) \ln(1-x) - v(0) \ln(x) + i\pi (v(1)-v(s)) + \int_0^1 v(s) \frac{ds}{s-x}.$$

After rearranging:

$$W_S(x) = \frac{1}{\pi} \int_0^1 v(s) \frac{ds}{s - x} - iv(x).$$
 (B.11)

For the velocity $u_S(x) =$, the real part of $W_S(x)$ is taken:

$$u_S(x) = -\frac{1}{\pi} \int_0^1 v(s) \frac{ds}{s - x}.$$
 (B.12)

B.2.2 Spline Formulation

Using linear theory as defined in Section 3.1.1 a cubic spline approximation is used to find the velocity $u_s(x)$:

$$\begin{split} g'(x) &= G_0^i + G_1^i \Delta x_i + G_2^i (\Delta x_i)^2 + G_3^i (\Delta x_i)^3, \\ &= \sum_{k=0}^3 G_k^i (\Delta x_i)^k, \\ &\text{where } \Delta x_i = x_i - x_{i-1}, \\ &\text{and } G_k^i \text{ are spline coefficients.} \end{split}$$

Now $v_S(x)$ can be written using linear theory:

$$v_S(x) = \sum_{k=0}^3 G_k^i (\Delta x_i)^k.$$

This can now be used to solve for $u_S(x)$:

$$u_{S}(x) = -\frac{1}{\pi} \int_{0}^{1} \left(\sum_{k=0}^{3} G_{k}^{i} (\Delta x_{i})^{k} \right)_{x=s} \frac{ds}{s-x},$$

$$= -\frac{1}{\pi} \sum_{i=1}^{N} \sum_{k=0}^{3} G_{k}^{i} \int_{x_{i-1}}^{x_{i}} (s-x_{i-1})^{k} \frac{ds}{s-x},$$

$$= -\frac{1}{\pi} \sum_{i=1}^{N} \sum_{k=0}^{3} G_{k}^{i} J_{k}^{i}(x),$$
where $J_{k}^{i}(x) = \int_{x_{i-1}}^{x_{i}} (s-x_{i-1})^{k} \frac{ds}{s-x}.$

B.2.3 Derivation of Integral $J_k^i(x)$

The integration for $J_k^i(x)$:

$$J_{k}^{i}(x) = \int_{x_{i-1}}^{x_{i}} (s - x_{i-1})^{k} \frac{ds}{s - x},$$

$$\det (s - x_{i-1})^{k} = \sum_{q=0}^{k} C_{q}^{k} s^{k-q} x_{i-1}^{q},$$

$$J_{k}^{i}(x) = \sum_{q=0}^{k} C_{q}^{k} x_{i-1}^{q} \int_{x_{i-1}}^{x_{i}} s^{k-q} \frac{ds}{s - x},$$

$$\det (s^{k-q} - x^{k-q}) = (s - x) \sum_{l=0}^{k-q-1} s^{k-q-l-1} x^{l},$$

$$J_{k}^{i}(x) = \sum_{q=0}^{k} C_{q}^{k} x_{i-1}^{q} \left\{ \sum_{l=0}^{k-q-1} x_{i-1}^{l} \int_{x_{i-1}}^{x_{i}} s^{k-q-l-1} ds + \underbrace{x_{i-1}^{k-q} \int_{x_{i-1}}^{x_{i}} \frac{ds}{s - x}}_{l_{9}} \right\},$$

$$I_{8} = \sum_{l=0}^{k-q-1} x_{i-1}^{l} \int_{x_{i-1}}^{x_{i}} s^{k-q-l-1} ds,$$

$$= \sum_{l=0}^{k-q-1} \frac{x_{i-1}^{l}}{k - q - l} (x_{i+1}^{k-q-l} - x_{i-1}^{k-q-l}),$$

$$I_{9} = x_{i-1}^{k-q} \int_{x_{i-1}}^{x_{i}} \frac{ds}{s - x},$$

$$= x_{i-1}^{k-q} \ln \left(\frac{x_{i-1} - x}{x_{i-1} - x} \right).$$

Noting that for integral I_9 , is restricted to no x between x_{i-1} and x_i . If this occurs:

$$I_{9} = x_{i-1}^{k-q} \left[-\int_{x_{i-1}}^{x-\epsilon} \frac{ds}{x-s} + \int_{x+\epsilon}^{x_{i}} \frac{ds}{s-x} \right],$$

$$= x_{i-1}^{k-q} \ln \left(\frac{x_{i}-x}{x-x_{i-1}} \right),$$
Hence $I_{9} = x_{i-1}^{k-q} \ln \left| \frac{x_{i}-x}{x_{i-1}-x} \right|.$

Putting integrals I_8 and I_9 into $J_k^i(x)$:

$$J_k^i(x) = \sum_{q=0}^k C_k^q x_{i-1}^q \left\{ \sum_{l=0}^{k-q-1} \frac{x_{i-1}^l}{k-q-l} (x_i^{k-q-l} + x_{i-1}^{k-q-l}) + x_{i-1}^{k-q} \ln \left| \frac{x_i - x}{x_{i-1} - x} \right| \right\}.$$
 (B.13)

B.3 Modified Expansion Field - Local Linearization

For Symmetrical aerofoils with rounded leading edges, a modified expansion field is required to treat this special case. This modified expansion:

$$v_S(x) = \sqrt{\frac{1-x}{x}} \sum_{k=0}^{3} G_k^i \Delta x_i^k,$$
 (B.14)

which treats the Kutta condition at the trailing edge and helps treat the infinite velocity at the leading edge. Putting the spline approximation into equation (B.12)

$$u_S(x) = -\frac{1}{\pi} \sum_{i=1}^{N} \sum_{k=0}^{3} G_k^i \int_{x_{i-1}}^{x_i} \sqrt{\frac{1-s}{s}} (s - x_{i-1})^k \frac{ds}{s-x},$$
 (B.15)

where the integral is represented by $J^{i}_{M_{k}}(x)$, now

$$u_S = -\frac{1}{\pi} \sum_{i=1}^{N} \sum_{k=0}^{3} G_k^i J_{M_k}^i(x).$$
 (B.16)

B.3.1 Derivation of Integral $J_{M_k}^i(x)$

$$J_{M_k}^i(x) = \int_{x_{i-1}}^{x_i} \sqrt{\frac{1-s}{s}} (s-x_{i-1})^k \frac{ds}{s-x},$$

$$\det (1-s) = (1-x) - (s-x),$$

$$= (1-x) \int_{x_{i-1}}^{x_i} \frac{(s-x_{i-1})^k}{\sqrt{s(1-s)}} \frac{ds}{s-x} - \frac{(s-x_{i-1})^k}{\sqrt{s(1-s)}} ds,$$

$$Using (s-x_{i-1})^k = \sum_{q=0}^k C_q^k s^{k-q} x_{i-1}^q,$$

$$= \sum_{q=0}^k C_q^k x_{i-1}^q \left\{ (1-x) \int_{x_{i-1}}^{x_i} \frac{s^{k-q}}{\sqrt{s(1-s)}} \frac{ds}{s-x} - \int_{x_{i-1}}^{x_i} \frac{s^{k-q}}{\sqrt{s(1-s)}} ds \right\}.$$

The last two integrals were already defined in Section B.1.3. Collecting all the integrals:

$$J_{M_k}^i(x) = \sum_{q=0}^k C_q^k x_{i-1}^q \left\{ (1-x) \left(\sum_{l=0}^{k-q-1} x^l \Lambda_{k-q-l-1} - \frac{\lambda_{k-q}}{x} \right) - \Lambda_{k-q} \right\}.$$
 (B.17)

Appendix C

Cubic Spline Formulation

C.1 Introduction

A series of different types of splines were researched and two types were found to give the best accuracy versus difficulty.

C.1.1 Cubic Spline Using Tri-Diagonal Matrix

This type of spline gives good accuracy without having to know the second derivative of the camberline coefficients h(x) and g(x). We start with a set of coordinates $\langle x, y \rangle$, where we want to find specific values of y at a given x coordinate, hence:

$$y = f(x). (C.1)$$

A function where the fourth derivative is zero is desired so a cubic order will be the best.

$$y_{i+1} = A_i + B_i \Delta x_i + C_i \Delta x_i^2 + D_i \Delta x_i^3, \tag{C.2}$$

where
$$\Delta x_i = x_i - x_{i-1}$$
. (C.3)

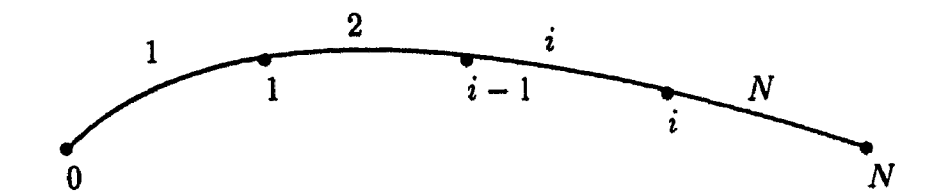


Figure C.1: Geometric notations of camberline panels used for the cubic spline representation of the aerofoil camberline

This cubic starts at point (i) and ends at (i + 1). This leads to (N) splines for (N + 1) points (Figure C.1 shows how the panels and points are numbered in this case). If the spline is evaluated at $x = x_i$:

$$y_i = A_i. (C.4)$$

Now B_i , C_i , and D_i are unknowns, requiring 3N-3 equations. Using equation (C.2), demanding continuity of the first and second derivatives:

$$y'_{i+1} = B_i + 2\Delta x_i C_i + 3\Delta x_i^2 D_i,$$
 (C.5)

$$y_{i+1}'' = 2C_i + 6\Delta x_i D_i, \tag{C.6}$$

setting:

$$y_i'(x_{i+1}) = y_{i+1}'(x_{i+1}),$$
 (C.7)

$$y_i''(x_{i+1}) = y_{i+1}''(x_{i+1}),$$
 (C.8)

which gives:

$$B_{i+1} = B_i + 2\Delta x_i C_i + 3\Delta x_i^2 D_i, \tag{C.9}$$

$$2C_{i+1} = 2C_i + 6\Delta x_i D_i. (C.10)$$

Two more conditions are now required to solve for the solution. By imposing and putting the second derivative to be zero at the ends (ie i = 0, i = N):

$$D_i = \frac{\Delta x_i}{3} (C_{i+1} - C_i), \tag{C.11}$$

$$B_i = \frac{y_{i+1} - y_i}{\Delta x_i} - \frac{\Delta x_i}{3} (C_{i+1} + 2C_i). \tag{C.12}$$

Using these conditions and putting into equation (C.7):

$$\Delta x_i \ C_i + 2(\Delta x_i + \Delta x_{i+1}) C_{i+1} + \Delta x_{i+1} \ C_{i+2} = Rhs_i, \tag{C.13}$$

$$Rhs_{i} = 3 \left[\frac{y_{i+2} - y_{i+1}}{\Delta x_{i+1}} - \frac{y_{i+1} - y_{i}}{\Delta x_{i}} \right]. \tag{C.14}$$

This results in a tri-diagonal matrix:

The spline can be changed by using different end conditions and redefining equations (C.12), (C.11), and (C.7).

For writing formulas the orientation of the spline is also found

$$y(x) = \sum_{k=0}^{3} H_k^i \Delta x_i^k, \tag{C.16}$$

where the spline coefficients A_i , B_i ,... are represented by H_0^i , H_1^i ,.... This is done so the coefficients can be written in a simple summation.

C.1.2 Cubic Spline Using Second Derivatives

This type of spline obtains very accurate results without any matrix operations. The downfall of the method is the need for the second derivative of the camberline coefficients h(x) and g(x). If the aerofoil is a function of x, the derivatives can be easily obtained, otherwise differencing methods have to be used. Differencing methods sometimes tend to lose accuracy near the ends (this is where the tri-diagonal matrix may be a better choice).

This method starts similarly to the tri-diagonal method using y as a function of x as in equation (C.1). This function may be written as equation (C.2), where its derivative is written as equation (C.5). If we evaluate these two functions at $x = x_i$:

$$A_i = y_i, (C.17)$$

$$B_i = y_i'. (C.18)$$

Evaluating these equations at $x = x_{i+1}$:

$$y_{i+1} - y_i - y_i' \Delta x_i = C_i \Delta x_i^2 + D_i \Delta x_i^3, \qquad (C.19)$$

$$y'_{i+1} - y'_i = 2C_i \Delta x_i + 3D_i \Delta x_i^2.$$
 (C.20)

Combining these two equations:

$$C_{i} = \left(\frac{3(y_{i+1} - y_{i})}{\Delta x_{i}^{2}}\right) - \left(\frac{y'_{i+1} + 2y'_{i}}{\Delta x_{i}}\right), \tag{C.21}$$

$$D_{i} = \left(\frac{y'_{i+1} + y'_{i}}{\Delta x_{i}^{2}}\right) - \left(\frac{2(y_{i+1} - y_{i})}{\Delta x_{i}^{3}}\right). \tag{C.22}$$

Appendix D

Imaginary Part of the Perturbation Functions

D.1 Imaginary Part of the Ridge Function

The ridge function denoted as $\cosh^{-1}\sqrt{\frac{(c-z)(s-c_o)}{(c-c_o)(s-z)}}$ becomes purely imaginary outside of the aerofoil regime. This becomes important when analyzing multi-section aerofoils. The hyperbolic cosh function is defined as:

$$\cosh^{-1}R = \ln(R + \sqrt{R^2 - 1}). \tag{D.1}$$

When the limits of z become outside of the aerofoil (ie z > c and $z < c_o$) the function $\sqrt{\frac{(s-c_o)(c-z)}{(c-c_o)(s-z)}}$ is less than one. Allowing this function to be denoted by R the upper formula becomes:

$$= \ln(R \pm i\sqrt{1 - R^2}), \tag{D.2}$$

$$= \ln(iR \pm \sqrt{1 - R^2}) - \ln i, \qquad (D.3)$$

$$= \pm i \sin^{-1} R \pm i \frac{\pi}{2}, \tag{D.4}$$

$$= \pm i \cos^{-1} R. \tag{D.5}$$

This function also poses a problem while s < z < c. This is on the aerofoil itself and doesn't contribute to the imaginary velocity field but contributes to the axial velocity function. The function $\sqrt{\frac{(s-c_o)(c-z)}{(c-c_o)(s-z)}}$ itself becomes imaginary giving $i\sqrt{\frac{(s-c_o)(c-z)}{(c-c_o)(z-s)}}$ which will again be denoted by R:

$$= \ln(iR + \sqrt{-R^2 - 1}), \tag{10.6}$$

$$= \ln(R \pm \sqrt{1 + R^2}) + \ln \iota, \tag{10.7}$$

$$= \sinh^{-1}R + \iota \frac{\pi}{2}. \tag{D.8}$$

These derivations are summed up in Table 6.1.

D.2 Imaginary Part of the Antisymmetrical Velocity Function outside the Aerofoil Contour

The complex conjugate perturbation function becomes outside of the aerofoil contour $(z = x < c_o, \text{ or } z = x > c)$

$$W(z) = \iota \sqrt{\frac{z-c}{z-c_o}} \left\{ -v(c_o) - \frac{2}{\pi} \underbrace{\int_{c_o}^c v'(s) \cos^{-1} \sqrt{\frac{s-c_o}{c-c_o}} ds}_{l_0} \right\} - \iota \frac{2}{\pi} \underbrace{\int_{c_o}^c v'(s) \cos^{-1} \sqrt{\frac{(c-z)(s-c_o)}{(c-c_o)(s-z)}} ds}_{l_0}.$$

Performing the integrals by parts gives:

• Integral I₀:

$$\int_{c_o}^{c} v'(s) \cos^{-1} \sqrt{\frac{s - c_o}{c - c_o}} ds = \left[v(s) \cos^{-1} \sqrt{\frac{s - c_o}{c - c_o}} \right]_{c_o}^{c} + \frac{1}{2} \int_{c_o}^{c} \frac{v(s)}{\sqrt{(s - c_o)(c - s)}} ds$$

$$= -\frac{\pi}{2}v(c_o) + \frac{1}{2} \int_{c_o}^{c} \frac{v(s)}{\sqrt{(s - c_o)(c - s)}} ds$$

• Integral I₁:

$$\int_{c_o}^{c} v'(s) \cos^{-1} \sqrt{\frac{(c-z)(s-c_o)}{(c-c_o)(s-z)}} ds$$

$$= \left[v(s) \cos^{-1} \sqrt{\frac{(c-z)(s-c_o)}{(c-c_o)(s-z)}} \right]_{c_o}^{c} + \frac{1}{2} \int_{c_o}^{c} v(s) \sqrt{\frac{(z-c_o)(c-z)}{(c-c_o)(s-c_o)}} \frac{ds}{s-z},$$

$$= -v(c_o) \frac{\pi}{2} + \frac{1}{2} \int_{c_o}^{c} v(s) \sqrt{\frac{(z-c_o)(c-z)}{(c-c_o)(s-c_o)}} \frac{ds}{s-z}.$$

Putting these two integrals back into the disturbance velocity function:

$$W_{A}(x) = i\sqrt{\frac{x-c}{x-c_{o}}} \left\{ -v(c_{o}) - \frac{2}{\pi} \left(-\frac{\pi}{2}v(c_{o}) + \frac{1}{2} \int_{c_{o}}^{c} \frac{v(s)}{\sqrt{(s-c_{o})(c-s)}} ds \right) \right\}$$

$$- i\frac{2}{\pi} \left\{ -v(c_{o})\frac{\pi}{2} + \frac{1}{2} \int_{c_{o}}^{c} v(s) \sqrt{\frac{(x-c_{o})(c-x)}{(c-c_{o})(s-c_{o})} \frac{ds}{s-x}} \right\}$$

$$= -i\frac{1}{\pi} \sqrt{\frac{x-c}{x-c_{o}}} \int_{c_{o}}^{c} v_{A}(s) \sqrt{\frac{s-c_{o}}{c-s} \frac{ds}{s-x}} + iv(c_{o}).$$

Taking the imaginary portions of the distrubance velocity function gives the perturbation velocity $v_A(x)$

$$v_A(x) = -\frac{1}{\pi} \sqrt{\frac{x-c}{x-c_o}} \int_{c_o}^c v_A(s) \sqrt{\frac{s-c_o}{c-s}} \frac{ds}{s-x}.$$
 (D.9)

This can be represented by a cubic spline notation such as

$$v_A(x) = -\frac{1}{\pi} \sqrt{\frac{x-c}{x-c_o}} \sum_{i=1}^{N} \sum_{k=0}^{3} V_k^{a,i} Q_k^i(x),$$
 (D.10)

where $Q_k^*(x)$ defines the integral.

D.2.1 Derivation of Integral $Q_k^i(x)$

While analyzing outside of the aerofoil contour the perturbation velocities are formulated as:

$$v_A(x) = -\frac{1}{\pi} \sqrt{\frac{x-c}{x-c_o}} \sum_{i=1}^{N} \sum_{k=0}^{3} V_k^i Q_k^i(x), \tag{1).11}$$

where the integral $Q_k^i(x)$;

$$Q_{k}^{i}(x) = \int_{c_{o}}^{c} (s - x_{i-1})^{k} \sqrt{\frac{s - c_{o}}{c - s}} \frac{ds}{s - x}$$

$$| \text{let } (s - x_{i-1})^{k} = \sum_{q=0}^{k} C_{q}^{k} s^{k - q} x_{i-1}^{q}$$

$$= \sum_{q=0}^{k} C_{q}^{k} x_{i-1}^{q} \int_{x_{i-1}}^{x_{i}} \frac{s^{k - q} (s - c_{o})}{\sqrt{(s - c_{o})(c - s)}} \frac{ds}{s - x}$$

$$| \text{let } (s^{k - q} - x^{k - q}) = (s - x) \sum_{l=0}^{k - q - l} s^{k - q - l - 1} x^{l}$$

$$= \sum_{q=0}^{k} C_{k}^{q} x_{i}^{q} \left\{ \sum_{l=0}^{k - q} x^{l} T_{k - q - l} - c_{o} \sum_{l=0}^{k - q - 1} x^{l} T_{k - q - l - 1} - 2x^{k - q} \sqrt{\frac{x - c_{o}}{x - c}} \cos^{-1} \sqrt{\frac{(c - x)(s - c_{o})}{(c - c_{o})(s - x)}} \right\}$$

in which

$$T_p = \int_{x_{i-1}}^{x_i} \frac{s^p ds}{\sqrt{(s - c_o)(c - s)}}. (1).12)$$

For the various p, the expressions of T_p are:

$$T_{0} = \left[\cos^{-1}\left(\frac{c+c_{o}-2s}{c-c_{o}}\right)\right]_{x_{i-1}}^{x_{i}},$$

$$T_{1} = \left[\left(\frac{c+c_{o}}{2}\right)\cos^{-1}\left(\frac{c+c_{o}-2s}{c-c_{o}}\right) - \sqrt{(s-c_{o})(c-s)}\right]_{x_{i-1}}^{x_{i}},$$

$$T_{2} = \left[\frac{3}{8}\left(c^{2}+6cc_{o}+c_{o}^{2}\right)\cos^{-1}\left(\frac{c+c_{o}-2s}{c-c_{o}}\right) - \left[\frac{s}{2}+\frac{3}{4}\left(c+c_{o}\right)\right]\sqrt{(s-c_{o})(c-s)}\right]_{x_{i-1}}^{x_{i}},$$

$$T_{3} = \left[\frac{1}{16}\left(-13c_{o}^{3}+21c_{o}^{2}c-15c^{2}c_{o}+5c^{3}+18c_{o}c\right)\cos^{-1}\left(\frac{c+c_{o}-2s}{c-c_{o}}\right) - \left(\frac{s^{2}}{3}+\frac{5sc}{12}+\frac{5c^{2}}{8}+\frac{c_{o}c}{12}+\frac{5c_{o}s}{12}+\frac{3c_{o}^{2}}{4}\right)\sqrt{(s-c_{o})(c-s)}\right]_{x_{i-1}}^{x_{i}}.$$

Appendix E

Computer Subroutines

All of these subroutines are coded using the C language. For some of the subroutines global variables exist. These are defined in the preamble of the main program.

```
#define N
             10
                       /* Number of chordline points
#define M
             N+2
                       /* Matrix size
                                                       */
             acos(-1) /* pi=3.14159...
#define PI
                                                       */
                      /* conversion from deg to rad
#define rad 180/PI
                                                       */
                       /* used to change x-coordinates */
#define diff 1e-13
                       /* used for jet flaps
#define L
                                                       */
```

E.1 Subroutine for Antisymmetrical Velocities

```
/* Subroutine AntiSpline calculates values of Cp by using Cubic Splines
  on aerofoils having antisymmetrical velocities only. Calculations are
  performed for 5 different angles of attack
  Recieves: x
                     - coordinates
             h'(x)
                     - camberline slope on aerofoil
                     - second derivative of aerofoil camberline
             h*(x)
                     - pressure coefficients for top and bottom of aerofoil
  Returns:
void AntiSpline(double x[M], double h[M], double hp[M], double Cp[2][5][N])
   double srt[N], K[5], H[5][M], u, v, A;
    int i,j,p,ii,aa;
    /* Calculate \sqrt{(1-x)/x} */
   for(i=0;i<N;i++)
      srt[i] = sqrt((1 - x[i]) / x[i]);
   /* Find Spline Coefficients H */
   Spline(x,h,hp,H);
    /* Find perturbation velocities and calculate pressure coefficients */
   for(aa=0;aa<5;aa++)
        A = aa * 5 / rad;
        for(i=0;i<N;i++)
            u = A * srt[i], v = -A + h[i];
            for (p=0;p<N;p++)
                KKK(x[p],x[p+1],x[i],K);
                for(j=0;j<4;j++)
                   u -= H[j][p] * K[j] * srt[i] / PI;
            Cp[0][aa][i] = 1 - (pow(cos(A) + u,2) + pow(sin(A) + v,2));
            Cp[1][aa][i] = 1 - (pow(cos(A) - u, 2) + pow(sin(A) + v, 2));
         }
    }
 }
```

E.2 Subroutine for Symmetrical Velocities

```
/* Subroutine SymmetSpline calculates values of Cp by using Cubic Splines
   on aerofoils of symmetrical thickness. Calculations are performed for
   5 different angles of attack
   Recieves: x
                      - coordinates
             g'(x)
                      - slope of thickness function
             g"(x)
                      - second derivative of thickness function
                     - pressure coefficients for top and bottom of aerofoil */
   Returns:
             Cp
void SymmetSpline(double x[M], double g[M], double gp[M], double Cp[2][5][N])
    double srt[N], J[5], G[5][M], Vs, Va, Us, Ua, A;
    int i,j,p,ii,aa;
    /* Calculate \sqrt{((1-x)/x)} */
    for(i=0;i<N;i++)
      srt[i] = sqrt((1 - x[i]) / x[i]);
    /* Find Spline Coefficients G */
    Spline(x,g,gp,G);
    /* Find perturbation velocities and calculate pressure coefficients */
    \times[0] = 0, \times[N] = 1;
    for(aa=0;aa<5;aa++)
         A = aa * 5 / rad;
         for(i=0;i<N;i++)
             Ua = A * srt[i], Us = 0, Va = -A, Vs = g[i];
             for (p=0; p<N; p++)
               {
                 JJJ(x[p],x[p+1],x[i],J);
                 for(j=0;j<4;j++)
                   u = G[j][p] * J[j] / PI;
            Cp[0][aa][i] = 1 - (pow(cos(A) + Ua + Us, 2) +
                                                 pow(sin(A) + Va + Vs, 2));
            Cp[1][aa][i] = 1 - (pow(cos(A) - Ua + Us, 2) +
                                                 pow(sin(A) + Va - Vs, 2));
          }
     }
```

}

E.3 Subroutine using Local Linearization

```
Subroutine ModSpline calculates values of Cp by using Cubic Splines
   on aerofoils of symmetrical thickness at zero incidence.
   Recieves: x
                      - coordinates
             g'(x)
                      - slope of thickness function
   Returns:
             Сp
                      - pressure coefficients for top of aerofoil */
void ModSpline(double x[M], double g[M], double Cp[M])
    double srt[M],G[5][M],J[5],gmod[M],gmodp[M],Vs,Va,Us,Ua,A,dx;
    int i,j,p;
    /* Calculate \sqrt{((1-x)/x)} and modified portion of g'(x) */
    dx = 1. / N;
    for(i=0;i<=N;i++)
        srt[i] = sqrt((1 - x[i]) / x[i]);
        gmod[i] = g[i] / srt[i];
    /* Find second derivative using forward and backwards second order
       differencing techniques */
    for(i=0;i<N-1;i++)
        dx = (x[i+2] - x[i]) / 2;
        gmodp[i] = (gmod[i+1]*2-1.5*gmod[i]-gmod[i+2]/2)/dx;
    for(i=N-2;i<=N;i++)
        dx = (x[i] - x[i-2]) / 2;
        gmodp[i] = (1.5*gmod[i] - 2*gmod[i-1] + gmod[i-2]/2) / dx;
    /* Find Spline Coefficients G */
   Spline(x, gmod, gmodp, G);
   /* Find perturbation velocities and calculate pressure coefficients */
   x[0] = 0, x[N] = 1;
    for(i=0;i<N;i++)
      {
        Us = 0:
        for (p=0; p<N; p++)
           JJM(x[p],x[p+1],x[i],J);
            for(j=0;j<4;j++)
              Us -= G[j][p] * J[j] / PI;
            Cp[i] = 1 - pow(1 + Us, 2) / (1 + pow(g[i], 2));
      }
 }
```

E.4 Subroutine for Integral $K_k^i(x)$

```
\prime^\star Subroutine KKK calculates the integration values for Kk(x) as needed
   by the antisymmetrical velocity field, defined by section appendix B.1.3
                     - first limit of integration
   Recieves: x1
                     - second limit of integration
             x^2
                     - position on velocity field
             XX
                     - integration values
   Returns:
           K
void KKK(double x1,double x2,double xx,double K[5])
    double ii[5], Io[5], I[5], t1, t2, temp1, temp2, temp3;
    int q,p;
    t2 = sqrt(x2*(1-x2)), t1 = sqrt(x1*(1-x1));
    if(x2 == xx)
                       temp2 = 0;
     else if (xx > 1)
                       temp2 = +acos(sqrt(x2*(1-xx)/(x2-xx)));
                       temp2 = acos(sqrt(x2*(1-xx)/(x2-xx)));
     else if (xx < 0)
     else if(x2 > xx) temp2 = acosh(sqrt(x2*(1-xx)/(x2-xx)));
                       temp2 = asinh(sqrt(x2*(1-xx)/(xx - x2)));
     else
   if(x1 == xx)
                       temp1 = 0;
     else if (xx > 1)
                       temp1 = +acos(sqrt(x1*(1-xx)/(x1-xx)));
                       temp1 = acos(sqrt(x1*(1-xx)/(x1-xx)));
     else if(xx < 0)
     else if(x1 > xx) temp1 = acosh(sqrt(x1*(1-xx)/(x1-xx)));
                       temp1 = asinh(sqrt(x1*(1-xx)/(xx - x1)));
   temp3 = sqrt(fabs(xx*(1-xx)));
   for(q=0;q<4;q++)
     Io[q] = -2 * pow(xx,q+1) / temp3 * (temp2-temp1);
   I[0] = acos(1-2*x2) - acos(1-2*x1);
   I[1] = I[0]/2 - (t2-t1);
   I[2] = .375*I[0] - (.75*(t2-t1) + (t2*x2-t1*x1)/2);
   I[3] = .3125*I[0] - (.625*(t2-t1) + 5/12.*(t2*x2-t1*x1) +
                                               (x2*x2*t2-x1*x1*t1)/3.);
   for(a=0;a<4;a++)
       ii[q] = Io[q];
       for (p=0; p <= q; p++)
         ii[q] += pow(xx,p) * I[q-p];
   K[0] = ii[0];
   K[1] = ii[1] - x1*ii[0];
   K[2] = ii[2] - 2*x1*ii[1] + pow(x1,2)*ii[0];
   K[3] = ii[3] - 3*x1*ii[2] + 3*pow(x1,2)*ii[1] - pow(x1,3)*ii[0];
 }
```

E.5 Subroutine for Integral $J_k^i(x)$

```
/* Subroutine JJJ calculates the integration values for Jk(x) as needed
  by the symmetrical velocity field, defined by section appendix B.2.3
  Recieves: x1
                     - first limit of integration
                     - second limit of integration
             x^2
             XX
                     - position on velocity field
             J
                     - integration values
  Returns:
void JJJ(double x1, double x2, double xx, double J[5])
   double ii[5], temp;
    int q,p;
    if(x1 == xx)
                        temp = log(fabs(x2-xx));
      else if (x2 == xx) temp = -\log(fabs(x1-xx));
      else
                        temp = \log(fabs((x2-xx)/(x1-xx)));
    for (p=0; p<4; p++)
        ii[p] = pow(xx,p) * temp;
        for(q=0;q<p;q++)
          ii[p] += pow(xx,q) / (p-q) * (pow(x2,p-q) - pow(x1,p-q));
   J[0] = ii[0];
   J[1] = ii[1] - x1*ii[0];
   J[2] = ii[2] - 2*x1*ii[1] + pow(x1,2)*ii[0];
   J[3] = ii[3] - 3*x1*ii[2] + 3*pow(x1,2)*ii[1] - pow(x1,3)*ii[0];
```

E.6 Subroutine for Integral $J_{M_k}^i(x)$

```
* Subroutine JJM calculates the integration values for JkM(x) as needed
   by the modified symmetrical velocity field, defined by section
   appendix B.3.1
                      - first limit of integration
   Recieves: x1
                      - second limit of integration
             x^2
                      - position on velocity field
             XX
                      - integration values
             J
   Returns:
void JJM(double x1, double x2, double xx, double J[5])
    double ii[5], Io[5], I[5], t1, t2, temp1, temp2, temp3;
    int q,p;
    t2 = sqrt(x2*(1-x2)), t1 = sqrt(x1*(1-x1));
                       temp2 = 0;
    if(x2 == xx)
      else if (xx > 1)
                       temp2 = +acos(sqrt(x2*(1-xx)/(x2-xx)));
      else if (xx < 0) temp2 = acos(sqrt(x2*(1-xx)/(x2-xx)));
      else if (x^2 > xx) temp2 = acosh(sqrt(x^2*(1-xx)/(x^2-xx)));
                        temp2 = asinh(sqrt(x2*(1-xx)/(xx - x2)));
      else
    if(x1 == xx)
                        temp1 = 0;
      else if (xx > 1) temp1 = tacos(sqrt(x1*(1-xx)/(x1-xx)));
      else if(xx < 0)
                       temp1 = acos(sqrt(x1*(1-xx)/(x1-xx)));
      else if (x1 > xx) temp1 = acosh(sqrt(x1*(1-xx)/(x1-xx)));
                        temp1 = asinh(sqrt(x1*(1-xx)/(xx - x1)));
      else
    temp3 = sqrt(fabs(xx*(1-xx)));
    for(q=0;q<5;q++)
      Io[q] = -2 * pow(xx,q) / temp3 * (temp2-temp1);
    I[0] = a\cos(1-2*x2) - a\cos(1-2*x1);
   I[1] = I[0] / 2 - (t2-t1);

I[2] = .375 * I[0] - (.75*(t2-t1) + (t2*x2-t1*x1)/2);
   I[3] = .3125*I[0] - (.625*(t2-t1) + 5/12.*(t2*x2-t1*x1) +
                                                      (x2*x2*t2-x1*x1*t1)/3.);
    for(p=0;p<5;p++)
      {
        ii[p] = Io[p] * (1 - xx) - I[p];
        for(1=0;1<p;1++)
          ii[p] += pow(xx,1) * I[p-1-1] * (1 - xx);
   J[0] = ii[0];
   J[1] = ii[1] - x1*ii[0];
   J[2] = ii[2] - 2*x1*ii[1] + pow(x1,2)*ii[0];
   J[3] = ii[3] - 3*x1*ii[2] + 3*pow(x1,2)*ii[1] - pow(x1,3)*ii[0];
 }
```

E.7 Subroutine for Spline Formulation

```
/* Subroutine Spline calculates spline coefficients using spline derived
   in appendix C.1.2
   Recieves: x
                       - coordinates
                       - coordinates to be splined
             y(x)
             y'(x)
                       - slopes of coordinates
                       - spline coefficients
   Returns:
void Spline(double x[M], double y[M], double yp[M], double G[5][M])
    double dx;
    int i;
    for(i=0;i<N;i++)
        dx = x[i+1] - x[i];
        G[0][i] = y[i];
        G[1][i] = yp[i];

G[2][i] = 3/dx/dx * (y[i+1] - y[i]) - (yp[i+1] + 2 * yp[i]) / dx;
        G[3][i] = (dx * (yp[i+1] + yp[i]) - 2 * (y[i+1] - y[i])) / pow(dx,3)
  }
```

E.8 Subroutine for Flexible Membranes

```
/* Subroutine SailSpline calculates values of Cp and shape of membrane
   by using Cubic Splines.
   Recieves: x
                      coordinates
   Returns:
             h(x)
                      - membrane shape
                      - pressure coefficients for membrane
                                                                              */
             Сp
void SailSpline(double x[M], double h[M], double Cp[M])
    double A(2*M)[2*M],t[4],t1[4],t2[4],srt[2][M],Rhs[2*M],b[2*M],h[M],hp[M],
           H[4][M], tt[4], dx, s1, a, xx;
    int i,j,ii,jj,q,end,More;
    /* Calculate \sqrt{(1-x)/x} */
    dx = 1. / N;
    for(i=0;i<N;i++)
      {
        xx = (x[i+1] + x[i]) / 2;
        srt[0][i] = sqrt((1 - x[i]) / x[i]);
        srt[1][i] = sqrt((1 - xx) / xx);
    srt[0][N] = sqrt((1 - x[N]) / x[N]);
    /* Set Matrix values to zero */
    for(i=0;i<2*M;i++)
      for(j=0;j<2*M;j++)
        A[i][j] = 0;
    /* Fill Matrix */
    end = 2*N+1;
    for(q=1;q=N;q++)
        i = q-1, ii = N + q,
        /* find midpoints and values for dx */
        xx = (x[q] + x[q-1]) / 2, dx = x[q] - x[q-1], dx2 = dx / 2;
        /* find values for v'(x) in eqn 4.7 */
        Temp1 (dx, dx, Ct/4, t1), Temp1 (dx2, dx, Ct/4, t2);
       s1 = So(x[q]), s2 = So(xx);
Rhs[i] = -Alpha * s1, Rhs[ii] = -Alpha * s2;
       A[i][i] += t1[0], A[i][i+1] += t1[1];
       A[i][ii] += t1[2], A[i][ii+1] += t1[3];
       A[ii][i] += t2[0], A[ii][i+1] += t2[1];
       A[ii][ii] += t2[2], A[ii][ii+1] += t2[3];
        /* find values for u(x) */
       for(j=0;j<N;j++)
           jj = N + j + 1, dx = x[j+1] - x[j];
          A[i][j] += s1 * dx/2, A[i][j+1] += s1 * dx/2;
           A[i][jj] += s1 * dx*dx/12, A[i][jj+1] -= s1 * dx*dx/12;
          KKK(x[j],x[j+1],x[q],tt), Temp(dx,tt,-srt[0][q]/PI,t);
          A[i][j] += t[0], A[i][j+1] += t[1];
```

```
A[i][jj] += t[2], A[i][jj+1] += t[3];
       KKK(x[j],x[j+1],xx,tt), Temp(dx,tt,-srt[1][q-1]/PI,t);
       A[ii][j] += s2 * dx/2, A[ii][j+1] += s2 * dx/2;
       A[ii][jj] += s2 * dx*dx/12, A[ii][jj+1] -= s2 * dx*dx/12;
       A[ii][j] += t[0], A[ii][j+1] += t[1];
       A[ii][jj] += t[2], A[ii][jj+1] += t[3];
  }
/* use equation 4.7 once more on first panel of membrane */
s = 1./N - .01/N, i = 0, do { i++; } while(s > x[i]), i--, ii = N+i+1;
Temp1(s-x[i], dx, Ct/4, t1), s1 = So(s), Rhs[N] = -s1 * Alpha;
A[N][i] += t1[0], A[N][i+1] += t1[1];
A[N][ii] += t1[2], A[N][ii+1] += t1[3];
for(j=0;j<N;j++)
    jj = N + j + 1;
    A[N][j] += s1 * dx/2, A[N][j+1] += s1 * dx/2;
    A[N][jj] += s1 * dx*dx/12, A[N][jj+1] -= s1 * dx*dx/12;
    KKK(x[j],x[j+1],s,tt), Temp(dx,tt,-sqrt((1-s)/s)/PI,t);
    A[N][j] += t[0], A[N][j+1] += t[1], A[N][jj] += t[2];
    A[N][jj+1] += t[3];
  }
/* Leading Edge singularity */
i = N-1;
for(j=0;j<=end;j++)
  A[end][j] = A[i][j], A[i][j] = 0;
Rhs[end] = Rhs[i], s1 = 16/PI*(.5/PI-Ct/8), Rhs[i] = -s1*Alpha;
for(j=0;j<N;j++)
  {
    jj = N + j + 1;
    A[i][j] += s1 * dx/2, A[i][j+1] += s1 * dx/2;
    A[i][jj] += s1 * dx*dx/12, A[i][jj+1] -= s1 * dx*dx/12;
    KKK(x[j],x[j+1],x[0],tt), Temp(dx,tt,-1/PI,t);
    A[i][j] += t[0], A[i][j+1] += t[1];
    A[i][jj] += t[2], A[i][jj+1] += t[3];
  }
/* Perform Guass-Jacobi Elimination */
Polynomial (A, Rhs, b);
for(i=0;i<=N;i++)
 h = b[i], hp = b[i+N+1];
/* Find Spline Coefficients */
Spline(x,h,hp,H);
/* Find Constant a as defined by equation 4.21 */
a = Alpha;
for(i=0;i<N;i++)
 for(j=0;j<4;j++)
    a += H[j][i] * pow(dx, j+1) / (j+1);
a *= -16 / PI;
```

```
/* Find membrane shape and pressure coefficients */
    for(i=0;i<=N;i++)
        Cp[i] = a*(.5-2*x[i])*srt[0][i];
        if(i == 0) Cp[i] += H[1][0], h[i] = s1 = 0;
        else
          {
            for(j=0;j<4;j++)
               s1 += H[j][i-1] * pow(dx,j+1) / (j+1);
               Cp[i] += j * H[j][i-1] * pow(dx,j-1);
           h[i] = s1 + a * Jo(x[i]) + Alpha * x[i];
       Cp[i] *= -Ct;
  }
void Temp(double x,double J[4],double s,double t[4])
    /* summation k=0..3 */
    t[0] = s * (J[0] + (2*J[3]/x-3*J[2])/x/x);
    t[1] = s * (3*J[2] - 2*J[3]/x)/x/x;
    t[2] = (J[1] - 2/x*J[2] + J[3]/x/x) * s;
    t[3] = (J[3]/x/x - J[2]/x) * s;
void Temp1(double s,double x,double temp,double t[4])
    /* Summation k = 1 ... 3 */
    t[0] = temp * 6*s/x/x * (s/x - 1);
    t[1] = temp * 6*s/x/x * (1 - s/x);
    t[2] = temp * (1 - 4*s/x + 3*s*s/x/x);
    t[3] = temp * (-2*s/x + 3*s*s/x/x);
  }
double So(double x)
  { return ((.5 - x + x*(1-x)*log((1-x)/x)) / PI - Ct/4*(.5-2*x)) *
         sqrt((1-x)/x) * 16 / PI;
/* equation 4.11 */
double Jo (double x)
  { return (.125*acos(sqrt(1-x)) - sqrt(x*(1-x))*(.125-7./12*x+x*x/3)); }
```

E.9 Subroutine for Jet Flapped Aerofoils

```
/* Subroutine JetSpline calculates values of Cp on the jet and aerofoil
   by using Cubic Splines.
   Recieves: x
                     - coordinates
            . h'(x)
                     - camberline slope on aerofoil
             h"(x)
                     - second derivative of aerofoil camberline
                     - pressure coefficients for aerofoil
   Returns:
             ďρ
                                                                         */
void JetSpline(double x[M], double h[M], double hp[M], double Cp[M])
    double xx[2][M], srt[2][M], E[5][M], H[5][M], A[2*M][2*M], Rhs[2*M], t1[4],
           t2[4],e[M],ep[M],t[4],b[2*M],bp[M],F[5],ff,fp,s1,s2,dx,u,dx2,a,hh
    int l,p,i,j,k,end,q;
    /* Calculate x and \sqrt{((1-x)/x)} */
    for(i=0;i<=N;i++)
      {
        xx[0][i] = 1+diff + (L - (1+diff)) * i/(N*1.);
        srt[0][i] = sqrt((L - xx[0][i]) / xx[0][i]);
        if(i > 0)
            xx[1][i-1] = (xx[0][i] + xx[0][i-1]) / 2;
            srt[1][i-1] = sqrt((L-xx[1][i-1])/xx[1][i-1]);
   dx = xx[0][1] - xx[0][0];
   /* special spline function given by equation 5.16 */
   fp = 2/PI*asinh(sqrt((L-xx[0][0])/L/(xx[0][0]-1)));
   ff = (xx[0][0]-1)*fp - sqrt(L-1)*2/PI*acos(sqrt(xx[0][0]/L));
   F[0] = ff, F[1] = fp, F[2] = -(3/dx*ff + 2*fp)/dx;
   F[3] = (fp + 2/dx*ff)/dx/dx;
   /* Find Spline Coefficients H for aerofoil surface */
   Spline(x,h,hp,H);
   /* Set matrix to zero */
   end = 2*N+2;
   for(i=0;i<=end;i++)
      {
        Rhs[i] = 0;
        for(j=0;j<=end;j++)
         A[i][j] = 0;
      }
   /* Fill Matrix */
   for(i=1;i<=N;i++)
         ii = N + i, dx = xx[0][i] - xx[0][i-1], dx^2 = dx / 2;
         if(i == 1)
              A[i][end] = Cj / 4 * F[0];
              for(k=1;k<4;k++)
                A[ii][end] += Cj / 4 * k * F[k] * pow(dx2,k-1);
```

```
Rhs[i] = srt[0][i-1] * Alpha, Rhs[ii] = srt[1][i-1] * Alpha;
     Temp1 (dx, dx, Cj/4, t1), Temp1 (dx2, dx, Cj/4, t2);
     A[i][i] += t1[0], A[i][i+1] += t1[1];
     A[i][ii] += t1[2], A[i][ii+1] += t1[3];
     A[ii][i] += t2[0], A[ii][i+1] += t2[1];
     A[ii][ii] += t2[2], A[ii][ii+1] += t2[3];
     for(j=0;j<N;j++)
         dx = xx[0][j+1] - xx[0][j], dx2 = dx / 2, jj = N + j + 1;
         KKK(x[j],x[j+1],xx[0][i-1],t1), KKK(x[j],x[j+1],xx[1][i-1],t2);
         for(k=0; k<4; k++)
             Rhs[i] = srt[0][i-1] / PI * H[k][j] * t1[k];
             Rhs[ii] -= srt[1][i-1] / PI * H[k][j] * t2[k];
         KKK(xx[0][j],xx[0][j+1],xx[0][i-1],t1);
         KKK(xx[0][j],xx[0][j+1],xx[1][i-1],t2);
         if(j == 0)
         for (k=0; k<4; k++)
             A[i][end] += srt[0][i-1] / PI * F[k] * t1[k];
             A[ii][end] += srt[1][i-1] / PI * F[k] * t2[k];
         Temp(dx, t1, srt[0][i-1]/PI, t), A[i][j] += t[0], A[i][j+1] += t[1];
         A[i][jj] += t[2], A[i][jj+1] += t[3];
         Temp(dx, t2, srt[1][i-1]/PI, t), A[ii][j] += t[0];
         A[ii][j+1] += t[1], A[ii][jj] += t[2], A[ii][jj+1] += t[3];
      }
/* boundary condition e'(c) = -tan(Beta) */
A[0][0] = 1, Rhs[0] = -tan(Beta);
A[0][end] = -sqrt(xx[0][1]-1) * 2 / PI * acos(sqrt(1/xx[0][1]));
/* boundary condition e'(1) = 0 */
for(i=0;i<=end;i++)
  A[end][i] = A[N][i], A[N][i] = 0;
Rhs[end] = Rhs[N], Rhs[N] = 0, A[N][N] = 1;
/* boundary condition e''(1) = 0 */
A[end-1][end-1] = 1, Rhs[end-1] = 0;
/* Perform Guass-Jacobi Elimination */
Polynomial (A, Rhs, b);
for(i=0;i<=N;i++)
  ii = i + N + 1, e[i] = b[i], ep[i] = b[ii];
/* Find spline coefficients E for jet */
Spline(xx[0],e,ep,E);
/* Find constant a for first panel */
a = b[end];
/* Find Pressure Coefficients on Aerofoil */
```

```
for(i=0;i<=N;i++)
        Cp[i] = Alpha;
        for(j=0;j<N;j++)
          {
            KKK(x[j],x[j+1],x[i],t1);
            KKK(xx[0][j],xx[0][j+1],x[i],t2);
            if(j == 0)
              Cp[i] = a / PI * (F[0]*t2[0]+F[1]*t2[1]+F[2]*t2[2]+F[3]*t2[3]);
            for(k=0;k<4;k++)
              Cp[i] = (H[k][j] * t1[k] + E[k][j] * t2[k]) / PI;
        Cp[i] *= sqrt((L-x[i])/x[i]) * 4;
      }
  }
void Temp(double x, double J[5], double s, double t[4])
    t[0] = s * (J[0] + (2*J[3]/x-3*J[2])/x/x);
    t[1] = s * (3*J[2] - 2*J[3]/x)/x/x;
    t[2] = (J[1] - 2/x*J[2] + J[3]/x/x) * s;
    t[3] = (J[3]/x/x - J[2]/x) * s;
  }
void Temp1(double s, double x, double temp, double t[4])
  {
    t[0] = temp * 6*s/x/x * (s/x - 1);
    t[1] = temp * 6*s/x/x * (1 - s/x);
    t[2] = temp * (1 - 4*s/x + 3*s*s/x/x);
    t[3] = temp * (-2*s/x + 3*s*s/x/x);
  }
```

E.10 Subroutine for Multi-Element Aerofoils

```
'* Subroutine Multi calculates values of Cp on aerofoil one and two
  by using Cubic Splines.
  Recieves: x
                     - coordinates
         h'(x)
                 - camberline slope on aerofoil
                 - second derivative of aerofoil camberline
         g'(x)
  Returns: Cp
                     - pressure coefficients for aerofoil
oid Multi(double x[2][M], double h[2][M], double g[2][M], double Cp[2][2][M])
     double t1[4], t[4], J[4], J2[4], G[2][4][M], H[2][4][M], srt[2][M], A[M1][M1],
     b[M1], Rhs[M1], x1, x2, dx, temp1, temp2, Ua, Us, Vs, Va, tus, tvs, dx1, dx2,
     ratio, det, temp, AA;
     int i,j,p,l,q,end,enn,ii,jj,perm,k,nn,ll;
     /* Calculate \sqrt{(1-x)/x} */
     end = 2*(N+1), enn = N + 1;
     for(i=0;i<=N;i++)
           srt[0][i] = sqrt(fabs((C1+dc+C2-x[0][i])/(x[0][i]-C1-dc)));
           srt[1][i] = sqrt(fabs((C1-x[1][i])/x[1][i]));
     /* Set Matrix to zero and fill Rhs[i] */
     for(i=0;i<=end;i++)
         for(j=0;j<=end;j++)
           A[i][j] = 0;
     for(i=0;i<=N;i++)
           Rhs[i] = -Alpha1 + h[0][i];
           Rhs[i+enn] = -(Alpha1 + Alpha2) + h[1][i];
         }
     /* Fill Matrix A */
     for(i=0;i<=N;i++)
           ii = enn + i;
           if(i == 0) x1 = x[0][i], x2 = x[1][i];
           else
                       x1 = x[0][i-1], x2 = x[1][i-1];
           if(i < (N-3))
               {
                   /* Equation one */
                   Temp1(x[0],x1,i,t), A[i][i] += t[0], A[i][i+1] += t[1];
                   A[i][i+2] += t[2], A[i][i+3] += t[3];
                   /* Equation two */
                   Temp1(x[1],x2,i,t), A[ii][ii] += t[0], A[ii][ii+1] += t[1];
                   A[ii][ii+2] += t[2], A[ii][ii+3] += t[3];
               }
```

```
else
          {
              /* Equation one */
              Templ(x[0],x1,i,t), A[i][i] += t[0], A[i][i+1] += t[1];
              A[i][i-1] += t[2], A[i][i-2] += t[3];
              /* Equation two */
              Temp1(x[1],x2,i,t), A[ii][ii] += t[0], A[ii][ii+1] += t[1];
              A[ii][ii-1] += t[2], A[ii][ii-2] += t[3];
      for (j=0; j< N-3; j++)
              jj = j + enn;
              /* Equation one */
              KKK(x[1][j],x[1][j+1],x1,t1,1);
              Temp(x[1],t1,-srt[0][i]/PI,j,t), A[i][jj] += t[0];
              A[i][jj+1] += t[1], A[i][jj+2] += t[2], A[i][jj+3] += t[3];
              /* Equation two */
              KKK(x[0][j],x[0][j+1],x2,t1,J,0,0);
              Temp(x[0], t1, -srt[1][i]/PI, j, t), A[ii][j] += t[0],
              A[ii][j+1] += t[1], A[ii][j+2] += t[2], A[ii][j+3] += t[3];
      for(j=N-3;j<N;j++)
              jj = j + enn;
              /* Equation one */
              KKK(x[1][j],x[1][j+1],x1,t1,J,1,0);
              Temp(x[1],t1,-srt[0][i]/PI,j,t), A[i][jj] += t[0],
              A[i][jj+1] += t[1], A[i][jj-1] += t[2], A[i][jj-2] += t[3];
              /* Equation two */
              KKK(x[0][j],x[0][j+1],x2,t1,J,0,0);
              Temp(x[0],t1,-srt[1][i]/PI,j,t), A[ii][j] += t[0],
              A[ii][j+1] += t[1], A[ii][j-1] += t[2], A[ii][j-2] += t[3];
          }
    }
/* Perform Guass-Jacobi Elimination */
end--;
for(j=0;j<end;j++)
    for (i=j+1; i \le end; i++)
          printf("\n%2d %2d",i,j);
          ratio = A[i][j] / A[j][j];
          for(q=j;q<=end;q++)
              A[i][q] -= A[j][q] * ratio;
          Rhs[i] -= Rhs[j] * ratio;
      }
```

```
/* Solve for b[j] */
for(i=end;i>=0;i--)
    {
      b[i] = Rhs[i];
      for(j=i+1;j<=end;j++)
          b[i] -= A[i][j] * b[j];
      b[i] /= A[i][i];
    }
/* Put solution vector into h for Splining Purposes */
for(i=0;i<=N;i++)
    h[0][i] = b[i], h[1][i] = b[i+enn];
/* Spline Velocities for both Aerofoils */
Spline(x[0],h[0],H[0]), Spline(x[1],h[1],H[1]);
Spline(x[0],g[0],G[0]), Spline(x[1],g[1],G[1]);
/* Find perturbation velocities and calculate pressure coefficients */
AA = Alpha1;
for(1=0;1<2;1++)
      for(i=0;i<=N;i++)
              x1 = x[1][i], Va = h[1][i], Ua = Us = 0, Vs = g[1][i];
              11 = 0;
              if(1==0) 11 = 1;
              x2 = x[11][i];
              for (p=0; p<N; p++)
                    KKK(x[1][p],x[1][p+1],x1,t1,J,1,0);
                    JJJ(x[1][p],x[1][p+1],x1,J);
                    JJJ(x[1][p],x[1][p+1],x2,J2);
                    for (j=0; j<4; j++)
                          Ua -= H[1][j][p] * t1[j] / PI;
                          Us -= G[1][j][p] * J[j] / PI;
                          Us -= G[11][j][p] * J2[j] / PI;
                         }
              if(1 == 0)
                          Ua *= sqrt(fabs(C1-x1)/x1);
                          Ua *= sqrt(fabs((C1+dc+C2-x1)/(x1-C1-dc)));
              Cp[1][0][i] = 1 - (pow(cos(AA) + Ua + Us, 2) + pow(sin(AA))
                                    + Va + Vs, 2));
              Cp[1][1][i] = 1 - (pow(cos(AA) - Ua + Us, 2) + pow(sin(AA))
                                    + Va - Vs,2));
     AA += Alpha2;
```

```
id Temp(double x[M], double J[5], double s, int i, double t[4])
      double h, dx1, dx2, tt[4];
      h = x[i+1] - x[i];
      tt[0] = s * (J[0] + (2*J[3]/h-3*J[2])/h/h);
      tt[1] = s * (3*J[2] - 2*J[3]/h)/h/h;
      tt[2] = (J[1] - 2/h*J[2] + J[3]/h/h) * s;
      tt[3] = (J[3]/h/h - J[2]/h) * s;
      if(i < (N-3))
          {
            dx1 = (x[i+2] - x[i]) / 2, dx2 = (x[i+3] - x[i+1]) / 2;
            tt[2] /= dx1, tt[3] /= dx2;
            t[0] = tt[0] - 1.5*tt[2];
            t[1] = tt[1] + 2*tt[2] - 1.5*tt[3];
            t[2] = 2*tt[3] - tt[2]/2;
            t[3] = -tt[3]/2;
      else
            dx1 = (x[i] - x[i-2]) / 2, dx2 = (x[i+1] - x[i-1]) / 2;
            tt[2] /= dx1, tt[3] /= dx2;
            t[0] = tt[0] + 1.5*tt[2] - tt[3]*2;
            t[1] = tt[1] + 1.5*tt[3];
            t[2] = tt[3]/2 - tt[2]*2;
            t[3] = tt[2]/2;
          }
void Temp1(double x[M], double xx, int i, double t[4])
      double dx1, dx2, dx, h, tt[4], tmp;
      if(i == 0) t[0] = 1, t[1] = t[2] = t[3] = 0;
      else
            h = x[i] - x[i-1], dx = xx - x[i-1], tmp = dx / h;
            tt[0] = 1 + pow(tmp, 2) * (tmp*2 - 3),
            tt[1] = pow(tmp, 2) * (3 - tmp);
            tt[2] = dx * (1 + tmp * (tmp - 2)), tt[3] = dx * (tmp * (tmp - 1));
            if(i < (N-3))
                    dx1 = (x[i+2] - x[i]) / 2, dx2 = (x[i+3] - x[i+1]) / 2;
                    tt[2] /= dx1, tt[3] /= dx2;
                    t[0] = tt[0] - 1.5*tt[2];
                    t[1] = tt[1] + 2*tt[2] - 1.5*tt[3];
                    t[2] = 2*tt[3] - tt[2]/2;
                    t[3] = -tt[3]/2;
            else
                {
                    dx1 = (x[i] - x[i-2]) / 2, dx2 = (x[i+1]-x[i-1]);
                    tt[2] /= dx1, tt[3] /= dx2;
                    t[0] = tt[0] + 1.5*tt[2] - tt[3]*2;
```

```
t[1] = tt[1] + 1.5*tt[3];
t[2] = tt[3]/2 - tt[2]*2;
t[3] = tt[2]/2;
```

}

}